DFT STUDY OF DOPED AND FUNCTIONALIZED FULLERENE BASED MATERIALS FOR LITHIUM-ION BATTERY APPLICATIONS

A Thesis
Presented to
The Academic Faculty

by

Parveen Sood

In Partial Fulfillment
of the Requirements for the Degree
Doctor of Philosophy in the
School of Materials Science and Engineering

Georgia Institute of Technology
May 2017

DFT STUDY OF DOPED AND FUNCTIONALIZED FULLERENE BASED MATERIALS FOR LITHIUM-ION BATTERY APPLICATIONS

Approved by:

Prof. Seung Soon Jang , Advisor
School of Materials Science and Engineering
Georgia Institute of Technology

Prof. Seung Woo Lee
School of Mechanical Engineering
Georgia Institute of Technology

Prof. Paul S. Russo
School of Materials Science and Engineering
Georgia Institute of Technology

Prof. Matthew McDowell
School of Materials Science and Engineering
Georgia Institute of Technology

Prof. Faisal Alamgir
School of Materials Science and Engineering
Georgia Institute of Technology

Date Approved: March 30, 2017

ACKNOWLEDGEMENTS

This work would not have been possible without the help, whole-hearted support, initiative and advisement of my advisor Prof. Seung Soon Jang. I have always found him to be very approachable and he always had his doors open for me. He has been very insightful, helpful, hands-on and always willing to offer constructive criticism from which I have learnt a lot professionally. As an academician, he is an inspiration to me and has shaped my view of life in multiple ways.

I also wish to thank my family, especially, my parents for all their patience and the wait that was foisted upon them. This work would not have been possible without their active support and encouragement. They have always been with me emotionally if not physically.

I also wish to thank all my colleagues and friends in GaTech for their support and from whom I have learnt a lot. Finally, I wish to thank all of the former and current members of the CNBT lab for their help and support.

TABLE OF CONTENTS

LIST OF TABLES

LIST OF FIGURES

LIST OF SYMBOLS AND ABBREVIATIONS

TMO	Transition metal oxide
NiMH	Nickel metal hydride
DFT	Density functional theory
MD	Molecular Dynamics
HOMO	(Energy of) Highest occupied molecular orbital
LUMO	(Energy of) Lowest unoccupied molecular orbital
HOMO-LUMO Gap	Energy of LUMO level minus Energy of HOMO level
OCFG	Oxygen containing functional group
SEWFG	Strongly electron withdrawing functional group
ESP	Electrostatic Potential
CNT	Carbon nanotubes
LCO	Lithium cobalt oxide
NCM	Lithium nickel cobalt manganese oxide
NCA	Lithium nickel cobalt aluminum oxide
LFP	Lithium iron phosphate
LTO	Lithium titanium oxide
LNO	Lithium nickel oxide
LTS	Lithium titanium sulfide
LFSF	Lithium iron fluorosulfate
SEI	Solid electrolyte interface

SUMMARY

The transition metal oxides (TMO) currently used as cathode materials are expensive, strategically scarce, toxic and have environmental implications. The crystal structure of these materials sets an upper bound on the amount of lithium they can intercalate which limits the energy density of the device. Consequently, there is intense effort to develop novel and better cathode materials.

Carbon based materials present a promising alternative because carbon is inexpensive, abundant and environmentally friendly. While the domain of carbon based materials is quite extensive, the high stability and electron affinity of C_{60} make C_{60} based materials attractive for positive electrode applications in lithium ion batteries (LIBs). The rich chemistry of carbon allows fullerene based materials to be doped and functionalized and thereby their properties can be tailored in a specific direction. Recently, devices based on functionalized CNTs and showing high energy and power densities have been fabricated. In these devices, the unique combination of properties has been attributed to the presence of oxygen containing functional groups.

In this work, we have systematically explored the domain of fullerene based materials for possible applications in Li-ion batteries. The electrochemical and electronic properties of pristine fullerene and highly reduced fullerene anions have been investigated using density functional theory. Because battery environment is complex and contains an electrolyte, solvation effects are important. Therefore, we have systematically studied the effect of solvation on the stability and redox potential of highly reduced fullerene anions. It has been reported that the redox potential of quinone derivatives is

reduced with increasing lithium adsorption thereby degrading cell potential. Correspondingly, the evolution of redox potential of C_{60} with increasing lithium adsorption is of interest and has been investigated in this work.

The effect of doping and functionalization on the redox and electronic properties of fullerene based materials has been studied. Our computation results show that some dopants and functional groups are quite effective in increasing the redox potential of C_{60}. Using DFT, we have quantitatively explored whether doping and functionalization have synergistic effect. The correlation between electronic properties and redox potentials of doped and functionalized C_{60} based materials has been investigated so as to be able to rapidly screen functionalized and doped fullerene based materials for cathode applications.

CHAPTER 1

INTRODUCTION

Energy on demand is a basic input for the sustenance of our technology dependent civilization and consequently the importance of energy producing and energy storage devices cannot be overemphasized. Although conventional energy producing devices vary considerably in scale from hydroelectric dams to solar cells, all such devices have in common that they convert energy from one form to another. At their cores, they are energy conversion devices. The dependence on fossil fuels, which are a finite natural resource, as a primary source of energy, has climatic[1] and geopolitical implications. This has led to an accelerated effort for development of cleaner and more efficient energy storage and conversion devices. Windmills, watermills and hydroelectric turbines have been providing clean energy for over a century. But the emergence of commercial electronic devices such as laptops and cell phones has required the development of portable, high energy density and high power density devices such as batteries and capacitors.

A battery is an energy conversion device that stores energy in the chemical form and transforms the stored chemical energy into electrical energy on demand[1]. The Galvanic cell was probably the earliest and the simplest prototype of a battery. Another example is the lead acid battery which has been extensively used in automobiles because of its low cost [2]. All batteries share a common feature in that they consist of a positive electrode called cathode and a negative electrode called anode which are physically separated but electrically connected through an electrolyte[1]. Oxidation and reduction

reactions take place at anode and cathode respectively. The electrolyte serves as a medium for transport of ionic species from one electrode to another, electrically connecting the two electrodes and maintaining charge neutrality for the uninterrupted, continuous working of the battery. The source of energy in the battery is the reduction in Gibbs free energy which appears in the form of electromotive force (emf) that drives current in the external circuit. Although inexpensive, lead acid batteries have low energy density[2] (energy to volume ratio) and specific energy (energy to weight ratio) and cannot be efficiently used for consumer electronics applications such as cell phones. Multiple commercial battery technologies such as NiMH, NiCd and Li-ion exist as possible alternatives to lead acid batteries, with their own advantages and limitations. Of these, Li-ion has the highest specific energy in the range[2] of 120-200 Wh/kg as shown [3] in Figure 1 and accordingly they have been extensively used in consumer electronics applications.

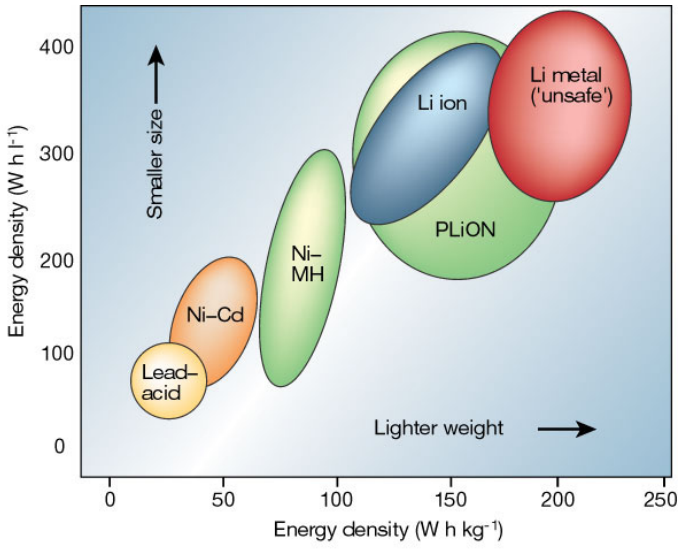

Figure 1: Energy density and specific energy of commercial battery technologies (source of graphic: Tarascon et al.[3])

Owing to intensive research and development, Li-ion battery technology has matured and become easily affordable. The energy density of Li-ion battery has been more than doubled[4] and they are ten times cheaper[4] since 1991 when the first commercial Li-ion battery was sold by Sony Corp. In 2013, consumers purchased an estimated 5 billion Li-ion cells[4] indicating that Li-ion battery technology has been a commercial success.

Li batteries are classified into primary and secondary batteries. If the electrode reactions are reversible, a discharged Li-ion battery can be reused i.e. it is rechargeable; otherwise it is non-rechargeable. Non-rechargeable and rechargeable batteries are also called primary and secondary batteries respectively.

A schematic[1] of a rechargeable Li-ion battery is shown in Figure 2.

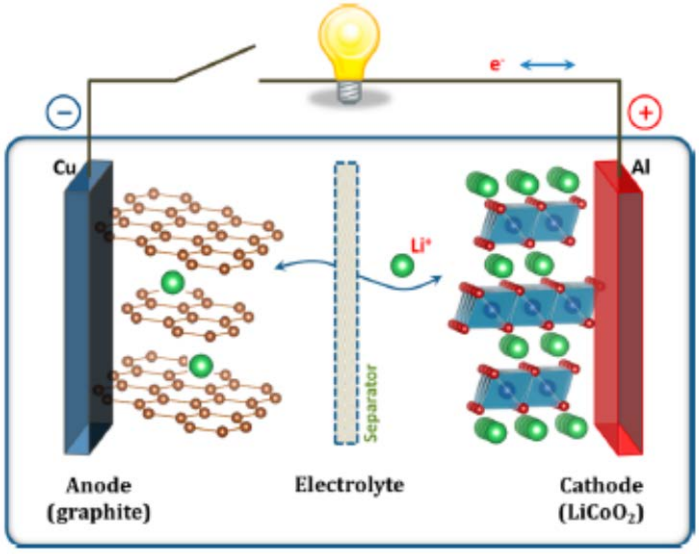

Figure 2: Schematic of a rechargeable Li-ion battery (source of graphic: Goodenough et al.[1])

The anode is made of graphite which is a layered structure. Lithium is intercalated between the graphite layers. On discharge, Li^+ ions from anode are transported through

the electrolyte to the CoO_2 cathode where they are intercalated to give $LiCoO_2$. The reaction at the cathode is termed as the insertion reaction. During the recharging of the battery, the reverse reaction occurs and lithium is deposited back at the anode and this cycle is repeated.

The current high performance of Li ion batteries is the result of extensive modifications in battery materials since the early stages of Li-ion battery development[5, 6]. A timeline for the evolution of energy density, a key performance parameter characterizing a battery, for several commercial batteries including Li-ion is shown [4] in Figure 3.

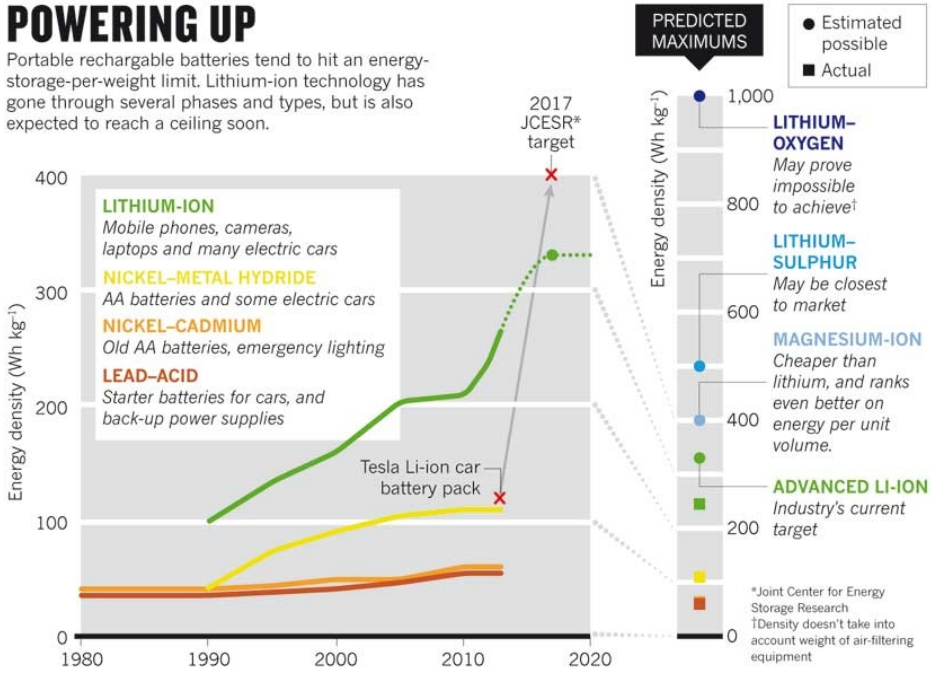

Figure 3: Timeline for evolution of energy density of commercial battery technologies(source of graphic: Van Noorden[4])

Although Li ion batteries perform much better than their other commercial competitors, it is expected that they will reach their peak performance[4] unless some novel advances are

made. Consequently, extensive research effort is in progress to improve the performance of Li-ion batteries by exploring new electrode materials[7].

Carbon allotrope materials such as fullerene (C_{60}), carbon nanotubes (CNTs), graphene and their derivatives are relatively recent materials[8] that hold promise as potential electrode materials[9-12]. The utility of carbon allotropes and their derivatives as possible electrode materials derives from multiple possible hybridization schemes for carbon, high chemical and mechanical stability of C-C bond, rich surface chemistry and the ability to form strong bonds with the adsorbed species[13]. Owing to these characteristics of the C-C bond, these allotropes of carbon and their derivatives have novel combinations of electronic, mechanical and thermal properties, a combination that is difficult to find in any other single component material. For example, single layer graphene has a thermal conductivity[14] of 5000 W/mK compared to 385 W/mK for copper. Since graphene is known to intercalate lithium [15], it an attractive electrode material with potential for further improvement with doping and functionalization .

The electrochemical environment inside the battery is complex[16]. Frequently, trade-offs in properties are required to design an optimum material for a given chemical environment and electrochemical specification. Although carbon allotropes and their derivatives have novel properties[13], a better understanding of their behavior and characteristics in the electrochemical aspect is highly desirable for practical applications. Experiments can be performed but they are tedious, expensive and sometimes may not be possible with the currently available instrumentation, especially while exploring new materials which may be unstable.

Computational studies can help narrow down the search space to be explored by experiments and cut cost. Ab-initio methods and atomistic simulations allow the material properties to be predicted and explained at the electronic and atomic level respectively. Such investigations also provide valuable inputs on values and trends for material properties such as diffusion coefficients, for modeling at systems level, which has direct commercial implications.

The focus of this work is to explore fullerene based materials and their derivatives using ab-initio density functional theory[17] (DFT). Such studies are important in their own right and also provide useful input for studies at higher temporal and spatial scales such as for Molecular Dynamics[18] (MD) simulation methodology at atomistic scale, Dissipative Particle Dynamics[19] (DPD) at mesoscale and Finite Difference Methods[20] (FDM) at continuum scale. It is anticipated that this approach will help in better understanding and improving the material selection and design process for electrodes in lithium ion batteries.

DFT has been used to model thermodynamic[21], kinetic[22] and electrochemical aspects[23] of batteries. Besides, batteries have been modeled at higher temporal and spatial scales[24], underscoring the complexity and multiscale nature of chemical, thermal and mechanical phenomenon underlying battery operation. A review of literature pertaining to these modeling studies will be presented in the next chapter.

CHAPTER 2

LITERATURE REVIEW

In order to improve the performance characteristics and safety of Li-ion batteries, many materials have been investigated for electrode and electrolyte applications[7]. An overview of the typical ranges of the average discharge potentials and specific capacity of some electrode materials from Nitta et al.[25], is presented in an Ashby chart[26] in Figure 4.

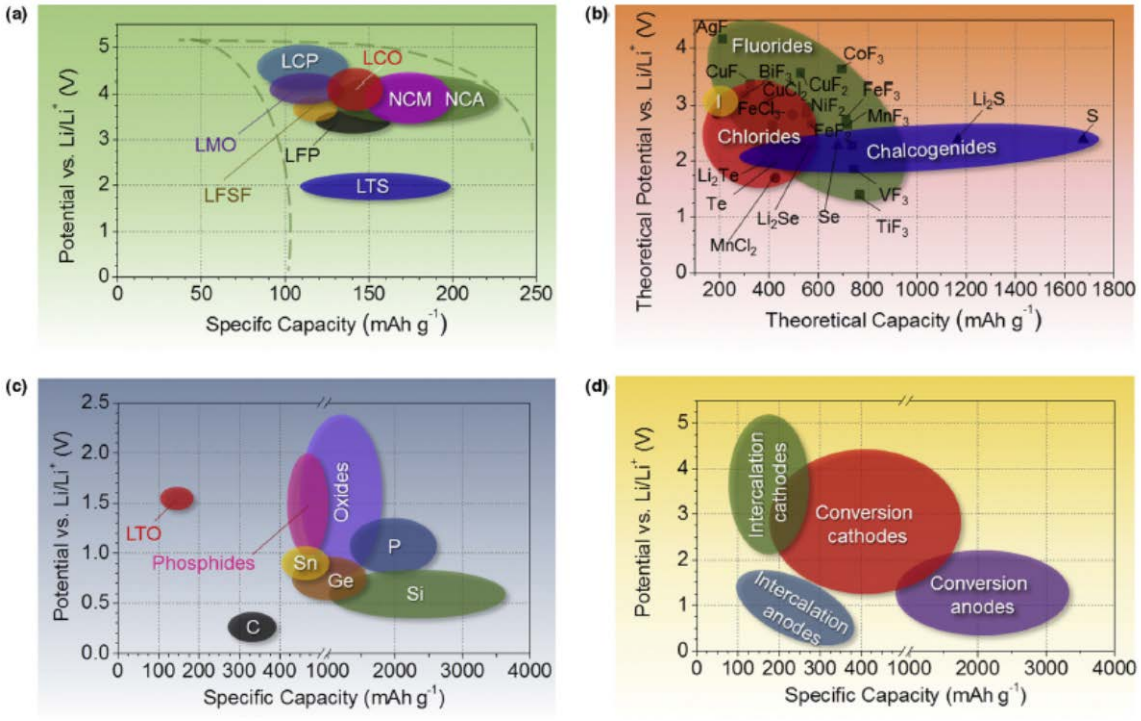

Figure 4: Range of average discharge potential as a function of specific capacity for (a) intercalation type cathodes (experimental) (b)conversion type cathodes (theoretical) (c) conversion type anode (experimental) (d)cumulative of a, b and c for all electrodes(source of graphic: Nitta et al.[25])

Several electrolyte materials have also been investigated. A schematic representation of some of the common electrolyte and electrode materials[27] considered for Li-ion battery applications is shown in a cell sandwich in Figure 5.

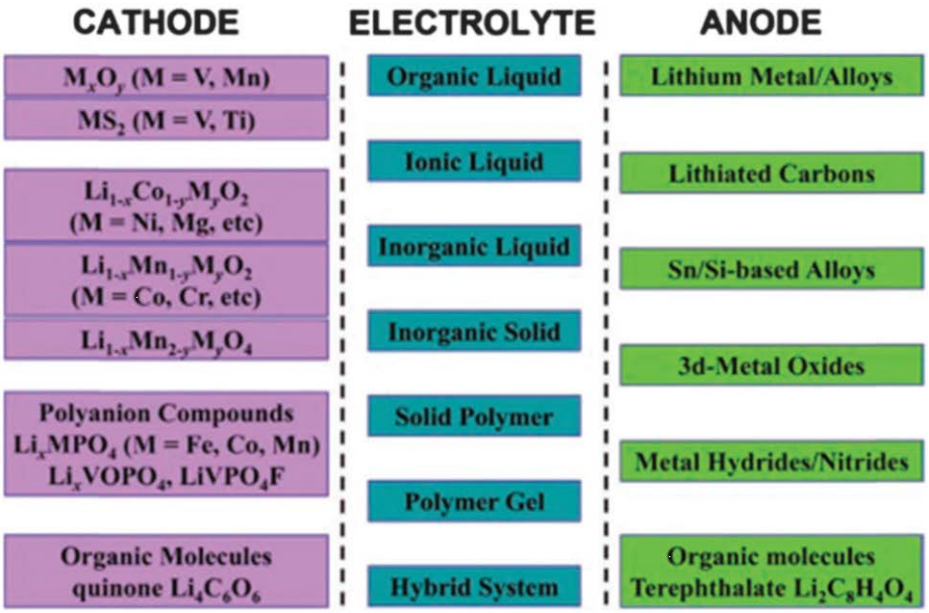

Figure 5: Electrode and electrolyte materials investigated for lithium ion battery applications (source of graphic: Bhatt et al.[27])

It is evident from Figure 4 and Figure 5 that the range of candidate materials currently under investigation for possible lithium ion battery applications is very extensive and is an ongoing and expanding area of research. Lithium ion batteries have been investigated across several temporal and spatial scales. The existence of such studies, in different spatial and temporal regimes, emphasizes that multiple aspects of their behavior at different scales need to be understood and correlated in order to fully understand their behavior and develop functional predictive capabilities. A complete survey of the available literature on materials and modeling for lithium ion batteries would fill several volumes. So, a focused survey of literature, which will cover the

current trends in computational and experimental investigations of lithium ion battery materials, relevant to this thesis, will be presented

2.1 Density functional theory studies on Li ion batteries

Functionally, battery materials can be subdivided into electrode and electrolyte materials. Electrode materials[28] have been investigated using DFT[17] for phase stability[29-34], intercalation phenomenon[35-38], crystal structure[39-43], electronic properties[44-47] and thermodynamic behavior[48-51]. Layered transition metal oxides are currently used as cathodes in lithium ion batteries. Kim et al.[52] investigated the increase in stability of $LiNiO_2$ (LNO) when doped with Co. They found that the formation energy of lithium and oxygen vacancies in LNO was smaller than that in $LiCoO_2$ (LCO). In addition, DFT study of the local configuration of vacancies showed that the energy of oxygen vacancy increased as the distance to the Co atom was decreased. The study also showed that the Ni-O bond strength was smaller than Co-O bond strength thus explaining the higher stability of LCO relative to LNO Hence, doping of LNO with Co increased the lithium and oxygen vacancy formation energy in LNO. The investigation of thermodynamics of lithium and oxygen vacancy formation carried out in this work is important as it suggests a way of increasing the stability of LNO by doping it with CoO, an insight useful from the industrial point of view.

Ceder et al.[53] used DFT[54] coupled with cluster variation method[55] to study the phase behavior of Li_xCoO_2. Density functional theory was used to determine the energy of the ground state as well as the relative energies of the various possible structures of Li_xCoO_2. Cluster variation method, utilizing DFT input,[54, 55] was used to generate a free energy model for finite temperature calculations and predict the stability of various phases of layered and spinel Li_xCoO_2 as a function of lithium content. This allowed the

generation of a phase diagram for the layered and spinel forms of Li_xCoO_2. The calculated free energies of the layered and spinel form of Li_xCoO_2 demonstrated the possibility of a phase transition from layered to spinel structure with increasing lithium concentration at 300 K. They also investigated the ability of specific transition metals to form stable spinel and layered structures by calculating the formation energies LiM_2O_4 (where M = Li, Cr, Mn, Fe or Ni). It was found that Mn formed the most stable spinel structure while Fe formed the most stable layered structure. Free energy calculations demonstrated that the layered structure was metastable around lithium mole fraction of 0.5 and there was a tendency to change to a spinel structure, the lower energy state. Calculated phase diagrams for $LiFePO_4$[56], Li-Mn-O system[57] and Li-Ni-O[58] system have also been reported. These works illustrate the application of DFT for predicting phase relationships in lithium ion battery materials at finite temperatures.

Kang et al.[59] investigated the effects of several factors on the ionic diffusivity of layered oxide materials. Although diffusion is a kinetic phenomenon, diffusivity depends upon the activation barrier for diffusion which can be calculated using density functional theory. They calculated the energy of Li ion in octahedral and tetrahedral sites as a function of c- parameter of the lattice. The calculated energies show that lithium in the octahedral site has a lower energy than the tetrahedral site. As lithium hops from one tetrahedral site to the next during diffusion, it transits via a tetrahedral site, a site of higher energy, which accounts for the diffusion barrier. They also investigated the effect of a and b lattice parameters on the activation barrier for lithium diffusion. It was found that the diffusion barrier was relatively insensitive to a or b spacing compared to c parameter. This was explained on the basis of the low sensitivity of the shortest Li-O

distance to change in a or b parameter. With the basic methodology established, they also investigated the effect of non-transition metal and transition metals dopants on diffusion and activation barrier. It was found that the activation barrier was considerably increased by doping with non-transition metals. Since the diffusion coefficient depends upon the activation energy through an Arrhenius type of relationship[60], such studies suggest ways of changing the diffusion coefficients of lithium by several orders of magnitude through slight changes in composition of the electrode. Similar studies on Li diffusion in LCO[61, 62], olivine phosphates[63, 64] and lithium manganese oxide (LMO)[65, 66] have also been reported.

Reed et al.[67] investigated the effect of cycling on the stability of Ni doped layered $LiMnO_2$. Their DFT calculations showed that electrochemical cycling of Ni doped $LiMnO_2$ resulted in changing the oxidation state of Ni from +2 to +4 while keeping the oxidation state of Mn to +4. This prevents the transformation from the layered to the spinel structure. The near constancy of Mn-O bond length, *irrespective of the Li* content in Ni doped $LiMnO_2$, demonstrated that the oxidation state of Mn remains unchanged and the base Mn-O structure intact, accounting for cyclic stability. This study illustrates a design concept that involves transferring the changes in oxidation state during cycling to an externally introduced doping material without degrading the base structure of the lithium transition metal oxide responsible for intercalation.

Winget et al.[68] have presented a computational methodology for calculating the equilibrium free energy of an oxidation/reduction process in terms of the ionization potential and electron affinity of the species in gas phase. The thermodynamic cycle applied in their approach [69] is based on Hess's law of heat summation. The free energy

change associated with the solvation of the electron is neglected. Since the oxidation/reduction potential of a species can be computed, the electromotive force (emf) of an electrochemical cell consisting of two electrodes can be obtained theoretically. Since the gas phase energies can be computed at various levels of theory[68], the redox potentials in solution can be computed with increasing accuracy depending upon the availability of computational resources. They demonstrated[68] the application of their computation protocol to both reversible and irreversible redox processes. Their methodology can be automated and used as a guideline for rapidly screening materials for electrode applications. Their approach has been used to determine the solvation free energies of metal halides in organic solvents[70], reduction potential of nitroxyl radicals[71], oxidation potentials for substituted anilines[69] and liquid phase reduction potentials of organic and biological molecules[72].

Shang et al.[49] used DFT to calculate phonon dispersion relations and phonon density of states for $LiMPO_4$ (M=Mn, Fe, Co and Ni). Based on the phonon density of states, they obtained the finite temperature properties of $LiMPO_4$ from 0 K to 1200 K i.e. the Gibbs free energy, entropy and enthalpy of $LiMPO_4$. It was found that the vibrational contribution to Gibbs free energy increased due to decreasing vibrational entropy from M=Mn, Fe, Co to Ni. These thermodynamic properties can be used as inputs in CALPHAD approach[73] to calculate phase behavior at different temperatures. This work demonstrated the possible application of DFT for calculating continuum level thermodynamic parameters for lithium ion batteries from first principle calculations. Goel et al.[74] have carried out experiments to measure the volume expansion coefficient, thermal expansion coefficient and inelastic scattering spectra of $LiMPO_4$ (M=Mn, Fe).

The inelastic scattering measurements were in good agreement with their DFT calculations. Lattice dynamics studies for Li_2CO_3 have also been reported[75].

Ganesh et al.[76] performed ab-initio MD simulations of $LiPF_6$ dissolved in ethylene carbonate (EC) and propylene carbonate (PC) to determine lithium diffusivities, lithium solvation energies and the structure of first solvation shell of lithium in EC and PC. The diffusivities of phosphorus and lithium ions were obtained from the computed mean square displacement of these ions in EC and PC while the structure of the first solvation shell was obtained from RDF analysis. The distribution of (carbonyl) O-Li-O (carbonyl) bond angle showed a sharp peak around 110 degrees indicating that lithium ion is tetrahedrally coordinated with four solvent molecules. This work was one of the first ab-initio MD studies reported for lithium ion batteries. Ab-initio MD simulations have also been carried out for negative electrode materials such as Si[77] and carbon nanotubes[78].

DFT has also been used to study anode materials [79-82]. The three main materials of interest[83] for negative electrode applications are graphite, silicon based materials and titanium oxide based materials. Currently, graphite is the most extensively used negative electrode material[10]. Because of the limiting reversible capacity and diffusion rates in graphite[10], which result in low power density, other materials are being explored. Tasaki[84] has used DFT to study the structural and energetic properties of several graphite intercalation compounds (GIC) with different solvents for lithium. When graphite is used as a negative electrode material in lithium ion batteries, lithium ion along with the solvent for lithium ions such as dimethysulfoxide is intercalated in graphite forming a ternary GIC. DFT with Grimme's dispersion correction [85-87] was used to describe Van der Waals interactions in graphite. Interlayer distances and intercalation energies were computed for

several GICs. Based on DFT studies, it was hypothesized that the stability of GIC depends on the electron affinity and the size of the intercalating species. Si has also been explored as negative electrode material[27]. Lithiation of silicon leads to a reduction in the strength of Si-Si bond and the continuous Si-Si tetrahedral network breaks down as a result of formation of Si-Li bonds[27]. This is accompanied by reduction in strength properties of silicon and the appearance of brittle to ductile transition in silicon. DFT calculations have shown that lithium prefers to occupy tetrahedral sites in Si network. DFT studies on lithium intercalation in Si nanowires have also been carried out[88]. The fast lithium transport in Si nanowires has been attributed to high surface area to volume ratio in nanowires. Computational studies on anode materials for lithium ion batteries have been extensively reviewed by Wu et al.[89] and Bhatt et al.[27].

In a series of related works, Koh et al.[90-93] used DFT to study the mechanism of Li adsorption on carbon nanotube (CNT) –fullerene hybrid system[90] and obtained lithium adsorption energies[91] on CNT-C_{60} hybrid systems as well as on pristine CNTs[91]. They found that Li adsorption on hybrid system was more favorable than that on pristine CNTs [90]and attributed it to high electron affinity of C_{60}. In addition, they have also obtained the HOMO and LUMO levels[90] for the CNT-C_{60} hybrid system for adsorption of multiple number of Li atoms on the hybrid system. They have also studied Li adsorption on graphene-fullerene nanobud system[92] as well as on graphene-fullerene nano-hybrid system[93]. They have calculated the binding energies for adsorption of multiple number of Li atoms on the graphene-fullerene nanobud[92] and hybrid system[93] and obtained their band structure and other electronic properties. While their work gives quantitative insight into the mechanism of Li adsorption on such systems and is quite useful in this regard, it

does not address the electrochemical aspects of these systems. A study on the electrochemical properties of nanobud and hybrid systems will be a good complement to their lithium adsorption investigation.

Summarizing, DFT has been extensively used to model electronic and atomic structures as well as their various manifestations such as response to doping and phase stability in Li ion batteries. Such studies are able to provide quantitative information on driving forces and activation barriers for atomistic interactions. However, systematic DFT studies on the electrochemical properties of fullerene based materials are quite limited.

While the effects of atomistic interactions can be measured in experiments, it is *only* through computational chemistry techniques such as DFT that a coherent understanding scheme can be constructed for these atomistic phenomenon; the averaged effects of these phenomenon being manifest and recorded in experiments. Hence, such studies provide insight for designing better materials for battery applications.

2.2 Atomistic level studies on Li ion batteries

DFT is computationally expensive and is limited to a couple of hundred atoms at most. It cannot be used to simulate a system consisting of even a few thousand atoms or to obtain information about the large scale atomic arrangement such as that obtained from radial distribution function and structure factor. While DFT can give useful information at the electronic scale, a large class of experiments measure average behavior over several hundred atoms. Molecular dynamics is quite suitable to such spatial scales. Besides, MD can be used to easily obtain temporal evolution of the system over several nanosecond timescale.

Molecular dynamics (MD) has been used to study the transport[94], structural[95] and interfacial properties[96] of electrolytic phase in Li ion batteries. Since these properties are obtained from representative systems consisting of several thousand atoms, DFT is not suitable for such studies because of the high computational cost associated with simulating systems of this size. Xing et al.[95] investigated the structure of several compositions of mixed solvent electrolyte, tetramethyleme sulfone/dimethyl carbonate, in close vicinity of the electrode surface, as a function of applied potential. They found[95] that charging the electrode has a profound effect on the adsorption and orientation of the electrolyte on the electrode surface. Based on changes in local coordination number of Li ion obtained from MD simulations, they were able to obtain profiles of distribution of electrolyte components[95] in different solvation shells of Li^+. They also obtained electrode double layer capacitance for electrolyte/electrode system which was found to be in the range of experimental values reported in literature

Marquez et al.[94] used MD simulations to study lithium ion diffusion coefficient, electrolytic structure, staging phenomenon and double layer formation at graphite-electrolyte interface as a function of lithium content. The electrolyte phase consisted of $LiPF_6$ dissolved in a mixture of ethylene carbonate and propylene carbonate. Inter-particle interactions were modeled using universal force field. Radial distribution function (RDF) was used to characterize the local distribution of phosphorus and fluorine atoms around lithium. RDF analysis showed well defined peaks for phosphorus and fluorine distribution around lithium ion indicating that atoms are arranged in anion-cation pairs. The distances between lithium cations and phosphorus/fluorine anions were in agreement with the optimized structures of $LiPF_6$ obtained using DFT. The computed

average interlayer spacing of graphite sheets, as a function of Li content, was found to be in agreement with the experimental results.

The accuracy and reliability of the information obtained from a molecular dynamics simulation is strongly dependent on the force field used to model the interactions between the species. One of the key inputs and challenges for molecular dynamics based atomistic simulations is the development of a reliable force field to accurately model interactions between the constituents of a model system. Electrolyte materials, owing to the presence of ionic species, present challenges in this respect since the underlying force field should be able to account for the polarizable nature of the ionic species when subject to an electric field. Borodin et al.[97] have developed a many body polarizable force field to accurately model ionic species in electrolytic environments existing in batteries. Molecular dynamics simulations performed on 30 ionic liquids using their force field[97] showed that the computed heat of vaporization, ion self- diffusion coefficient, conductivity and viscosity were in good agreement with the experimental data. This validated the force field parameters and functional forms. Borodin et al.[98] used a variation of this force field to model lithium ion transport in dilithium ethylene dicarbonate (Li_2EDC). The conductivity of Li_2EDC obtained from MD simulations in this study[98] was found to be in good agreement with the experiment. The force field allowed the effect of polarization on transport to be investigated[98]. It was found that the neglect of polarization in the force field led to slower diffusion rate[98] and a higher activation energy for diffusion in the simulation compared to when the polarization was switched on.

In addition to transport and structural properties, molecular dynamics has also been used to model the mechanical behavior of batteries[99]. An understanding of the

mechanical behavior of batteries is important since phase transitions, thermal effects and intercalation phenomenon lead to dimensional changes which would introduce stresses in the system and affect the structural integrity, performance and lifetime of a battery. Lee et al.[99] performed MD simulations and obtained the elastic constants of $Li_xMn_2O_4$ as a function of lithium concentration, x. The analysis of elastic constants showed that elasticity resulted from the three main contributions to the stress tensor: kinetic energy, long range coulomb and pair interactions. While the kinetic and coulomb contributions were almost unaltered with changing lithium content x, the pair contribution was observed to be sensitive to the state of discharge. It was observed[99] that the stress contribution resulting from Mn^{+4} and O^{-2} pair interaction was the dominant interaction at low doping levels. At high doping levels, Mn^{+3}/O^{-2} and Li^{+}/O^{-2} interactions were dominant[99].

Based on our survey of literature, we found that the atomistic simulation studies on Li-ion batteries are quite limited and are focused mainly on the structure and diffusion in solid electrolyte interface[100] (SEI), a transition layer in the immediate vicinity of electrode. Agubra [101] has reviewed literature on the formation and stability of SEI on graphite anode. From the kinetic perspective, a very limited number of studies on the Li-C_{60} system have been reported. For example, Tachikawa[102-104] has used ab-initio MD to study the kinetics of lithium diffusion on C_{60}. Although important in their own right, owing to the limitations on the computational resources needed for DFT, ab-initio MD cannot substitute for atomistic MD simulations.

In conclusion, molecular dynamics, in its own right, can be seen as a technique to average over the electronic effects modeled by DFT. MD is also useful since it can act as

a bridge between the DFT simulations and continuum level modeling in the multi-scale modeling framework.

2.3 Continuum level studies on Li ion batteries

Although a majority of chemical processes involve redox reactions, a battery is a special type of chemical system because in contrast to normal molecular reactions, charge transfer in batteries occurs over macroscopic distances. Because macroscopic distances are involved, at least for charge transport, continuum level studies of batteries are quite natural. Secondly, electrochemical experiments which are carried out using instruments such as voltmeters and ammeters are closely tied to continuum level simulations of batteries. Potentials and currents, as measured in electrochemical experiments, are respectively measures of the driving forces and rates of the underlying electrochemical reactions which power the battery. Such electrochemical measurements, therefore, correlate the battery performance, an engineering viewpoint, to driving forces and reaction rates, a chemistry viewpoint. Thirdly, the actual usage of batteries, at systems level, is modeled by continuum level simulations[24]. These continuum level models[24], formulated in terms of currents and voltages, simulate those aspects of batteries which are experienced directly by a commercial user on a day to day basis[24]. The modeling of such continuum level phenomena is, therefore, important to gain insight into performance of batteries from the application side.

Thermodynamics, mass transport in electrolyte, electron transfer kinetics at the electrode surface, heat transport, electrostatics and interfacial phenomenon[105-107] are usually the major factors in macroscopic electrochemical systems. These phenomena are described using partial differential equations, which are coupled to one another, requiring a multi-physics approach[108]. The imposition of physical conditions such as

microelectrode environment in experiments, translate into boundary conditions for mathematical models[109]. In addition, measurements made in experiments also provide empirical relationships between the physical quantities of the mathematical models e.g. for modeling a cell sandwich, an expression for the over-potential and its parameters is required and is obtained from experimental measurements[24].

The modeling of these coupled phenomena in batteries has been extensively carried out by Newman and coworkers[24]. Their work on porous electrode theory[20], concentrated solution theory as applied to batteries[24, 110] and the finite difference method approach which is based on implicit Crank-Nicolson method for solving the coupled ODEs in the context of batteries[111, 112] forms the basis of large number of continuum level simulations in this area. A brief description of porous electrode theory[20], concentration solution theory[110] and the numerical technique[111] for solving coupled ODEs will now be provided.

A nonporous electrode consists of a plane, well- defined, sharp interface between the metal electrode and the underlying electrolytic solution. However, the rate of the reaction at the electrode surface can be significantly increased by using a porous electrode. A porous electrode[20] consists of a porous matrix of a mixture of active non-conducting material and an inert conducting material in which the pores are fully infiltrated by the electrolyte. For example, the active material could be TiS_2 or a lithium metal oxide that can intercalate lithium and the inert conducting material can be carbon particles which are introduced to increase electrical conductivity. The electrolyte can be a solution of a binary electrolyte in a polymer, which acts as a solvent for the binary salt, for example, lithium trifluoromethane sulphonate salt in polyethylene oxide polymer[24].

The increase in reaction rate comes from the increased surface area per unit volume of the porous electrode relative to a simple metal electrode. In the porous electrode theory[20], the geometric details of the porosity are neglected and the electrode is characterized by spatially averaged quantities such as the average fraction of pores in the electrode. The detailed structure of the heterogeneities is neglected and the electrode is treated as a continuum. Two separate potentials Φ_1 and Φ_2 are defined, one for the matrix and other for the electrolytic phase in the pores respectively. Similarly, two current densities, i_1 and i_2 are defined, corresponding to the matrix phase and the electrolytic phase respectively[24]. Charge conservation is enforced by requiring that the total current density entering into the electrode phase from the electrolytic phase, i, is equal to the sum of charge densities in the matrix phase and the electrolytic phase (infiltrated into the pores) of the porous electrode, i_1+i_2. The equations of the porous electrode theory for the charge transport in porous electrode are have been formulated by Newman for one dimensional transport and used extensively in battery modeling[24].

The multicomponent mass transport of ions in the electrolyte phase can be modeled using either the dilute solution theory[113] or the concentrated solution theory[24]. In the dilute solution theory, the fluxes are governed by Fick's law. The dilute solution theory only considers the interactions between the solute and the solvent. In the concentrated solution theory, which is based on Stefan-Maxwell equations[110, 114], the driving forces for diffusion are expressed in terms of the combination of fluxes of *all* the components in the solution. For electrolytic solutions, even in dilute regime, Fick's law does not provide an adequate description because of the long range interactions between the diffusing species[110]. For ideal mixtures, the Fick's law is replaced by the Stefan-

Maxwell equation[110] which expresses driving forces in terms of the fluxes of the component species. However, these equations are coupled. These coupled equations can be inverted and put in a form similar to Fick's law. This is the form in which they are used in modeling transport phenomenon in analogy to Fick's law. Stefan-Maxwell equations have been generalized to non-ideal case[115, 116] and for modeling thermal diffusion[117-119]. Newman has presented solution to Stefan-Boltzmann equations for several model problems of engineering interest[110].

The equations for electrode kinetics describing a porous electrode and for mass transport in electrolytes using concentrated solution theory are coupled differential equations that need to be solved simultaneously subject to specified initial and boundary conditions. The method, as implemented in BAND(J) subroutine[120] developed by Newman and coworkers[111, 120], for solving the coupled differential equations for modeling batteries has been extensively used in its original[121, 122] and modified form[120] in literature. The method was developed originally for coupled non-linear ordinary differential equations and uses finite difference approximation and the implicit Crank-Nicolson scheme[120], to convert a set of coupled differential equations to non-linear algebraic equations. The non-linear algebraic equations are solved using the Newton-Raphson procedure. The method can also be used for solving coupled PDEs by first converting them to coupled ODEs.

All of the above described three constituents, the porous electrode theory, the concentrated solution theory and the BAND(J) subroutine were developed over a span of about 30 years and brought together in a coherent manner in the seminal work by Newman and coworkers[24] on the modeling of the charge and discharge of the Li-ion

battery[24]. The ideas discussed in this work[24] form the basis of numerous other works on modeling Li-ion batteries in their original and modified form[123-125]. Consequently, this work will be described in some detail. The model presented in this work[24] simulates a full cell sandwich consisting of a lithium anode, a solid polymer electrolyte containing a binary salt and a composite porous electrode. Temperature is an input parameter in the model but temperature effects on the material properties of the cell components are neglected. Film formation at the electrode-polymer interface is also neglected. Porous electrode theory is used for composite cathode which is assumed to be a continuum. The electrolyte is modeled using concentrated solution theory and mass transport in the electrolyte is characterized by the transference number of lithium ions, the diffusion coefficient of the Lithium ion and the electrical conductivity of the electrolyte. Lithium insertion in intercalating cathode is modeled using superposition. Although it is a simplified model[24] in the sense that it does not take into account the temperature effects and the interfacial phenomenon at the electrolyte-electrode interface, the model[24] captures the core electrochemical aspects of transport and discharge of active ionic species in a Li ion battery. The model is able to predict the evolution of cell potential as a function of average utilization of cathode for different charge and discharge rates. Based on the predictions of this model, several optimization strategies for maximizing cell performance can be inferred[24].

$LiFePO_4$ has also been demonstrated as promising intercalation materials for Li ion batteries[5]. These materials differ from conventional active materials such as TiS_2 in that they undergo a phase change as lithium is intercalated in the material. Shrinking core model[126-128] has been used to model the moving phase boundary and incorporate this

phenomenon in mathematical models of Li ion batteries. Figure 6 shows[129] a schematic representation of the shrinking core model.

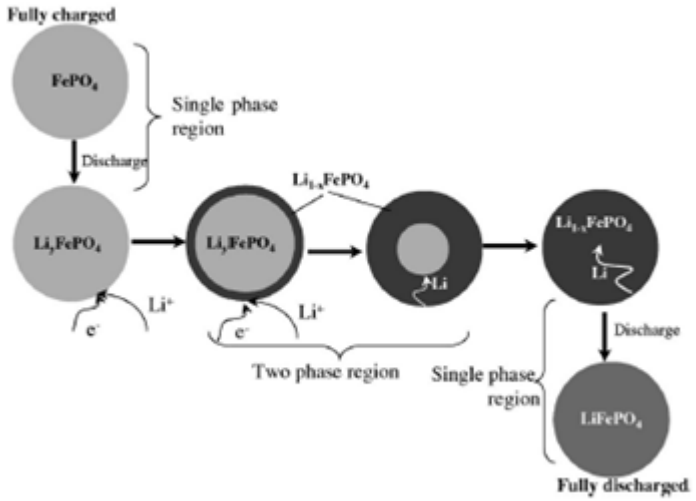

Figure 6: Schematic representation of the shrinking core model showing the formation of lithiated phase on the boundary and the gradual progression of the phase boundary towards the center. (source of graphic: Srinivasan et al.[129])

Srinivasan et al.[129] have incorporated the phase transition behavior observed in lithium iron phosphate cathodes in the porous electrode theory and were able to predict the cell potential as a function of charge capacity for different current densities. This model can be viewed as an extension of cell sandwich model in Doyle et al.[24], extended to incorporate phase transition in active cathode material.

Ferguson et al.[130] have presented a generalization of porous electrode theory to non-ideal active materials based on non-equilibrium thermodynamics. Unlike other models, which require open-circuit potential, exchange current and diffusion properties to be obtained from an empirical fit and then input into the model, in the model of Ferguson et al.[130], these quantities relate to and emerge from the underlying physics incorporated into this model. A generalization of Butler-Volmer equation[131] that is applicable to both

conventional active materials as well as to active materials undergoing phase transition is presented. Their formulation incorporates Cahn-Hilliard based phase field models[132] for simulating phase change in lithium transition metal oxide cathodes.

Because of space and time constraints, it is not possible to give an exhaustive discussion of all the continuum level battery models and so a few excellent review articles will be cited. Gomadam et al.[133] have presented a detailed review of the strengths and drawbacks of various mathematical models for lithium ion and nickel battery systems. They observe that a large number of battery models incorporate several simplifying assumptions such as the neglect of volume changes and side reactions occurring during battery operation, the constancy of transference number and diffusivity during the operation of battery and the assumption of spherical active intercalation particles. These assumptions are also inbuilt into the work of Newman and coworkers[24]. Botte et al.[134] have reviewed several mathematical models used for secondary lithium ion batteries. Different mathematical models that capture the electrochemical as well as the thermal aspects of secondary lithium ion batteries have been discussed[134]. Multiple discretization schemes and numerical approaches to solving the governing equations have been discussed by Botte et al[134]. Inferring that most of the current battery models are one dimensional, the review stresses the need for a mathematical model of batteries that includes detailed material and energy balances in a three dimensional framework. The review also acknowledges the importance of ab-initio and molecular level simulations in understanding the mechanism of lithium intercalation in li ion battery cathode.

To summarize, while DFT and MD can provide atomic and molecular level insights into the workings of batteries, the actual usage of batteries is modeled by

continuum level simulations. DFT and MD studies can be used to provide input parameters for continuum models in a cost effective manner, without resorting to experiments at least in the preliminary stages of modeling. DFT, MD and continuum level simulations are needed in conjunction to provide a full spectrum view of a system as complex as a battery.

2.4 Electrochemical studies on Carbon-Based Materials

Chabre et al.[135] have used cyclic voltammetry to study the electrochemical intercalation of Lithium on C60. The voltage vs. current curve showed well defined reduction peaks. On integrating the voltage vs. current curve, they were able to attribute the peak positions to the formation of Li_xC_{60} where X =0.5, 2, 3, 4 and 12 respectively corresponding to the reduction peaks (vs. Li) at 2.3 V, 1.9 V , 1.5 V, 1.0 V and 0.8 V. The relaxation rate of the current was found to be sluggish which meant slow diffusion in the system which is characteristic of a solid state intercalation process. Synthesis of other alkali metal fullerites such as K_xC_{60}[136] and Rb_3C_{60}[137] through wet synthesis has also been reported. However, as Chabre et al. [135] have pointed out, in the case of K and Rb, only the peaks corresponding to X=3 and 4 have been observed. One possible reason can be the large size of K and Rb which causes steric hindrance for intercalation on fullerene. In addition, the intercalation of Li in C_{60}, as reported by Chabre et al.[135] , is a solid state process and utilizes a polymer electrolyte. Since polymer electrolytes are more stable and less corrosive than liquid electrolytes, their work demonstrated the experimental feasibility of using C_{60} and C_{60} based materials as possible electrode materials.

Yokoji et al.[138] have studied electron-deficient benzoquinones using cyclic voltammetry for possible applications as cathode materials. Perfluoroalkyl groups, with a

strong tendency to attract electrons, were used to generate electron deficient benzoquinone. They demonstrated experimentally that electron-deficient benzoquinones showed higher cell voltage compared to electron-rich benzoquinone due to the presence of electron withdrawing functional group in the molecular structure. This is an important advancement as it illustrates an important design principle for synthesizing new promising organic cathode materials, namely, functionalize with an electron withdrawing functional group. We have investigated such materials in this work.

Kim et al.[23] have used density functional theory to study the electrochemical and thermodynamic aspects of lithium adsorption on quinone derivatives. Their computation results showed that the presence of electron withdrawing functional groups can be used to selectively modify the properties of quinone derivatives, an effect also demonstrated by Yokoji et al.[138] experimentally. They also investigated the most favorable binding sites for lithium adsorption on quinone derivatives and studied the effect of Lithium adsorption on the discharge potential of the battery.

Lee et al.[139] have demonstrated the design and fabrication of high energy and power density battery device based on carbon nanotubes functionalized with oxygen containing functional groups[140]. They constructed a carbon based electrode with reversible gravimetric capacity (per gram of electrode) of ~200mAh and power density of ~0.1kW with a lifetime of several thousand cycles[139]. The device had a power density which was one order of magnitude higher than commonly use Li-ion battery technology and within the range of electrochemical capacitors. The high energy density was attributed to the presence of faradaic reaction[139] between the adsorbed Lithium ions and the functional group used to functionalize the CNT surface. Similar enhancement in

properties was reported for composite electrodes composed of Graphene Oxide and functionalized CNTs[140]. Their work[139, 140] demonstrated that higher properties can be obtained for the Li-ion battery system by functionalizing carbon based materials and utilizing the Faradaic reaction. Coupled with the low cost and almost limitless supply of carbon based materials, this was a very important development in the search for novel electrode materials. Several other studies[141] have demonstrated the beneficial effect of oxygen containing functional groups[142-144] and nitrogen[145-147] on CNTs and graphene.

Burkhardt et al.[148] have studied the redox properties of small organic molecules functionalized with violene cations as redox active sites on conducting polymers. Based on this study[148], they have formulated a set of empirical rules for quick screening of promising electrode materials. Their computational studies showed that molecular structure has a profound effect on the electrochemical properties of the molecule. They found that the electrode potential is quite sensitive to the type, number and specific position of the heteroatom on the molecule and the redox properties can be tailored by controlling these aspects. Their work demonstrates[148] that significant changes in redox potentials can be obtained through the presence of specific heteroatoms in the structure. Pseudo-capacitance[141, 149] in carbon based materials has also been studied in activated carbons[149] and other nanostructures.

Liang et al.[150] have presented an exhaustive review of organic electrode materials for Li ion batteries. Xie et al.[151] have reviewed positive and bifunctional organic electrode materials in addition to organic anode materials in their work.

Based on a review of literature, we observe that fullerene based materials, for which the basic raw material is carbon which is abundant in nature, have not been investigated systematically for their electrochemical aspects. In this work, we will investigate fullerene based materials for electrochemical applications. In the next chapter we outline the rationale and objectives of this study.

CHAPTER 3

OBJECTIVES

Based on the survey of literature in the previous chapter, it is concluded that electrode materials have been the subject of extensive study, both at electronic and atomistic level. Such studies have focused either on developing new materials or on understanding the mechanism of working of existing materials and using this insight to design better electrode materials. The experimental design of new materials for electrode applications is an expensive process owing to the large search space that needs to be explored. The design process is also quite tedious and intrinsically random unless some promising direction for synthesis is indicated in advance by computation. For example, a computational study may indicate that an envisioned electrode material is thermodynamically improbable and save the experimentalists months of resources in trying to synthesize it. Besides, some advanced information on the redox properties of an envisioned electrode material can indicate a promising direction which the synthesis process can take, thereby saving time and expenses. Computations can also reveal useful trends in the structure-property relationship paradigm which may not be accessible from experiments alone. *In this work, therefore, we will use computation to investigate novel electrode materials*.

Because currently used anode materials have a higher storage capacity for Lithium than cathode materials[152], one of the main factors limiting the performance of present day Li ion batteries is the upper limit on the amount of Lithium that can be intercalated at the cathode[152]. This upper limit is determined by the crystal structure of

the cathode material which is fixed once the cathode material is chosen. Therefore, new cathode materials are being explored actively[152, 153]. Besides, Nickel and Cobalt based materials, which are currently in use are costly, environmentally toxic and strategically scarce[3, 6]. Carbon, which is the main raw material for carbon based electrodes is relatively inexpensive, environmentally friendly, easily available and abundant in nature. Besides, in the light of recent advances in making high energy and power density electrodes using carbon based materials[139, 144] , they appear promising and worthy of further exploration.

There are large numbers of carbon based materials. So, based on our understanding of electrochemistry and chemical intuition, the search space had to be narrowed down with battery applications in mind. The energy density of the battery is determined by cell potential and for a given anode material the cell potential is determined by the redox potential of the cathode[152]. For a high cell potential, it is desirable to have an anode with a highly negative redox potential and a cathode with a highly positive redox potential. It is the molecular structure that determines the redox potential of electrodes[68] which in turn determines the working voltage of the cell and hence the energy density. Fullerene is known to have high electron affinity[154] and it is anticipated to have a high positive redox potential, a very desirable attribute for a promising cathode material.

Fullerene materials are a relatively recent discovery[155] and have novel electronic and structural properties[155] along with high stability[156]. They are also amenable to tailoring to specific needs owing to the presence of carbon-carbon bonds, which are known to have a rich chemistry[13], and the possibility of on-cage[157] and endohedral

doping[158]. Fullerene materials are being actively explored for functionalization[159-161] and doping[162, 163] with various adducts and the synthesis of newly functionalized, fullerene based materials is being continuously reported in literature[161]. Batteries have traditionally been devices with high energy densities but low power densities[139]. Ideally, a device with a high energy *and* power density is desirable. Working devices fabricated from carbon based materials such as carbon nanotubes and graphene, with high energy and power density have already been demonstrated[139]. In these devices, the high energy density coupled with high power density has been attributed to electron transfer due to the presence of oxygen containing functional groups[139, 140]. The ability to functionalize fullerenes with various functional groups and dopants in multiple ways when coupled with the high positive redox potential of fullerene, is therefore a desirable attribute. It is anticipated, based on chemical intuition, that similar electron transfer processes may be accessible in fullerene. In this work, the stability, thermodynamic, electrochemical and electronic aspects of fullerene based materials, as they relate to their possible applications in batteries, will be studied.

From the thermodynamics and electrochemical point of view, we will study the redox and electronic properties of three classes of functionalized, fullerene based materials. The first class of materials that will be investigated are pristine fullerene functionalized with oxygen containing functional groups (OCFGs) namely, hydroxyl (-OH), carboxylic (-COOH), epoxide(-O-) and aldehyde(-CHO). Yokoji et al.[138] have experimentally demonstrated that functionalizing a material with a strongly electron withdrawing functional group (SEWFGs) creates electron deficiency in the parent chemical structure resulting in a higher redox potential[138]. Therefore, we have also

investigated the effect of functionalizing fullerenes with SEWFGs, namely, trifluoride (-CF_3), cyano (-CN), nitro(-NO_2) and sulfonate (-SO_3H). *This group of materials i.e. fullerene functionalized with OCFGs and SEWFGs will be designated as Series 1.*

We will also explore the electrochemical and electronic properties of fullerene doped with various elements, $C_{59}X$ (X=B, N, S, Si and P) to search for interesting electrochemical properties and trends in electronic properties across a period and down the group. *This group of materials will be designated as Series 2.*

In *Series 3*, the combined effect of functionalization and doping on the electronic and electrochemical properties of fullerene based materials will be investigated. The *first material system to be investigated in Series 3* would be nitrogen doped fullerene[164], $C_{59}N$, functionalized with abovementioned OCFGs and SEWFGs. The effect of functionalizing $C_{59}N$ with OCFGs and SEWFGs at the ortho, meta and para position relative to nitrogen atom, on the electrochemical and electronic properties of $C_{59}N$ will be explored. We will also explore the effect of doping C_{60} with multiple nitrogen atoms, i.e., $C_{58}N_2$ for ortho, meta, para and dispersed position of two nitrogen atoms on the hexagonal face of C_{60}. $C_{57}N_3$ will be explored for dispersed configuration of nitrogen atoms on the fullerene cage. The *second material system to be studied in Series 3* would be boron doped fullerene[165], $C_{59}B$, functionalized with OCFGs and SEWFGs. The effect of functionalizing $C_{59}B$ with OCFGs and SEWFGs at the ortho, meta and para position relative to boron atom will be explored. The effect of doping C_{60} with multiple boron atoms, i.e., $C_{58}B_2$ for ortho, meta, para and dispersed position of two boron atoms on the redox potential will be investigated.

Materials in Series 1 were chosen since fullerene is known to be a material with relatively high electron affinity[93, 154] and the addition of OCFGs and SEWFGs is expected to enhance this tendency. Oxygen containing functional groups have also been experimentally demonstrated to participate in electron transfer processes responsible for high energy and power densities in CNT based devices[139]. The functional groups chosen for the functionalization of fullerene are the fundamental functional groups of organic chemistry and their effects on the redox properties in other carbon based electrode materials has already been investigated[23]. Material with one OCFG/SEWFG moiety attached to fullerene will also give insight into the effect of attaching multiple moieties to fullerenes, and several of these materials with multiple hydroxyl[166]and carbonyl groups[167] have already been synthesized.

Materials in Series 2 were chosen to address a very interesting question: What will be the effect of on-cage doping of C_{60} with elements, which are close to carbon in the periodic table, on the redox potential of fullerene? The addition of one dopant atom, which is close to carbon in the periodic table, to C_{60} is not expected to drastically change the structure, and so based on chemical intuition, it is expected that the resulting molecules will give atleast the properties of C_{60} or may be better. This would also help us discern useful trends, if any, to intelligently design new materials. To the best of our knowledge, no systematic study on the redox properties of fullerenes with the abovementioned functional groups and dopants has been carried out.

Materials in Series 3 were chosen to study the combined effect of functionalization and doping with high electronegativity species, such as nitrogen atom, on the redox properties of fullerenes. The interesting questions that we aspired to

investigate were: Do functionalization and doping have a synergistic effect or do they nullify one another? Quantitatively, how are the redox potentials for C_{60} affected when doping and functionalization are harnessed together? Based on our chemical intuition, the presence of nitrogen dopant on the fullerene cage is expected to further enhance the electron attracting tendency of fullerene. On-cage nitrogen doped fullerene materials[164] have already been synthesized and can act a base material for adding functional groups. The study of redox properties of nitrogen-doped-fullerenes with OCFGs and SEWFGs is a novel design idea and we have not come across any systematic experimental or computational study on the redox properties of such materials. In *Series 2*, we had investigated $C_{59}X$ (X=B, N, S, Si and P) to look for interesting electrochemical properties and trends in them as we move across/down the periodic table. Based on our DFT calculations on materials in *Series 2*, it was observed that doping C_{60} with B i.e. $C_{59}B$ gave a redox potential that was about 50 percent higher than pristine fullerene. *This is an example of computation helping in the search and design of novel materials with interesting properties*. Besides, $C_{59}B$ has already been synthesized[165]. So, the material exists but it has not been studied for its electrochemical properties in a systematic manner. Since our computations showed that $C_{59}B$ is an intrinsically high positive redox potential material, we were interested in investigating the effect of functionalization of $C_{59}B$ with OCFGs and SEWFGs and inquire if they can act synergistically. Based on the interesting redox potentials obtained by doping fullerene with one boron atom, it was natural to investigate the effect of doping fullerene with two ($C_{58}B_2$) and three atoms ($C_{57}B_3$) respectively

The accumulation of lithium at an electrode results in a decrease in cell potential[23, 135] with continued operation of the battery. This degrades performance of the battery. Based on previous studies of lithium adsorption on quinone derivatives[23], it is expected that the electron affinity of pristine fullerene will decrease with increasing adsorption of Li on C_{60}. Therefore, in addition to studying the redox properties of above three classes of materials in this work, the effect of lithium on the redox properties of pristine fullerene will also be investigated[168-170].

In this study, Fullerene is the base material from which other materials are derived by functionalization and/or doping. In all of these materials, we are interested in the tendency of the material to accept electrons. Different charge states for pristine fullerene have been reported in literature[171, 172]and fullerene is known to act as a buffer for electrons[173]. This begs an important question: What is the maximum electron adsorption capacity of pristine fullerene both in vacuum and in the presence of electrolyte? Could the presence of electrolyte, in the battery environment, stabilize a highly charged fullerene anion which may otherwise be unstable in the vacuum? In order to answer these questions, we will also investigate the electrochemical and electronic properties of highly reduced states of fullerene anion.

To summarize, the redox properties of three classes of materials *Series 1, Series 2* and *Series 3* will be studied using DFT. This will give quantitative information about the electrochemical and thermodynamic aspects of fullerene based electrode materials. Specifically, the study of the redox properties of abovementioned materials will help discern as to which functional groups and dopants are effective in improving the electrochemical properties of fullerene based materials. In this study, the geometry

optimized structures, converged wavefunctions and orbital energies of various fullerene based materials will be computed from which other electronic, structural and bonding properties of these materials can be obtained. For example, activation energies for diffusion[174], polarizabilities[175] and dielectric constants are important inputs for continuum level modeling and design[24] of Li-ion batteries and can be obtained from converged wavefunctions. Thermodynamic functions such as heat capacity, enthalpy and entropy which are required for thermodynamic modeling of C_{60} based Li-ion batteries will be obtained in this study. The converged structures and wave functions obtained in this study will also be the starting point for other computational studies such as the effect of electrolyte and operating conditions on the newly designed electrode materials. Interaction energies for C_{60}-Li system, that is the energies of interaction between C_{60} and Li for different number and configurations of Li on $C_{60,}$ will be computed in this work . This would be an essential input for developing, training and testing a reliable force field for molecular dynamics (MD) based atomistic simulations of C_{60}-Li system. To the best of our knowledge and information, an accurate and reliable force field to model C_{60}-Li interactions has not been developed till date. It is also expected that this work would lay the ground work for future studies on the electrochemical aspects of fullerene based materials which are functionalized with more complex functional groups.

In the next chapter, the simulation methodologies that are used in this work to study the electrochemical and electronic properties of fullerene based materials will be briefly described.

CHAPTER 4

SIMULATION METHODOLOGY

Li-ion batteries are complex systems with multiple aspects which manifest at different spatial and temporal scales. These aspects are coupled, e.g. phenomena at the electronic and atomic level determine what is observed subsequently at the molecular scale and this determines the continuum level behavior. This bottom up multi-scale simulation paradigm, in which information is shared across scales, is shown schematically[176] in Figure 7 .

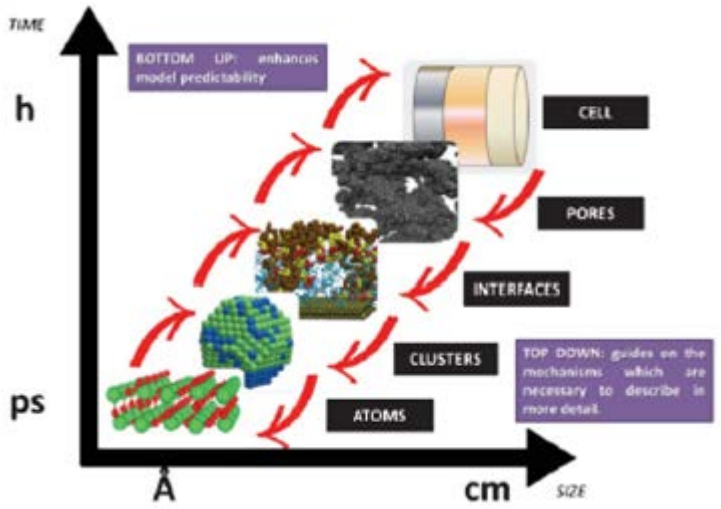

Figure 7: Schematic representation of a bottom up simulation paradigm **(**source of graphic**:** Franco[176])

The behavior at any length scale is determined ultimately by quantum interactions at the atomic scale, and in principle can be predicted solely using quantum mechanics based modeling. In practice, owing to the limitations of computational resources and the way computational requirements scale with increasing number of atoms[177], quantum

mechanics based modeling is limited to a few hundred atoms at best. Besides, from the experimental point of view, only the spatially and temporally averaged behavior of a collection of atoms is accessible. Consequently, the behavior of a single atom, in a collection of one mole of atoms or higher, is not of much interest even if it could be computed. This has necessitated the development of different methodologies which correspond to different time and length scales as shown schematically[178] in Figure 8.

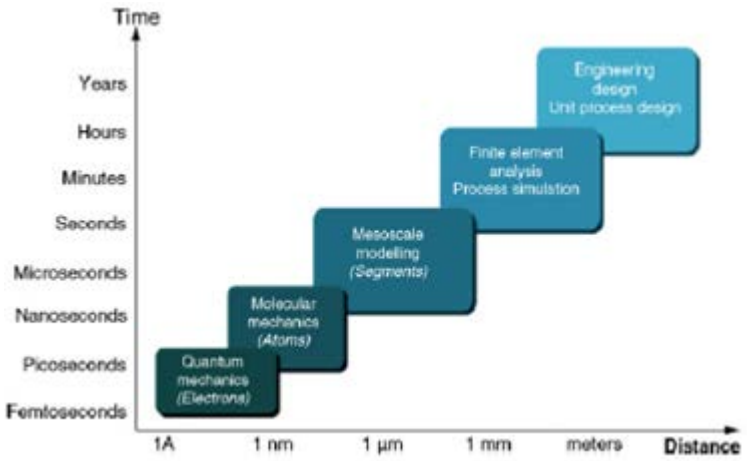

Figure 8: Simulation methodologies at different temporal and spatial scales (source of graphic: Fermeglia et al.[178])

The focus of this work is to use density functional theory[17] (DFT) to study the electrochemical and electronic structure aspects of fullerene based electrode materials for Li-ion battery applications. A brief description of the simulation methodologies used in this work will be provided in the subsequent sections of this chapter.

4.1 Density Functional Theory (DFT)

The motivation behind DFT[179] is that the description of a system of N particles in three dimensions requires the specification of wave function which is a function of 3N

independent variables, neglecting the spin degrees of freedom. For a small molecule such as water, this will give rise to a wave function which will be a function of 39 variables (30 degrees of freedom for the electrons and 9 for the nuclei). Even if the Born-Oppenheimer approximation[180] is invoked and motion of the nuclei is neglected, the wave function is still a function of 30 variables which presents a challenging problem. Any increase in the number of atoms further increases the number of independent variables and increases the complexity of the problem. The basic idea underlying density functional theory (DFT), as formulated by Hohenberg and Kohn[179], is that the ground state density $n(\mathbf{r})$ uniquely determines the external potential v, for any system of interacting particles in an external potential[179]. Conversely, two external potentials, $v^a(\mathbf{r})$ and $v^b(\mathbf{r})$, cannot result in the same ground state density $n(\mathbf{r})$ if they differ by more than a constant[179]. Since the external potential determines the Hamiltonian and hence the wave function of a system of interacting particles, if follows that **any** property of a system of interacting particles, to the extent that it is determined by the wave function, is determined from the knowledge of ground state particle density[179]. Since ground state density is a function of 3 variables and continues to be so even with the increase in the number of particles, the consideration of ground state density as a basic variable which determines all the properties of the system, makes the problem significantly simpler. The validity of this postulate, based on proof by contradiction[179], was first presented by Hohenberg and Kohn[179].

The Hamiltonian[54, 181], H, for calculation of electronic structure can be written as

$$H = T_e + T_n + V_{ee} + V_{en} + V_{nn} \tag{1}$$

Here, T_e is the kinetic energy of interacting electrons, T_n is the kinetic energy of nuclei, V_{ee} is the electron-electron interaction for the interacting electrons and includes correlation effects, V_{en} is the interaction of electrons with nuclei and V_{nn} is the coulomb interaction between the nuclei. The term V_{en} is the energy term that accounts for the external potential. Owing to their large mass, compared to the electrons, the motion of nuclei is sluggish at the time scales of interest for electronic structure calculations. Hence, the Born-Oppenheimer[54, 180, 181] approximation can be invoked and the term T_n can be neglected. Equation (1) can be written as

$$H_{HK} = T_e + V_{ee} + V_{en} + V_{nn} \tag{2}$$

where H_{HK} denotes Hohenberg-Kohn Hamiltonian. Hohenberg and Kohn[179] also showed that the ground state energy of a system of interacting particles can be formulated as a universal functional of the ground state electron density, independent of the external potential. In the context of molecules and solids, the specific form of external potential results from the position and charges of the nuclei forming the molecule and/or solid. In general, the different functional forms of the particle density will yield different values of energies when substituted into the universal functional[54, 181]. Of all the energy values that can be obtained from this functional by using different expressions for ground state particle density, the true ground state energy would be the minimal value and the function $n(\mathbf{r})$ which minimizes the energy functional will be the correct ground state particle density. The form of the functional is universal in the sense that it is independent of the number of particles and the externally applied potential. Hohenberg and Kohn[179] do not

specify the detailed form of this functional but postulates the existence of such a functional. From the point of view of actually computing numbers with this theory, the form of functional or an approximation to it is needed and that is the content of Kohn and Sham[17] (KS).

Kohn and Sham[17] constructed an ansatz[181] and mapped the problem of many-body interacting particles to a system of non-interacting particles so that the interacting particle problem can be solved using the independent particle techniques. This ansatz[17] is the foundation for the development of a numerical method for solving the Schrodinger wave equation for multi-body interacting system. Consequently, the basic postulates of DFT as presented by Hohenberg and Kohn[179] along with the numerical scheme that is spawned by Kohn and Sham[17] has been collectively called DFT in literature.

In the Kohn and Sham[17] formulation of approximation scheme for DFT, the system was composed of non-interacting particles having the same ground state density as the original system. By Hohenberg and Kohn[179], since the densities are the same and the energy functional is universal, the solution of the independent particle system yields the properties of the interacting system. In KS[17], the Hamiltonian for a system of non-interacting particles is written as

$$H_{KS} = T_{e-n} + V_{ee-n} + V_{en} + V_{nn} + E_{xc} \tag{3}$$

Here, T_{e-n} and V_{ee-n} are respectively the kinetic energies and coulomb energies for non-interacting particles whose form is well established. E_{xc} is the exchange and correlation energy which will be explained below. V_{en} and V_{nn} are the same in equations (2)and (3)

respectively and their form is known. Since equations (2) and (3) should give the same energy, it follows that

$$E_{xc} = \left(T_e - T_{e-n}\right) + \left(V_{ee} - V_{e-n}\right) \tag{4}$$

and thus *all the correlation effects that were present in the original interacting system have been accumulated into* E_{xc} *in equation* (3), *in the auxiliary non-interacting system*[182]. Exchange and correlation contribution to energy of interacting many-body system stems from quantum many-body effects that do not have a classical analogue[182]. Quantum mechanics classifies particles as bosons or fermions based on whether their spin is integral of half integral. Exchange interactions arise from the indistinguishability of identical particles. The wave function of a system of identical particles is symmetric or anti-symmetric to exchange depending upon whether the particles are bosons or fermions respectively. If the particles are bosons, they tend to be in the same quantum state and the average distance between them is smaller compared to the situation where indistinguishability effects could be neglected. On the other hand, for a system of fermions such as electrons, the antisymmetric behavior of wave function to exchange requires that no two electrons can be in the same quantum state. This implies that when the wave functions of two electrons overlap, they tend to be, on an average, at a greater distance than if the indistinguishability effects were absent. Consequently, there is an energy associated with the exchange of identical particles and the exchange energy functional accounts for this effect. Exchange effects will be present even if the identical particles were un-charged since they are the consequence of the indistinguishability of identical particles. In actual computation, this only requires that the wave function of a

system of particles, constructed from non-interacting particles, to be of the form of slater determinant[183]. This effect is already present in Hartree–Fock theory[184] which neglects coulomb correlation and therefore over estimates the energy. If the particles are indistinguishable *and charged*, their motions will be further correlated because the coulomb interaction[185] will alter the energy of the configuration compared to the case where the particles are uncharged. For repulsive interactions between electrons, which exist in solids, the presence of an electron at any location reduces the probability of finding another electron in the vicinity[185] thereby creating a hole, a region of low probability of finding an electron. The presence of hole has a net effect of increasing the distance between the electrons and reducing their interaction energy[185]. The correlation energy term accounts for such effect arising from coulomb correlation.

From equation(3), it is clear that the forms of all the terms other than E_{xc} are known and the functional for E_{xc} needs to be approximated. Two approximations are used to model exchange-correlation effects in DFT: the local density approximation[17, 186] (LDA) and the generalized gradient approximation[187] (GGA). The GGA[187] is an improvement over the LDA[17] in that the functional depends upon the local density as in LDA[181] as well as the gradient of the density, similar to the first and second term of the Taylor series expansion. LDA is based on the assumption[17] that the exchange and correlation effects experienced by an electron in a solid, which constitutes a non-homogeneous electron gas, are the same as experienced by an electron in a homogeneous gas with the same density as at the position of the electron in the solid. Homogeneous electron gas has been simulated using quantum Monte-Carlo methods[186] and the results have been parametrized[188-190].

LDA[181] neglects the local variations in density around an electron and assumes the energy at the local constant density as the true energy. In molecules, where density changes are rapid, LDA is not a good approximation. GGA[187] overcomes this shortcoming of LDA by accounting for the local variations of density. GGA preserves the advantages of LDA for systems such as solids, where the approximation of slow varying density is valid and at the same time is applicable to molecules where density changes are rapid.

The computational efficiency of Kohn-Sham[17] numerical scheme can be further enhanced by introducing the concept of pseudopotentials[191] in DFT calculations. The numerical solution[192] of the Schrodinger equation is obtained by expanding the wave function in terms of a basis set to convert the differential eigenvalue problem to a matrix eigenvalue problem that can be solved iteratively[193] using a digital computer. The wave function of an electron in close proximity to the nucleus oscillates rapidly and can have multiple nodes. A large basis[194] set is required to accurately model the rapidly fluctuating wave function in the core region. It is well known that the chemical properties of molecules are determined mostly by valence electrons, and the core electron wave functions remain unperturbed and quite similar to their isolated atom state[195]. The same applies when isolated molecules form condensed phases: their core electron states remain unaltered[195]. The computational resources and time needed to solve the Schrodinger equation can therefore, be substantially reduced by replacing the effect of nucleus and core electrons with a simpler effective potential, the pseudopotential[196], that has a simpler form in the core region and matches the true potential beyond some cutoff radius r_c. Other than the reduction in the size of basis set and the number of electrons to be

explicitly represented in the calculation, pseudopotentials also offer the advantage that they can be developed for isolated atoms[197] and transferred to solids and molecules. This becomes feasible because the essential idea, that the core states remain unchanged, remains valid. In literature[197, 198], the pseudopotential have been classified as soft or hard depending upon the size of cutoff radius. Higher cutoff implies a softer potential. However, there is a tradeoff involved in that increasing the cutoff radius generally also makes the pseudopotential less transferable. Plane wave codes such as VASP[192, 199] make extensive use of pseudopotentials.

4.2 Methodology for computing redox potential

DFT-based simulations yield the geometrically optimized structure, converged wave function and the energies of the molecular orbitals. The thermodynamic quantities needed for computation of redox potentials as well as the electron affinities are obtained starting from the geometry optimized structures[68]. The frequencies of the converged molecular structures are obtained from the Hessian computed at the end of geometry optimization stage. The computed frequencies should all be real in order for the system to be in a local energy minimum. The frequency calculation, therefore, provides a check on the stability of the structure. The computational methodology of Winget et al.[68, 69] is employed for calculating the equilibrium free energy of an oxidation/reduction process in terms of the ionization potential and electron affinity of the species in gas phase. The thermodynamic cycle employed in this work is based on their approach[68] and is shown in Figure 9 .

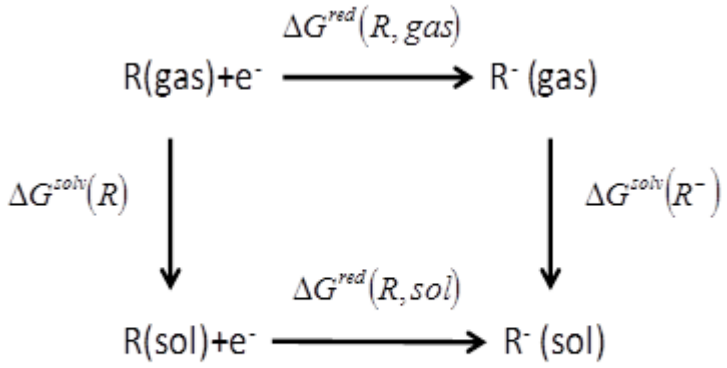

Figure 9: Thermodynamic cycle[68] to calculate the redox potential of a species R in solution phase

In this method[68], the free energy changes associated with the electrochemical reduction reaction in solution phase (bottom horizontal line in Figure 9) can be expressed in terms of the free energy change for the reduction reaction in gas phase (top horizontal line in Figure 9) and the solvation free energies of each species (vertical lines in Figure 9). The solvent was a 3:7 (mol:mol) mixture of ethylene carbonate and dimethyl carbonate, respectively, whose dielectric constant is 16.14. The solvation free energies were calculated using Poisson-Boltzmann solver[200] as implemented in Jaguar[201]. The solvation free energy of an electron is neglected.

Based on the thermodynamic cycle shown in Figure 9, the redox potential of the species R is given as

$$E^0_{w.r.t.Li/Li^+} = \left(-\frac{\Delta G^{red}\,(R,sol)}{nF} - E_H\right) - E_{Li/Li^+} \qquad (5)$$

where $E^0_{w.r.t.Li/Li^+}$ is the redox potential of species R w.r.t. Li/Li^+ electrode, $\Delta G^{red}\,(R,sol)$ is the reduction free energy of the species R in the solution state. E_H and

E_{Li/Li^+} are the absolute redox potential of hydrogen electrode and the electrode potential of lithium electrode w.r.t. the standard hydrogen electrode (SHE), respectively. F and n are the Faraday constant and the number of electrons transferred in the reaction, respectively. The absolute redox potential of the hydrogen electrode and the redox potential of Li electrode w.r.t. SHE are taken to be -4.44 V and -3.05 V, respectively. $\Delta G^{red}\ (R, sol)$ corresponds to the free energy change for the bottom horizontal line in the thermodynamic cycle in Figure 9 and is given as

$$\Delta G^{red}\ (R, sol) = \Delta G^{red}\ (R, gas) + \Delta G^{solv}\ (R^-) - \Delta G^{solv}\ (R) \qquad (6)$$

where $\Delta G^{red}(R, gas)$ is the reduction free energy in gas phase. The method used to calculate redox potentials in this study has been validated through comparison with experiments in several previously published works[68, 69].

In the next chapter, we will present the investigations for redox and electronic properties for pristine C_{60}, materials in *Series 1*, *Series 2* and for multiply charged C_{60} anions and discuss them.

CHAPTER 5

DFT STUDY OF REDOX AND ELECTRONIC PROPERTIES OF FUNCTIONALIZED AND DOPED FULLERENE

In this chapter, the computed redox properties and electronic structures of functionalized and doped C_{60} will presented and discussed. We will also explore the relationship between the electronic structure and redox properties of these materials. Using DFT[17], as implemented in Jaguar[201], we have obtained the geometry optimized structures, converged wave functions and energies of occupied and virtual molecular orbitals of fullerene functionalized with OCFGs and SEWFGs. As described in chapter 3, the functionalized fullerenes constitute *Series 1*. The hetero-fullerenes, $C_{59}X$ (X=B, N, S, Si and P), constitute *Series 2*. The simulation parameters used for DFT based geometry optimization are given in table 1.

Table 1 Simulation parameters for geometry optimization

Parameter	Value
Theory	DFT
Functional	PBE0
Basis Set	6-31+G (d,p)
Energy Convergence Criterion	$5x10^{-5}$ Ha
Energy convergence Criterion(Solvation)	$15x10^{-5}$ Ha
Dielectric Constant of solvent	16.14
Probe radius of solvent	2.5124 Å
Reference Temperature	298.15 K

As described in detail in chapter 4, we have used the methodology of Truhlar and coworkers[69], which is based on a thermodynamic cycle[69], to compute free energy changes

in solvent environment. The solvent is a 3:7 (v/v) mixture of ethylene carbonate (EC) and dimethyl carbonate (DMC). Solvation effects are modeled using a Poisson-Boltzmann solver[200] as implemented in Jaguar[201] simulation package. The representative geometry optimized structures for molecules in *Series 1 and Series 2* along with the description of their nomenclature are shown in Figure 10.

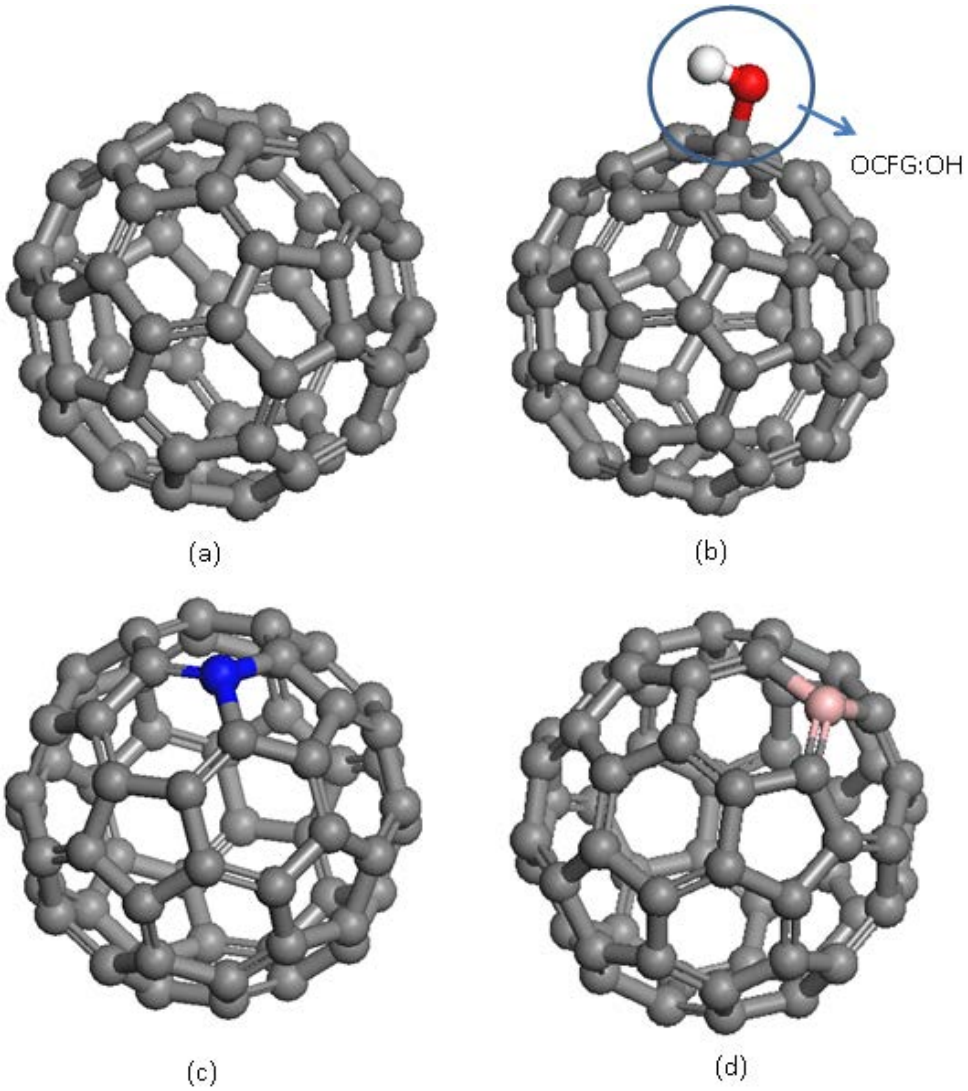

Figure 10: Nomenclature and representative geometry optimized structure of (a) Pristine C_{60} (b) C_{60} functionalized with hydroxyl group (c) $C_{59}N$ and (d) $C_{59}B$. In (b), the OCFG attached to C_{60} is explicitly designated for the sake of clarity and nomenclature. As described in the text, we have investigated functionalization of C_{60} with OCFGs and SEWFGs

The computed redox and electronic properties for each of the molecules in *Series 1* and *Series 2* as designated in chapter 3, will be presented now.

5.1 Computed redox potentials and electronic properties for *Series 1*

As designated in detail in chapter 3, *Series 1* consists of pristine fullerene functionalized with two classes of functional groups. The first class consists of OCFGs, namely, hydroxyl(-OH), carboxyl(-COOH), epoxide(-O-) and aldehyde (-CHO). The second class consists of SEWFGs, namely, trifluoride ($-CF_3$), cyano (-CN), nitro ($-NO_2$) and sulfonates ($-SO_3H$). The OCFGs were chosen for functionalization because the high energy and power densities in the carbon based cathode materials were attributed to the electron transfer reaction between OCFG and adsorbed lithium[139, 140]. The SEWFGs were chosen because Yokoji et al.[138] have experimentally demonstrated that functionalization with electron withdrawing functional group can make the parent structure electron deficient and result in a high redox potential material. It is interesting to investigate, in a quantitative sense, the ability of SEWFGs to create electron deficiency on the C_{60} cage and compare it with pristine C_{60} and OCFGs. Figure 11 shows the molecular electrostatic potential, expressed in kcal/mole, on an iso-charge density surface corresponding to the charge density of 0.001 a.u. for SEWFG functionalized C_{60}.

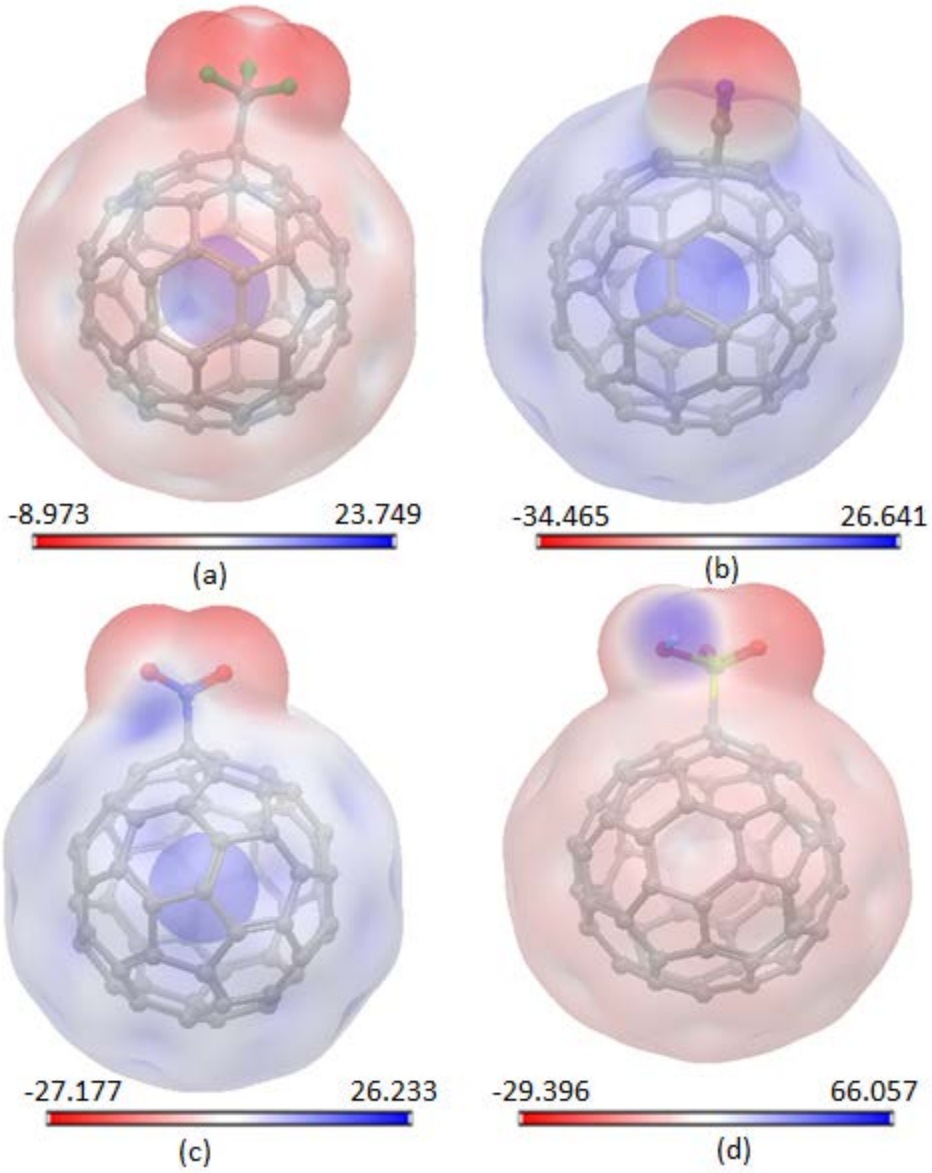

Figure 11: Electrostatic potential profiles, in kcal/mole, superimposed on a 0.001 a.u. charge density profile for SEWFG-functionalized C_{60} (a) Trifluoride ($-CF_3$) (b) Cyano (-CN) (b) Nitro ($-NO_2$) (b) Sulfonate ($-SO_3H$). Notice that functionalization with cyano and nitro makes almost the entire fullerene cage electron deficient.

It is evident from Figure 11 that cyano and nitro group render the fullerene cage almost entirely electron deficient. The effect of sulfonate group in creating an electron deficient region is higher but is primarily localized on the functional group. For reference, the maximum value of electrostatic potential pristine C_{60} is 19.29 kcal/mole.

We observe that SEWFGs are quite effective in creating highly electron deficient region on the fullerene cage and this is reflected in the high redox potentials obtained by functionalizing C_{60} with SEWFGs

In addition to the redox potentials, we have calculated the electron affinity, the HOMO and LUMO level and the HOMO-LUMO gap (calculated as LUMO-HOMO) for the molecules. We anticipate that the electronic structure would determine the redox properties of the material. Because the electronic properties are descriptors of the electronic structure of the material, we hope to extract correlation between the redox and electronic properties of the materials investigated in this work. Such correlations of electronic properties to redox potential will serve as guidelines for designing promising, high positive redox materials for electrochemical applications. It is anticipated that such correlations can be used as screening criteria for selecting promising materials from a group of electronic structures for further investigation. The values of HOMO, LUMO and HOMO-LUMO gap have other significance as well. A high negative value of HOMO level indicates[202, 203] that the neutral species will have a lower tendency to spontaneously lose electrons and will be more stable. A relatively large negative value of LUMO indicates that anion formed by the addition of electron to the neutral species would be correspondingly more stable. A high positive value of the HOMO-LUMO gap for neutral species indicates high stability and lower reactivity for the molecule[204, 205]. The calculated redox and electronic properties of materials in *Series 1* are given in Table 2 below. The redox potential for pristine C_{60} is also computed as a reference value.

Table 2 Redox potentials and electronic properties of pristine C_{60}, OCFG-functionalized C_{60} and SEWFG-functionalized C_{60}.

	Redox Potential (V vs. Li/Li^+)	Electron affinity (eV)	HOMO (eV)	LUMO (eV)	Gap (eV)
Pristine C_{60}	2.462	-2.666	-6.648	-3.614	3.034
Hydroxyl	3.322	-3.516	-6.041	-3.613	2.428
Carboxyl	3.145	-3.314	-5.877	-3.623	2.254
Epoxide	2.589	-2.792	-6.595	-3.709	2.887
Aldehyde	3.162	-3.417	-4.953	-3.630	1.323
Trifluoride	3.214	-3.456	-6.058	-3.718	2.340
Cyano	3.287	-3.562	-6.147	-3.820	2.327
Nitro	3.433	-3.680	-6.257	-3.817	2.440
Sulfonate	3.341	-3.644	-6.133	-3.801	2.332

The electron affinity of C_{60} computed in this work is 2.666 which is in very good agreement with values reported in literature[154, 206]. Wang et al.[207] have experimentally measured the electron affinity of C_{60} and reported a value of 2.650 ± 0.050 eV. Zettergren et al.[154] have used DFT and reported a value of 2.59 eV for the electron affinity of C_{60}. The close agreement between our computed value of electron affinity of C_{60} and the experimental[207] and theoretical[154] values reported in literature validates the choice of simulation parameters and calculation procedure used in this work.

It is clear from table 2 that both the OCFGs and SEWFGs, which are investigated in this work, are effective in increasing the redox potential of fullerene. OCFGs on C_{60} give a 5 percent to 40 percent increase in redox potential. Hydroxyl functional group on pristine C_{60} was found to be quite effective but its effect on doped C_{60} i.e. on $C_{59}N$ and $C_{59}B$ was quite limited and in some cases detrimental. All the SEWFGs investigated in this work were quite effective in increasing the redox potential of fullerene with increments from 30 percent to 40 percent. The quantum of increment is dependent on the specific functional group attached to fullerene. Our chemical intuition that OCFGs and

SEWFGs can be used to give an increase in redox potential and tailor it in specific direction has been validated by computation.

Figure 12 shows the relationship between redox potentials and electronic properties for molecules listed in table 2.

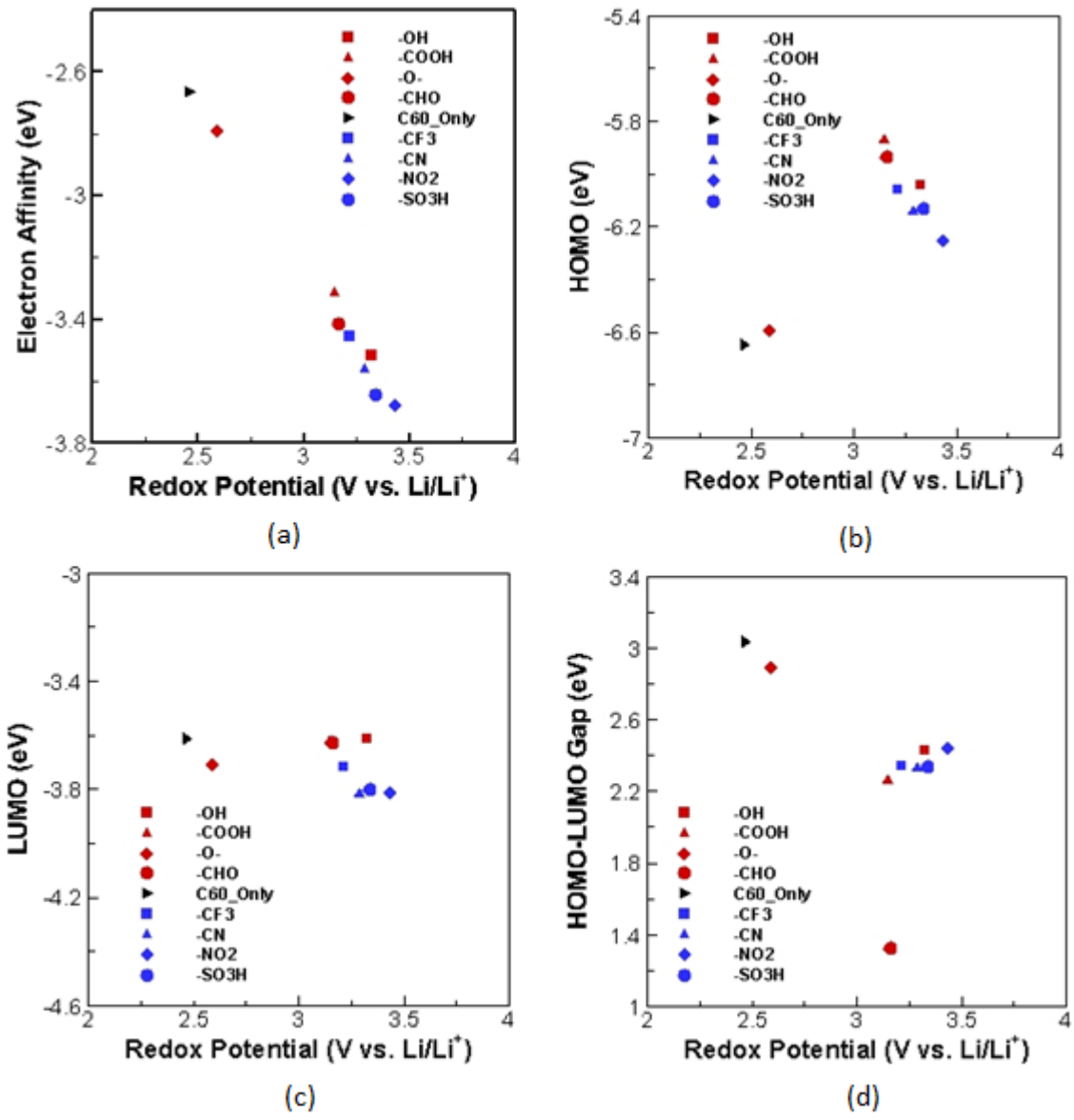

Figure 12: Relationship between computed electronic properties and redox potential for OCFG and SEWFG functionalized C_{60}: (a) Electron affinity; (b) HOMO level; (c) LUMO level; (d) HOMO-LUMO gap. Values for pristine C_{60} are included for comparison.

A strong correlation is observed between the computed redox potential and the electron affinity of the molecule in Figure 12. It is expected that the electron affinity, computed as a difference in the Gibbs free energy (anion minus neutral species) at reference temperature, would decrease with increasing redox potential and this trend is clearly evident in Figure 12. A negative electron affinity means that the anion is more stable than the neutral species and is a quantitative measure of the molecule to accept an electron. The HOMO level, the LUMO level and the HOMO-LUMO gap (computed as LUMO minus HOMO) as a function of redox potentials of the neutral species for functionalization with OCFGs and SEWFGs is also shown in Figure 12. While electron affinity is observed to correlate strongly with the redox potential, the correlation between other electronic properties and the redox potential is not so strong. This is because the overall redox potential is composed of an intrinsic electronic structure part and a solvation part. The solvation part is dependent on the nature of the solvation medium and hence the correlation of *overall* redox potential with any electronic property will be medium dependent.

It is insightful to consider how the redox potential is calculated from the electronic structure of the molecule. The energy decomposition of the redox potential is shown schematically in Figure 13.

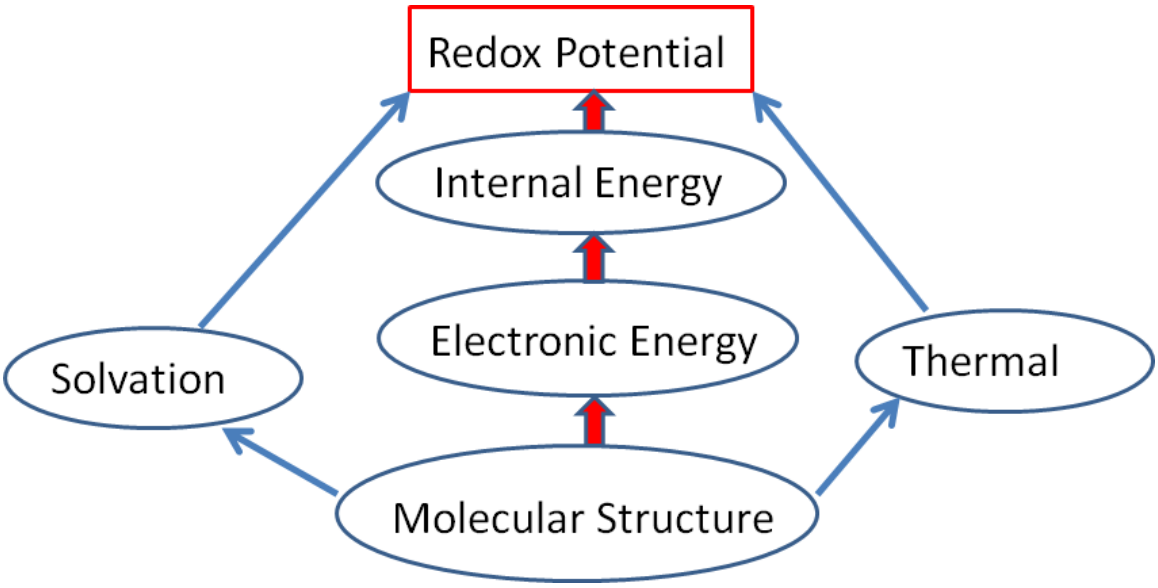

Figure 13: Decomposition of redox potential into its component energies

Figure 13 shows that the computed redox potential is mainly composed of an molecular structure contribution and a solvation contribution. The molecular structure contribution is intrinsically determined by the molecular electronic structure while the solvation contribution is determined by the interactions with implicit solvent phase. The molecular structure contribution is also composed of the internal energy and the vibrational entropic contribution. Since the vibrational entropic contribution is just one order of magnitude smaller than the internal energy the internal energy is the main contributor to the redox potential. To study the relative importance of electronic structure and solvation to the redox potential of the molecule and to develop molecular descriptors which can be used to rapidly screen promising materials for redox potentials, we have analyzed the overall redox potential into the electronic structure contribution and solvation contribution as shown in Figure 14, showing that the solvation contributes 10 to 20% of the redox potential.

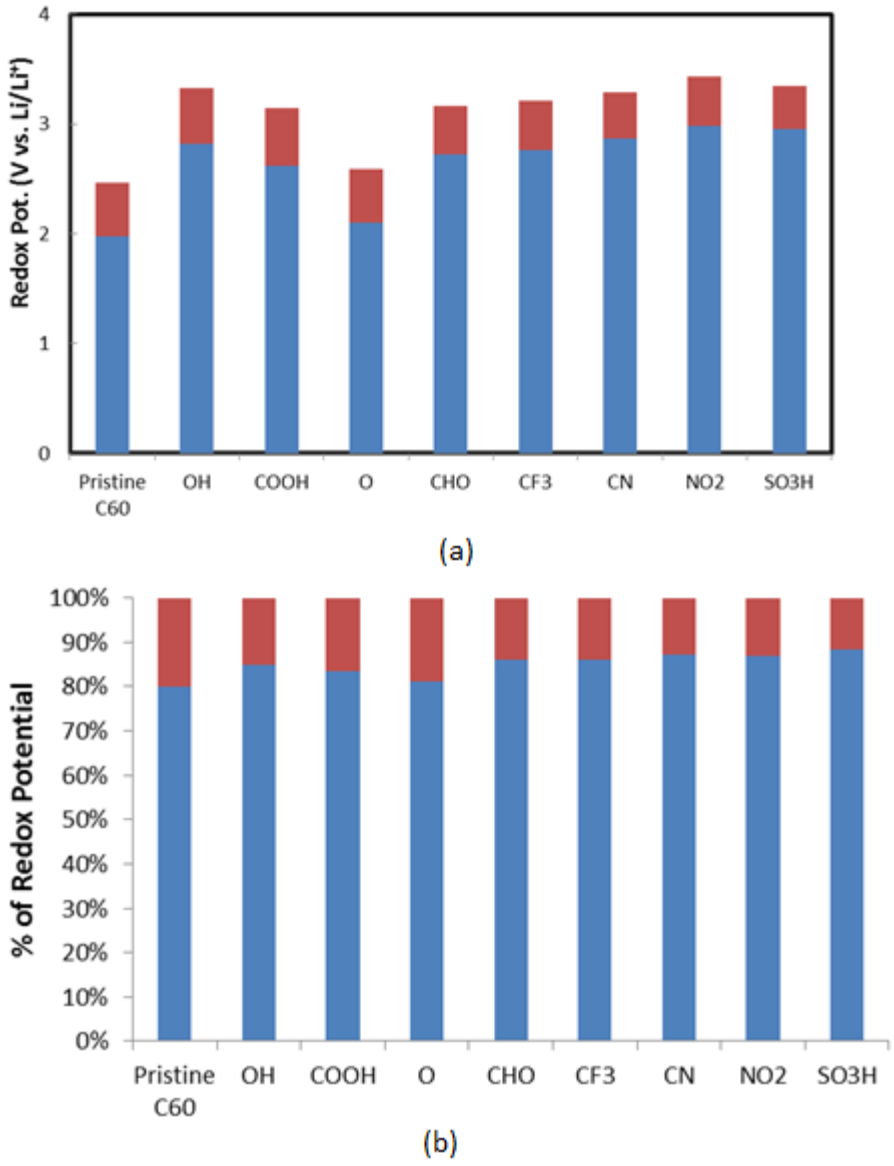

Figure 14: Contributions of electronic structure (blue) and solvation (red) to redox potential for OCFG and SEWFG functionalized C_{60} (a) absolute values (b) percentage contributions

It is observed from Figure 14(b) that solvation contributes up to a maximum of 20 percent to redox potential and mostly less than 20 percent. Intrinsic electronic structure contributes atleast 80 percent to redox potential. It is more meaningful to look for correlations between the electronic properties and the electronic structure part of the redox potential. Figure 15 shows the correlation between the intrinsic electronic structure

part of redox potential and HOMO level for open shell OCFG and SEWFG functionalized C_{60}. Surprisingly, it is observed in Figure 15 that the correlation is very strong. From this result, it is inferred that the HOMO is responsible for the redox potential 1) if the open shell is commonly applied for the electronic structure; 2) if the solvation free energy is not significantly changed as a function of functional groups. It would be interesting to investigate whether correlations of this nature are incidental or repeatedly reproducible by investigating other materials.

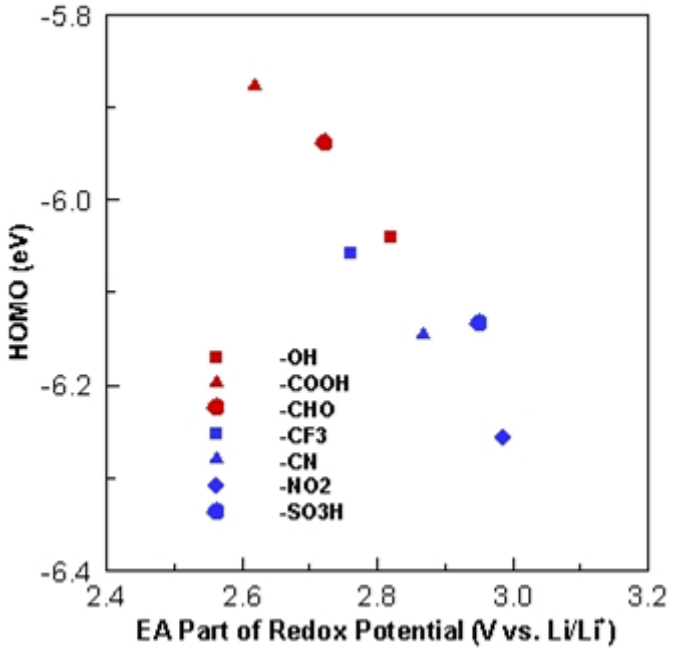

Figure 15: Correlation of HOMO with the redox potential contributed from the electron affinity for open shell OCFG and SEWFG functionalized C_{60}.

5.2 Computed redox potentials and electronic properties for *Series 2*

As described in chapter 3, materials in *Series 2* are obtained by substituting one of the carbon atoms on the C_{60} cage with another atom to yield doped fullerene, $C_{59}X$ (X=B, N, S, Si, P). The calculated redox and electronic properties of materials in *Series 2* are given in table 3 below. The redox potential for pristine C_{60} serves as a reference.

Table 3 Redox potentials and electronic properties of doped C_{60}, $C_{59}X$ (X=B, N, S, Si, P)

	Redox Potential (V vs. Li/Li^+)	Electron affinity (eV)	HOMO (eV)	LUMO (eV)	Gap (eV)
C_{60}	2.462	-2.666	-6.648	-3.614	3.034
$C_{59}B$	3.709	-3.835	-6.327	-3.603	2.724
$C_{59}N$	2.760	-2.947	-5.148	-3.685	1.463
$C_{59}S$	2.367	-2.621	-5.748	-3.639	2.109
$C_{59}Si$	2.878	-3.113	-6.379	-3.941	2.438
$C_{59}P$	3.040	-3.254	-5.775	-3.628	2.148

From table 3, it is observed that doping fullerene with boron results in more that 50 percent increase in redox potential. Since boron is poor in electrons and fullerene by itself is an electron withdrawing group, an increase in redox potential was expected based on chemical intuition. But the magnitude of the effect was unexpected. This is an example of computation reveling promising directions for experimental synthesis and helping to reduce the randomness and tedium which is intrinsic to experimental design of novel materials. Based on our computation results, another material that seems promising, so far as the redox potential is concerned, is $C_{59}P$. It shows approximately 25 percent increase in redox potential over the baseline potential of C_{60}. Nitrogen gives approximately 10 percent increase in redox potential. Nitrogen has a high electronegativity. Therefore, it is anticipated that it would withdraw electrons from the fullerene cage and $C_{59}N$ will be a high redox potential material. However, calculated redox potentials show that the effect of nitrogen substitution is quite mild. This somewhat unexpected result is due to the electronic structure of $C_{59}N$ which will be discussed in more detail in next chapter.

Figure 16 shows the relationship between redox potentials and electronic properties for doped fullerene molecules, $C_{59}X$, listed in table 3.

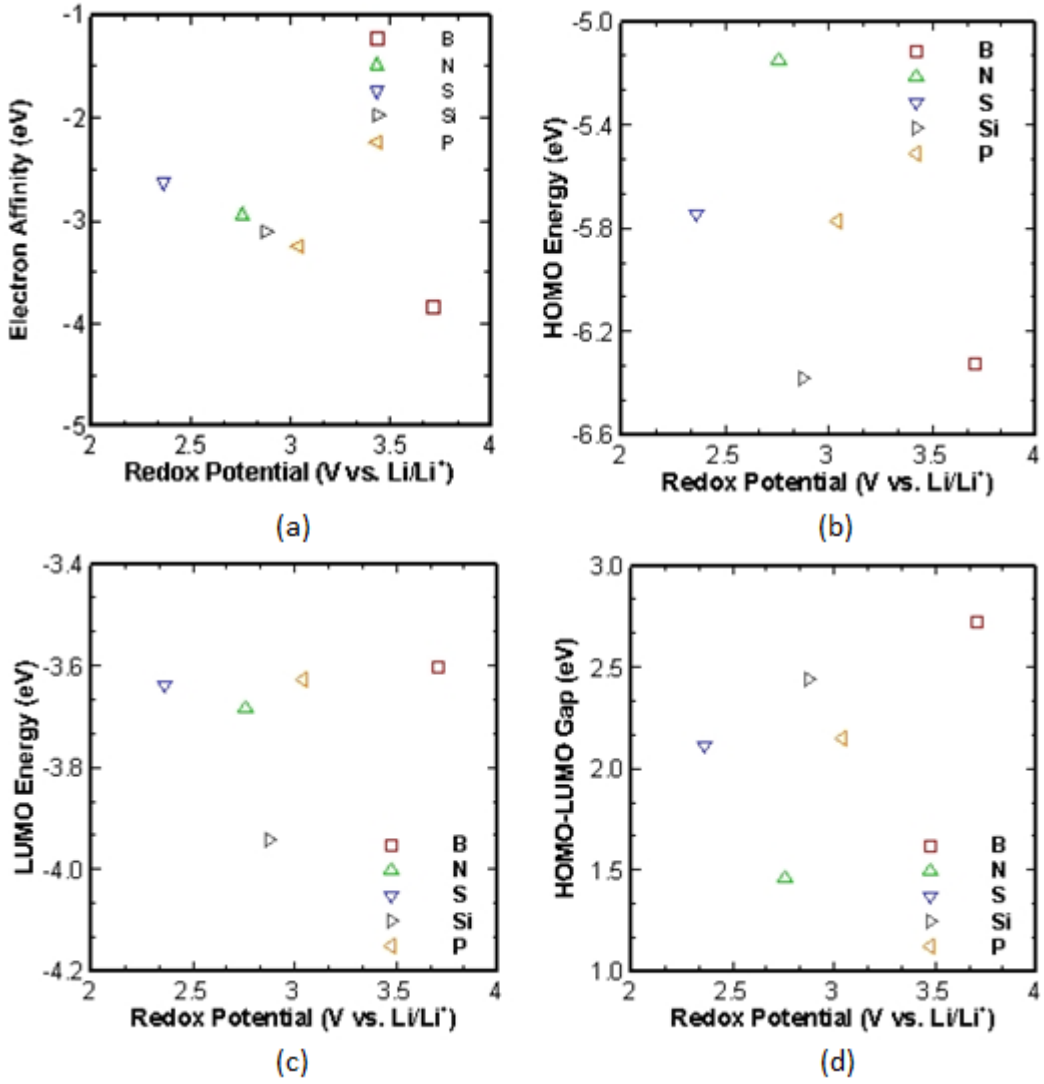

Figure 16: Relationship between computed electronic properties and redox potential for doped C_{60}, $C_{59}X$ (X=B, N, S, Si, P): (a) Electron affinity; (b) HOMO level; (c) LUMO level; (d) HOMO-LUMO gap.

A strong correlation is observed between the computed redox potential and the electron affinity of the molecule. The HOMO level, the LUMO level and the HOMO-LUMO gap (computed as LUMO minus HOMO) as a function of redox potentials of the neutral

species for OCFGs and SEWFGs is also shown in Figure 16. The correlation between the redox potential and HOMO level, LUMO level and HOMO-LUMO gap is not so strong.

5.3 Lithium adsorption capacity of C_{60} for redox applications

This work investigates C_{60} and materials obtained by doping and functionalizing C_{60} because high electron affinity[154] of C_{60} makes it a promising candidate for high positive redox material. The energy density that can be obtained by using C_{60} based materials depends on the electron affinity of C_{60}, the evolution of electron affinity with increasing negative charge on C_{60} and the amount of lithium that can be adsorbed on C_{60}. It has been reported that the redox potential of carbon based cathode materials decreases with increasing lithium adsorption[23]. Therefore, we investigate the evolution of redox potential of C_{60} with increasing lithium content and determine the threshold at which the redox potentials become negative, indicating saturation of redox capability of C_{60} with increasing lithium adsorption. Figure 17 presents the evolution of redox potential of C_{60} with increasing lithium adsorption on the pentagonal faces of C_{60}.

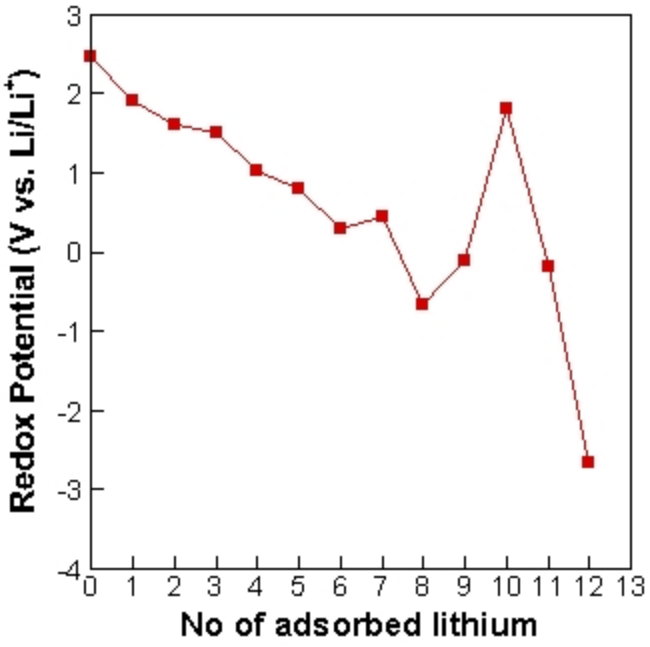

Figure 17: Evolution of redox potential of C_{60} with increasing lithium adsorption

It is observed from Figure 17 that redox potential decreases monotonically with increasing lithium adsorption upto 6 lithium atoms and is positive. A peak in redox potential is observed when the number of adsorbed lithium is 10. We believe that this is because in going from 9 lithium atoms to 10 lithium atoms, the additional lithium was placed on the pentagonal face rather than on the position of minimum energy.

The number of lithium atoms that can be adsorbed on C_{60} depends on the stability of higher anionic charge states of C_{60}. The higher anionic states of C_{60} are also of interest because the continued high performance of C_{60} cathode with increasing lithium adsorption would depend upon the evolution of the electron affinity and redox potential with increasing anionic charge on $C_{60.}$ To investigate the evolution of electron affinity and stability of C_{60} with increasing anionic charge, we have calculated the electronic properties of multiple charged stated of $C_{60,}$ C_{60}^{-n}. The evolution of electron affinity,

HOMO level, LUMO level and HOMO-LUMO gap with increasing anionic charge on C_{60} is presented in Figure 18.

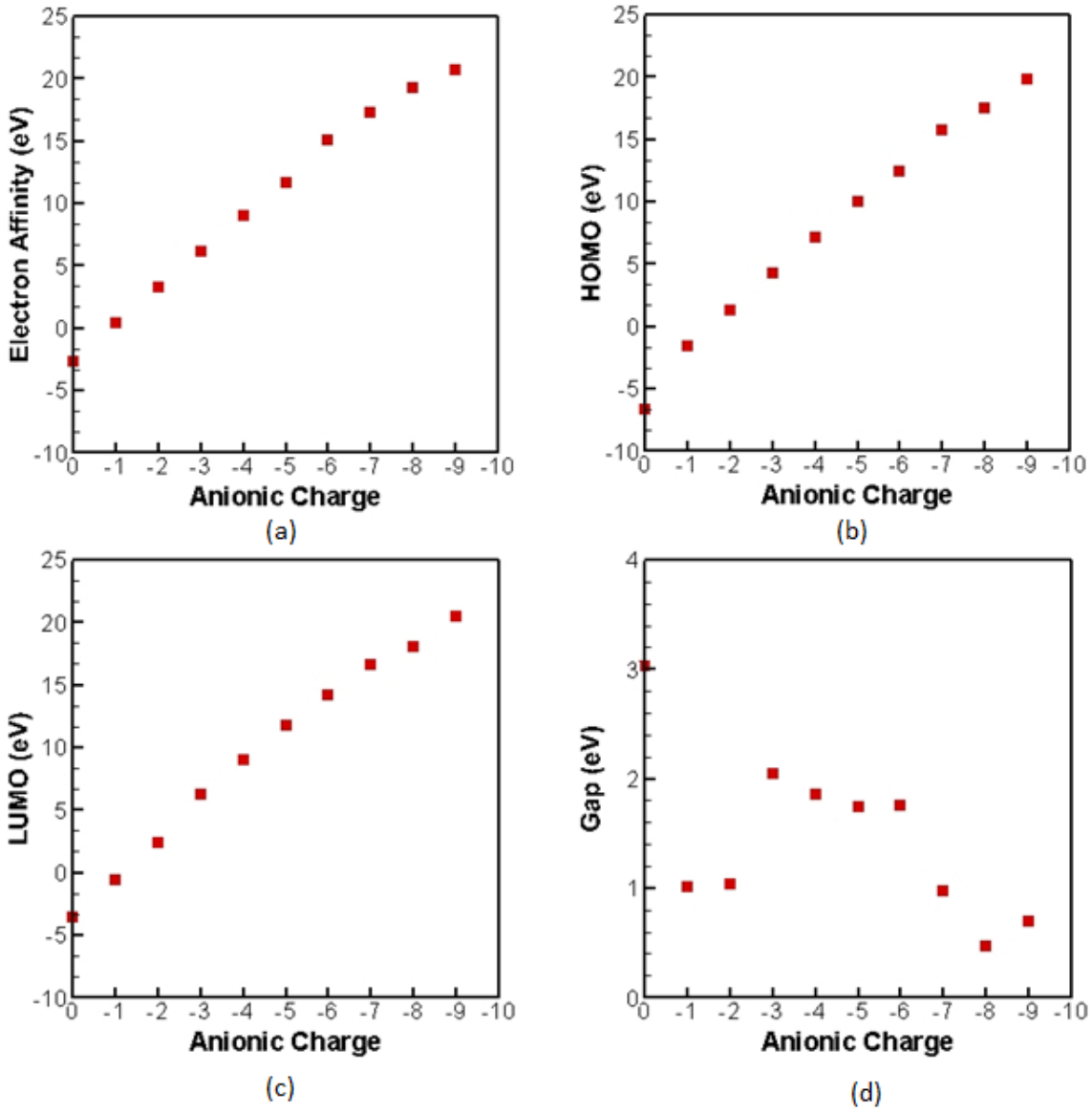

Figure 18: Computed electronic properties for multiply charged C_{60} anions, C_{60}^{-n} (n=0 to 9) (a) Electron affinity; (b) HOMO level; (c) LUMO level; (d) HOMO-LUMO gap

It is observed from Figure 18 that despite the high electron affinity and large size of C_{60}, all electron affinities for C_{60} beyond the first one are positive. This means that any higher charged state of C_{60} beyond C_{60}^{-1} is energetically unfavorable. The HOMO and LUMO

levels of C_{60} and C_{60}^{-1} are negative but for higher anionic charge they are positive indicating a spontaneous tendency to lose an electron. It is also observed that electron affinities, HOMO and LUMO vary almost linearly with anionic charge of $C60^{-n}$ from n=1 to n=6. These results indicate that despite its high electron affinity, isolated C_{60} is not stable in anionic states with more than one electron. This result seems to limit the utility of C_{60} as a cathode material. The question arises that if C_{60} anion is unstable for anionic charge states -2 and higher, how is it that upto 6 lithium atoms can be adsorbed on C_{60}. It would be interesting to investigate if the result obtained for isolated C_{60} anions also holds in the battery environment. In the battery environment, C_{60} will be in a solvated state and hence we have calculated the redox potential of C_{60} anions and the results are displayed in Figure 19.

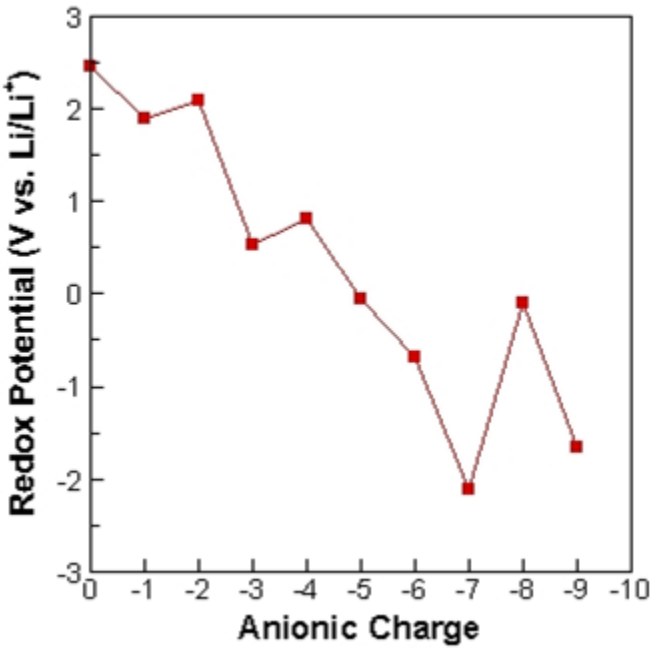

Figure 19: Computed redox potentials for multiply charged C_{60} anions, C_{60}^{-n} (n=0 to 9)

It is observed from Figure 19 that the reduction potential of C_{60}^{-n} is positive from n=0 to n=4 indicating that solvated C_{60} has the capacity absorb upto 5 electrons before its

redox potential becomes negative. Our computation results are supported by the experimental observations of Dubois et al.[172]. Dubois et al.[172] have reported detection of highly reduced fulleride anions C_{60}^{-n} with the highest reduction state of n=5 for C_{60} in benzene solvent. Solvation was found to stabilize C_{60}^{-n} anions upto n=5 and account for the adsorption of six lithium on C_{60}.

5.4 Conclusions

We have investigated the redox and electronic properties of pristine fullerene, functionalized fullerene and doped fullerene materials in this work. Our investigations show that the redox potential of fullerene can be increased up to 30 to 40 percent by functionalization with OCFGs and SEWFGs. Functionalization of pristine C_{60} with SEWFGs investigated in this work show that SEWFGs especially cyano and nitro have a strong effect in making the fullerene cage electron deficient and resulting in a high redox material. It was observed that electronic affinity correlated strongly with redox potential while the correlation of other electronic properties namely HOMO, LUMO and HOMO-LUMO gap with redox is not so strong. It was found that the intrinsic electronic structure is the major contributor to the redox potential contributing atleast 80 percent of the redox value while the solvation contributes only upto 20 percent. Our investigations show that the intrinsic electronic structure part of redox correlates quite strongly with the HOMO of the open shell functionalized fullerenes investigated in this work. Hence, for open shell functionalized C_{60}, HOMO level can be used as a criterion for rapidly screening materials for high redox potentials. It was observed that on cage doping of C_{60} with boron was quite effective in giving a high redox material with upto 50 percent increase in redox potential. Phosphorus doping was also found to be beneficial for obtaining a high redox

material. This work gives quantitative information on the structure –property relationship, relating the descriptors of electronic *structure* to redox *properties* and can be used to discern trends for designing novel fullerene based materials for electrochemical applications. Studies on the evolution of the redox potential of C_{60} with increasing lithium adsorption showed that C_{60} can adsorb upto seven lithium before its redox potential becomes negative. It was found that despite the high electron affinity and large size of C_{60} molecule, the higher reduced states of isolated C_{60}, beyond C_{60}^{-1} are energetically unstable. However, in a solvation medium, the higher reduced states of C_{60} are stable and the redox potential of C_{60}^{-n} anions was found to be positive for n=4. This accounts for the possibility of adsorption of multiple lithium on C_{60}, despite C_{60}^{-2} and subsequent higher reduced states of isolated C_{60} molecule being energetically unstable. Our computation results on higher reduced states of C_{60} are supported by the experimental observations of Dubois et al.[172]

CHAPTER 6

REDOX AND ELECTRONIC PROPERTIES OF FUNCTIONALIZED AZAFULLERENE

In this chapter, we will present our investigations on nitrogen doped fullerene, $C_{59}N$, functionalized with OCFGs and SEWFGs. It was observed in chapter 5 that nitrogen doping gives an increase in the redox potential of fullerene but the increment is small. We are interested in the effect of functionalization on the redox potentials of $C_{59}N$. As described in chapter 3, the OCFGs considered in this work are hydroxyl (-OH), carboxyl (-COOH), epoxide (-O-) and aldehyde (-CHO). The SEWFGs explored in this work are triflouride ($-CF_3$), cyano (-CN), nitro ($-NO_2$) and sulfonates ($-SO_3H$). We have also used DFT to study the effect of doping C_{60} with multiple numbers of nitrogen atoms i.e. $C_{58}N_2$ and $C_{57}N_3$, to investigate if the effect of doping with one nitrogen atom can be synergistically enhanced by doping with multiple number of nitrogen atoms.

6.1 Electronic structure of Pristine C_{60} and $C_{59}N$

Substitution of carbon with nitrogen on the C_{60} cage results in the creation of an electron deficient region in the vicinity of nitrogen. In order to quantitatively visualize the changes in electron distribution caused by the introduction of nitrogen on the fullerene cage, we have computed the molecular electrostatic potential on an iso-charge density surface corresponding to the charge density of 0.001 a.u. for C_{60} and $C_{59}N$. This is shown in Figure 20.

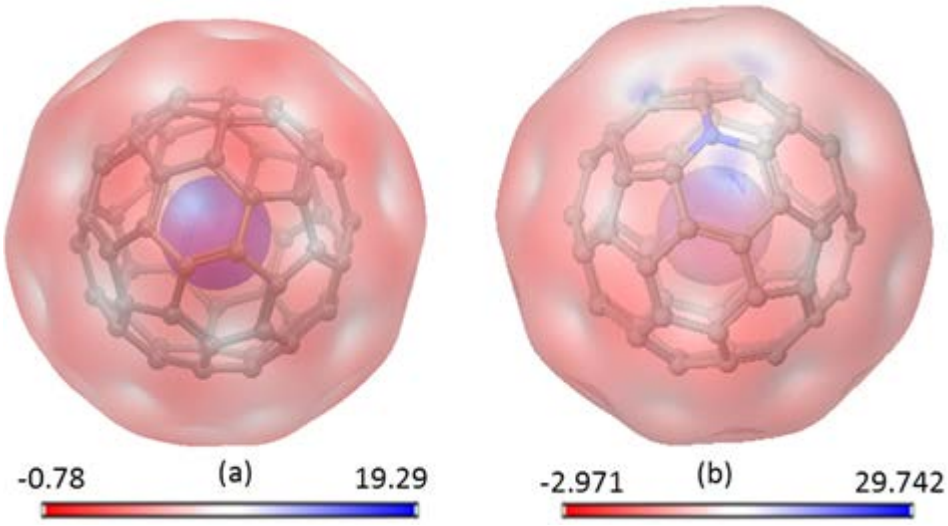

Figure 20: Electrostatic potential profiles, in kcal/mole, superimposed on a 0.001 a.u. charge density profile for (a) Pristine C_{60} and (b) $C_{59}N$. There is an electron deficient region in the vicinity of nitrogen in (b).

From Figure 20, it is clear that in contrast to C_{60}, an electron deficient region develops in close vicinity to nitrogen in $C_{59}N$ as indicated by high positive value of electrostatic potential close to nitrogen. This shows that nitrogen substitution results in a redistribution of electronic charge creating a region of positive potential which can attract electrons.

Chemical activity is governed by the distribution, occupancies and energies of HOMO and LUMO orbitals. The calculated energy levels of C_{60} and $C_{59}N$ in the vicinity of HOMO and LUMO energy levels are shown below in Figure 21 .

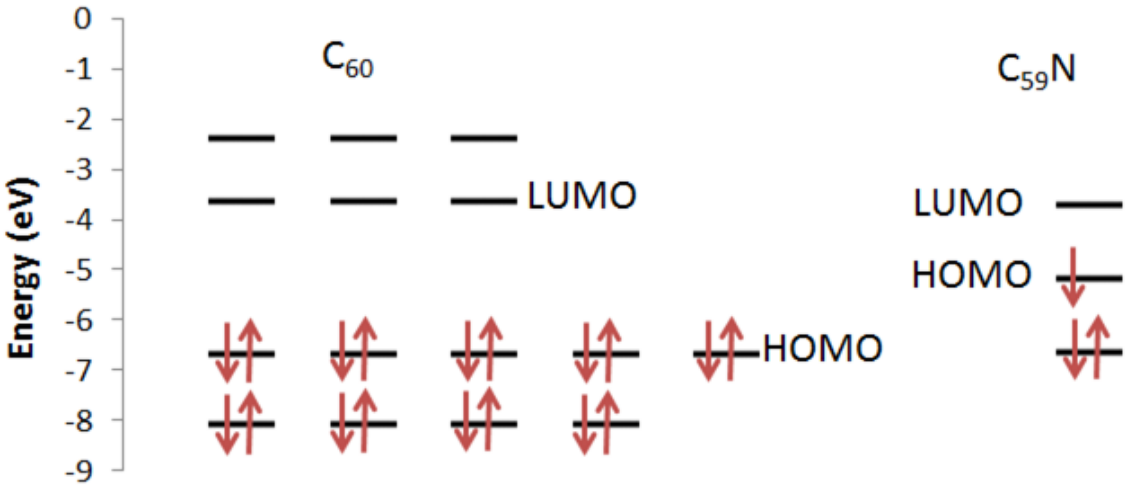

Figure 21: Energy levels and degeneracies in the vicinity of frontier orbitals for pristine C_{60} (left) and $C_{59}N$ (right).

On substituting carbon with nitrogen on the fullerene cage, the degeneracy of the penta-degenerate HOMO level of C_{60} is lifted. In $C_{59}N$, there is an additional electron in the system, compared to C_{60}, which is unpaired. This creates a singly occupied HOMO which is 1.5 eV above the HOMO level of pristine C_{60}. The HOMO orbital of $C_{59}N$ at -5.148 eV is below the LUMO of pristine C_{60} at -3.614 eV but at a higher energy than the HOMO level of C_{60}. This partially occupied HOMO of $C_{59}N$ can accept another electron to form a closed shell system but because of the high energy of partially occupied HOMO, the system also has the tendency to lose this electron to form a closed shell system. These two competing tendencies make $C_{59}N$ have a slightly higher redox potential than C_{60} and that accounts for the rather small effect of nitrogen substitution on redox potential of C_{60}.

The iso-contour of HOMO orbitals at the iso-value of 0.05 for C_{60} and $C_{59}N$ is shown in Figure 22(a) and Figure 22(b) respectively.

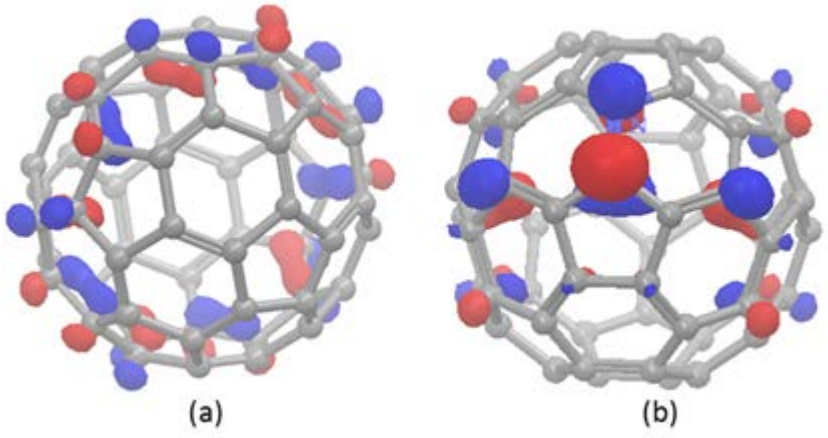

Figure 22: Iso-profile of highest occupied molecular orbital at iso-value of 0.05 (a) Pristine C_{60} and (b) $C_{59}N$. Notice the larger lobe of HOMO on nitrogen atom in (b) indicating that nitrogen makes a substantial contribution to HOMO.

It is observed that in C_{60}, the HOMO is delocalized over the entire molecule. In contrast, in $C_{59}N$, the HOMO is prominently localized on the nitrogen atom. This indicates that nitrogen contributes substantially to the HOMO in $C_{59}N$ and hence determines the properties of the molecule. The HOMO in $C_{59}N$ is singly occupied; therefore, the region around nitrogen is reactive. Therefore, in this work functionalization and doping of $C_{59}N$ on positions in close vicinity to nitrogen has been investigated.

6.2 Redox and electronic properties of pristine C_{60}, $C_{59}N$ and functionalized $C_{59}N$

The representative geometry optimized structures for molecules obtained by functionalizing and doping $C_{59}N$, along with the description of their nomenclature is shown in Figure 23.

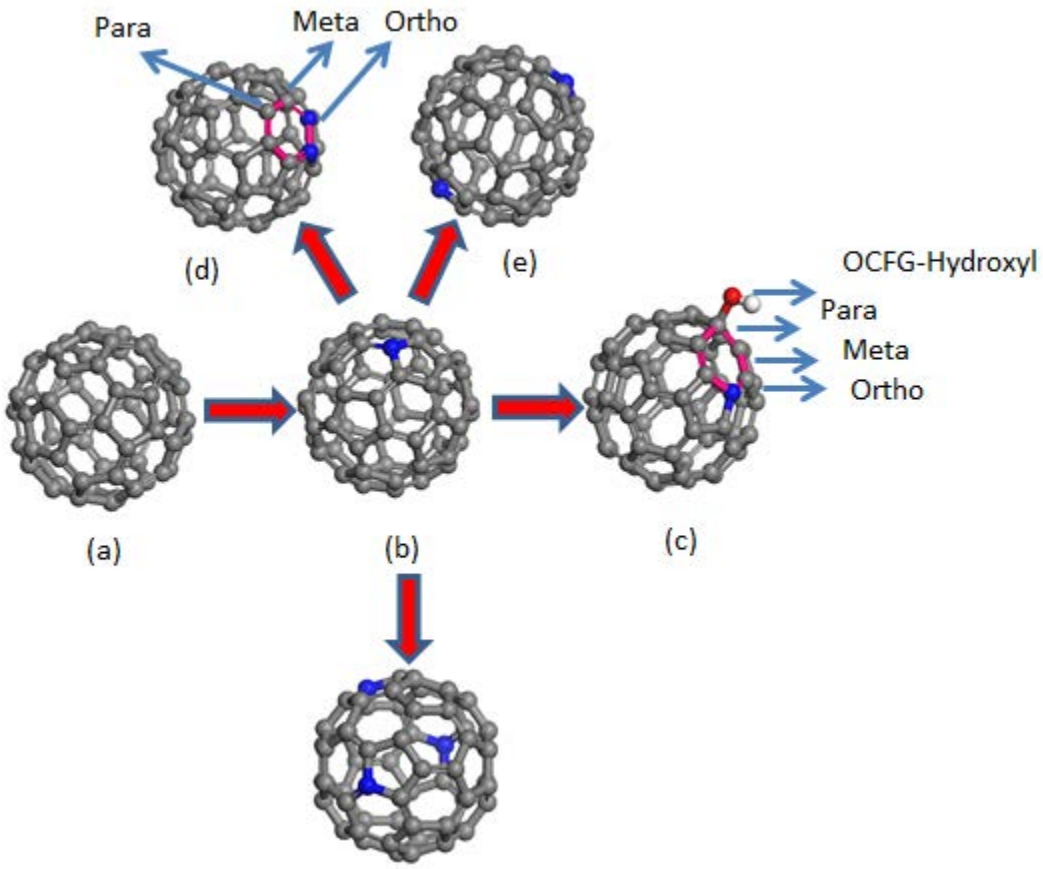

Figure 23: Nomenclature of functionalized and doped $C_{59}N$ based materials investigated in this study (a) Pristine C_{60}, for reference (b) Nitrogen doped C_{60}, $C_{59}N$ (c) $C_{59}N$ functionalized with OCFGs and SEWFGs at different positions relative to nitrogen atom as described in the text: *Ortho, meta and para* positions are indicated for clarity (d) $C_{58}N_2$ with possible *ortho, meta and para* configurations of two nitrogen atoms. (e) $C_{58}N_2$-dispersed configuration (f) $C_{57}N_3$.

All chemical structures considered in this work were optimized for multiple multiplicities to find the multiplicity with the lowest energy. The computed redox potentials and electronic properties of $C_{59}N$, functionalized with OCFGs at ortho, meta and para position relative to the nitrogen atom, as shown schematically in Figure 23, are presented in Table 4.

Table 4 Redox potentials and electronic properties of C_{60}, $C_{59}N$, and OCFG-functionalized $C_{59}N$s. Ortho, meta, and para are the position of OCFG with respect to nitrogen atom as described in the text.

	Redox Potential (V vs. Li/Li^+)	Electron affinity (eV)	HOMO (eV)	LUMO (eV)	Gap (eV)
C_{60}	2.462	-2.666	-6.648	-3.614	3.034
$C_{59}N$	2.760	-2.947	-5.148	-3.685	1.463
Ortho					
Hydroxyl	2.464	-2.679	-6.296	-3.652	2.644
Carboxyl	2.502	-2.888	-6.366	-3.809	2.556
Epoxide	3.135	-3.283	-5.672	-3.703	1.969
Aldehyde	2.499	-2.792	-6.266	-3.736	2.530
Meta					
Hydroxyl	2.619	-2.854	-5.789	-3.869	1.920
Carboxyl	2.724	-3.114	-5.820	-4.080	1.740
Epoxide	2.777	-2.977	-5.304	-3.706	1.598
Aldehyde	2.742	-3.023	-5.692	-3.934	1.758
Para					
Hydroxyl	2.486	-2.722	-6.260	-3.703	2.558
Carboxyl	2.535	-2.921	-6.374	-3.890	2.485
Epoxide	3.072	-3.228	-5.477	-3.745	1.733
Aldehyde	2.527	-2.810	-6.197	-3.778	2.419

The HOMO and LUMO levels are negative as expected for a stable chemical structure. The HOMO-LUMO gap for the neutral species is positive which shows that the geometry optimized structure of the neutral species corresponds to a ground state. It is observed that other than epoxide group at ortho and para positions, which give approximately 25 to 30 percent increase in redox potential, the redox potentials are relatively insensitive to the presence OCFGs attached to $C_{59}N$. It is observed that OCFGs which were effective in pristine fullerene are relatively ineffective in $C_{59}N$. The slight

increase in redox potential, relative to pristine C_{60}, can be attributed to the presence of nitrogen on pristine fullerene since OCFGs other than epoxide have minor effect on the computed potentials.

The relationship between the redox potentials and electronic properties of $C_{59}N$-OCFG materials investigated in this work is displayed in Figure 24.

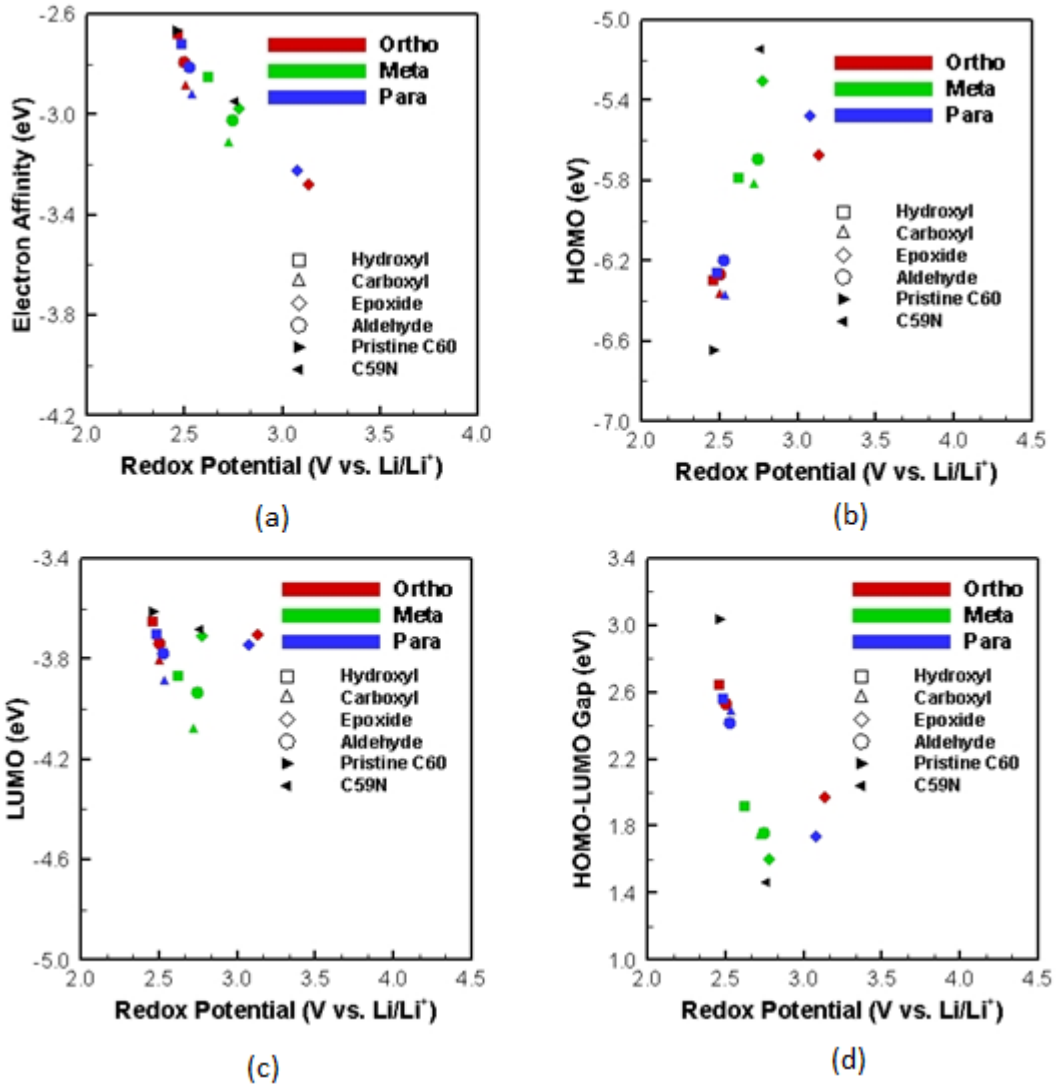

Figure 24: Relationship between computed electronic properties and redox potential for OCFG functionalized $C_{59}N$ in *ortho, meta and para* position with respect to nitrogen: (a) Electron affinity; (b) HOMO level; (c) LUMO level; (d) HOMO-LUMO gap. The *ortho, meta and para* positions are designated with red, green and blue color respectively. Values for pristine C_{60} and $C_{59}N$ are also included for comparison.

It is observed from Figure 24 that the electron affinity shows a good correlation with redox potential. However, neither of the HOMO, LUMO and HOMO-LUMO energy gap seems to correlate clearly to redox potential as shown in Figure 24(b), Figure 24(c) and Figure 24(d) respectively.

The computed redox potentials and electronic properties of $C_{59}N$, functionalized with SEWFGs at ortho, meta and para position relative to the nitrogen atom, as shown schematically in Figure 23, are presented in Table 5.

Table 5 Redox potentials and electronic properties of C_{60}, $C_{59}N$, and SEWFG-functionalized $C_{59}N$. Ortho, meta, and para are the position of SEWFGs with respect to nitrogen atom as described in the text.

	Redox Potential (V vs. Li/Li$^+$)	**Electron affinity (eV)**	**HOMO (eV)**	**LUMO (eV)**	**Gap (eV)**
C_{60}	2.462	-2.666	-6.647	-3.614	3.034
$C_{59}N$	2.760	-2.947	-5.148	-3.685	1.463
Ortho					
Trifluoride	2.447	-2.717	-6.350	-3.748	2.602
Cyano	2.531	-2.857	-6.453	-3.855	2.598
Nitro	2.534	-2.858	-6.511	-3.863	2.648
Sulfonate	2.569	-2.937	-6.428	-3.826	2.603
Meta					
Trifluoride	2.814	-3.105	-5.787	-4.005	1.782
Cyano	2.830	-3.165	-5.875	-4.116	1.759
Nitro	2.777	-3.106	-6.000	-4.068	1.931
Sulfonate	2.830	-3.201	-5.882	-4.120	1.762
Para					
Trifluoride	2.544	-2.822	-6.283	-3.810	2.473
Cyano	2.598	-2.930	-6.391	-3.915	2.475
Nitro	2.650	-2.971	-6.439	-3.902	2.537
Sulfonate	2.580	-2.939	-6.348	-3.891	2.458

The HOMO and LUMO levels are negative[202, 203] and the HOMO-LUMO gap is positive[204 205]as expected. It is observed from Table 5 that amongst the SEWFGs, the cyano group is most effective in increasing the redox potential when it is present at the meta position. In contrast to OCFGs, functionalization of $C_{59}N$ with SEWFGs at the meta position is consistently more effective in giving an increased redox potential relative to the ortho and para positions. Functionalizing $C_{59}N$ with SEWFGs is not quite effective in increasing the redox potentials. Functionalization of $C_{59}N$ with SEWFGs at the ortho and para position is detrimental to redox potential and depresses the redox potential relative to $C_{59}N$. The relationship between the electronic properties of $C_{59}N$-SEWFG materials investigated in this work is shown in Figure 25

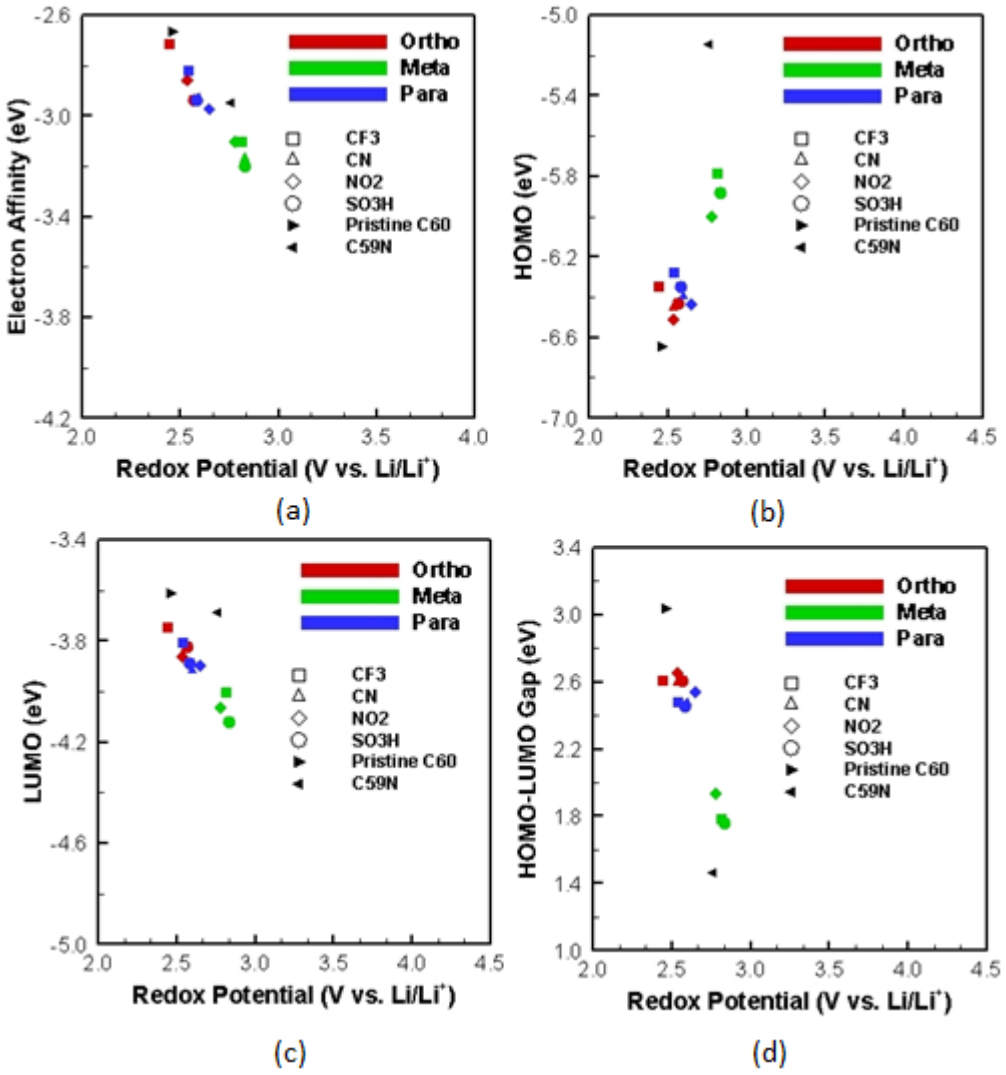

Figure 25: Relationship between computed electronic properties and redox potential for SEWFG functionalized $C_{59}N$ in *ortho, meta and para* position with respect to nitrogen: (a) Electron affinity; (b) HOMO level; (c) LUMO level; (d) HOMO-LUMO gap. The *ortho, meta and para* positions are designated with red, green and blue color respectively. Values for pristine C_{60} and $C_{59}N$ are also included for comparison.

It is observed from Figure 25 that the electron affinity shows a good correlation with redox potential. However, HOMO, LUMO and HOMO-LUMO gap do not correlate so well with the redox potential. A similar feature was observed for $C_{59}N$ functionalized with OCFGs in Figure 24.

In order to study the correlation between the redox potential and electronic properties, we have decomposed the overall redox potential into an intrinsic electronic structure part and a solvation part. The intrinsic electronic structure part depends only on the molecular structure while the solvation part depends also on the interaction of the molecule with the solvation medium. The decomposition of redox potential into electronic structure part and solvation part for $C_{59}N$ based materials functionalized with OCFGs is shown in Figure 26.

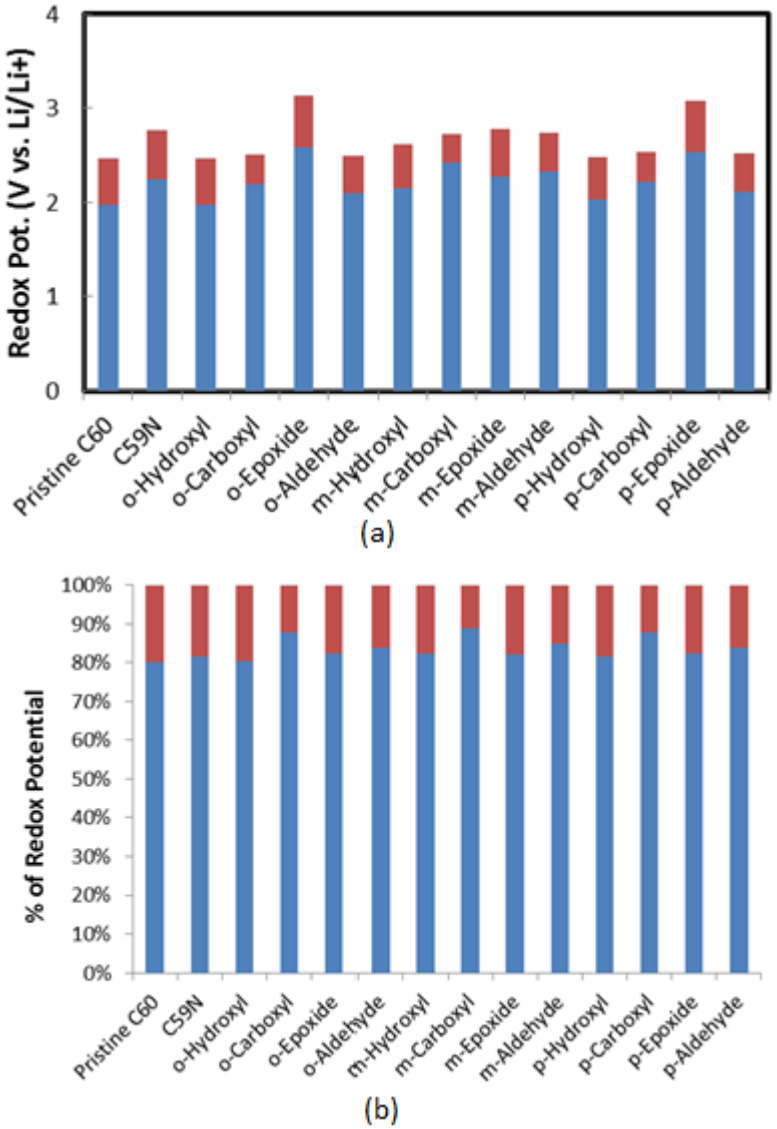

Figure 26: Contributions of electronic structure (blue) and solvation (red)

to redox potential for OCFG-functionalized $C_{59}N$ (a) absolute values (b) percentage contributions

For $C_{59}N$ functionalized with SEWFGs, the decomposition of redox potential is presented in Figure 27 .

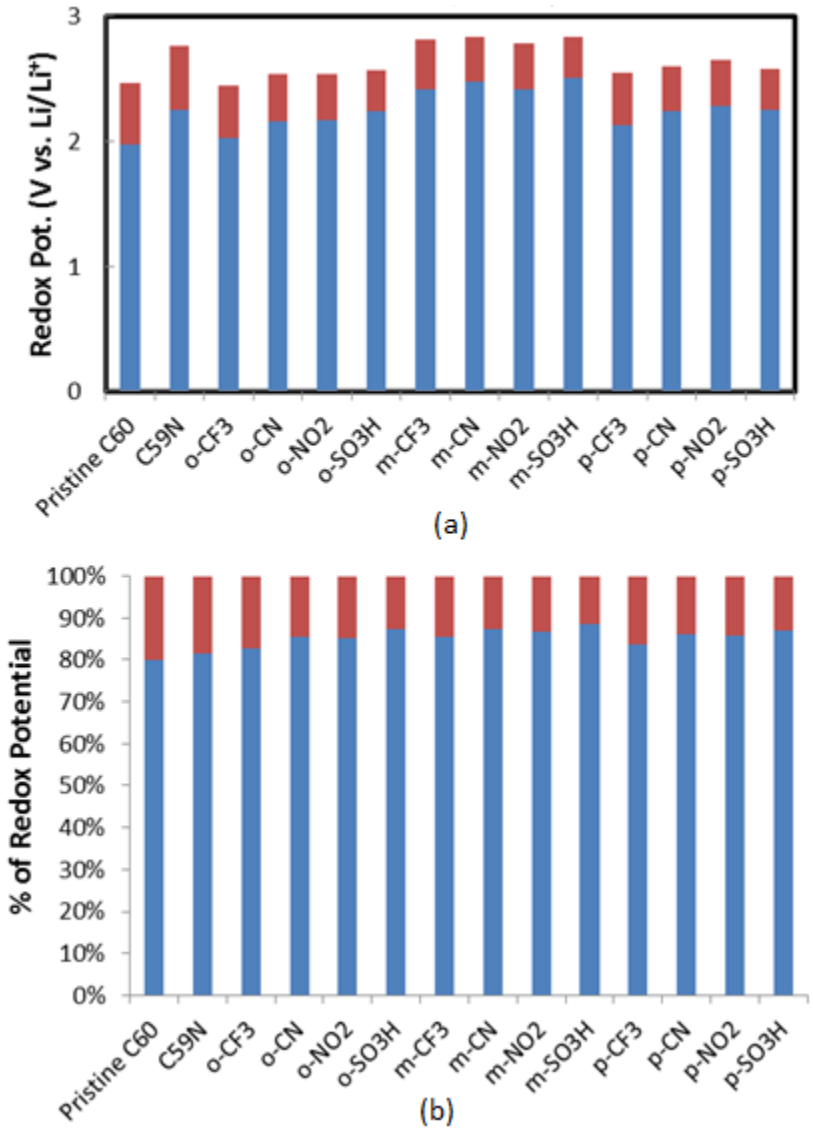

Figure 27: Contributions of electronic structure (blue) and solvation (red) to redox potential for SEWFG-functionalized $C_{59}N$ (a) absolute values (b) percentage contributions

Both absolute and percentage contributions are shown in Figure 26 and Figure 27. It is observed from Figure 26 (b) and Figure 27 (b) that solvation contributes at most 20 percent of the redox potential and usually lower. The contribution of intrinsic electronic structure to redox potential for both the OCFGs and the SEWFGs is atleast 80 percent. Therefore, the intrinsic electronic structure is the major determinant of the redox potential of the material. Since the details of intrinsic electronic structure can be predicted and investigated using DFT, this emphasizes the utility of computational approaches in research, development and design of new materials for redox applications. From Figure 26 (b) and Figure 27 (b), it is observed that the percentage of solvation contribution depends on the functional group but is relatively independent of the position of the functional group relative to the nitrogen atom. Since solvation medium can be changed, the solvation contribution can be altered. This suggests that it would be more meaningful to look for correlations between the intrinsic electronic structure contribution to redox potentials and the electronic properties of the molecules. We have, therefore, investigated the correlation between the intrinsic electronic structure contribution to redox and the LUMO of the closed shell systems. The results are presented in Figure 28 (a) and Figure 28 (b) for OCFGs and SEWFGs respectively.

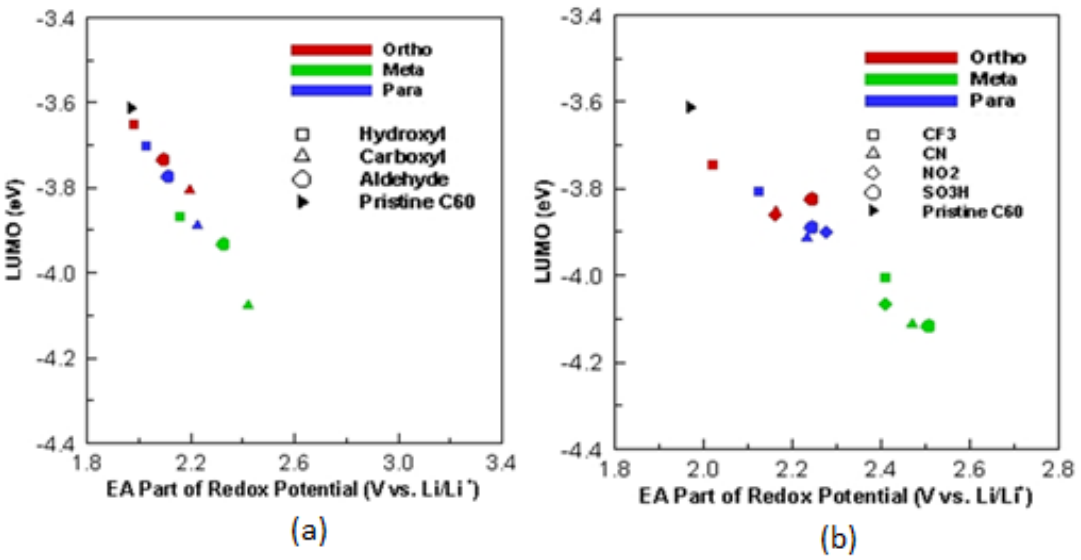

Figure 28: Correlation of LUMO with the redox potential contributed from the electron affinity for (a) closed shell OCFG- functionalized $C_{59}N$ (a) closed shell SEWFG-functionalized $C_{59}N$

Clearly, a very strong correlation is observed between the intrinsic electronic structure part and LUMO for both closed shell OCFGs and SEWFGs. Hence, we infer that LUMO level, which is one of the descriptors of the electronic structure, can be used to rapidly screen closed shell, high redox potential $C_{59}N$ materials provided solvation contributions are small. This strong correlation can be explained because the LUMO level is the lowest energy level available for the closed shell system to gain an electron to form an anion.

The relative stabilities of ortho, meta and para positions of OCFG and SEWFG functionalized $C_{59}N$ are presented in Table 6.

Table 6 Relative stabilities (kcal/mole), of ortho, meta and para positions of OCFGs and SEWFGs in functionalized $C_{59}N$ at 298.15K

	Ortho	Meta	Para
Hydroxyl	0.000	23.708	11.881
Carboxyl	0.000	23.286	5.360
Epoxide	0.000	0.240	11.462
Aldehyde	0.000	20.835	7.250
Trifluoride	0.000	22.917	7.518
Cyano	0.000	21.384	6.231
Nitro	0.000	21.021	8.621
Sulfonate	0.000	21.230	6.806

The relative stabilities can give useful information about the relative amounts of ortho, meta and para functionalized molecules that will be obtained during the synthesis process. It is observed that ortho position relative to the nitrogen is the most stable for all the functional groups. Assuming Boltzmann distribution and using weights obtained from Boltzmann distribution, the position averaged redox potentials for all of the functional groups investigated in this work can be estimated.

6.3 Electronic structure and redox properties of $C_{58}N_2$ and $C_{57}N_3$

The computed redox potentials and electronic properties for multi-nitrogen doped fullerenes are presented in Table 7

Table 7 Redox potentials and electronic properties of multi-nitrogen doped C_{60}

	Redox Potential (V vs. Li/Li^+)	Electron affinity (eV)	HOMO (eV)	LUMO (eV)	Gap (eV)
C_{60}	2.462	-2.666	-6.648	-3.614	3.034
$C_{59}N$	2.760	-2.947	-5.148	-3.685	1.463
$C_{58}N_2$-Ortho	2.735	-2.932	-5.381	-3.864	1.517
$C_{58}N_2$-Meta	2.762	-2.970	-5.316	-3.921	1.394
$C_{58}N_2$-Para	2.559	-2.751	-5.655	-3.728	1.927
$C_{58}N_2$-Dispersed	2.593	-2.803	-5.101	-3.765	1.336
$C_{58}N_2$-Dispersed	2.652	-2.844	-4.985	-3.763	1.222

It is observed that the redox potentials are relatively insensitive to the number of dopant nitrogen atoms. The variation of computed electronic properties with redox potentials for multi-nitrogen doped fullerenes is presented in Figure 29. The insensitivity of redox potentials to the number of dopant nitrogen atoms can be attributed to the shift in LUMO level as is evident from the strong correlation in Figure 29 (c). It is also observed from Figure 29 (a) that the electron affinity shows a good correlation with redox potential.

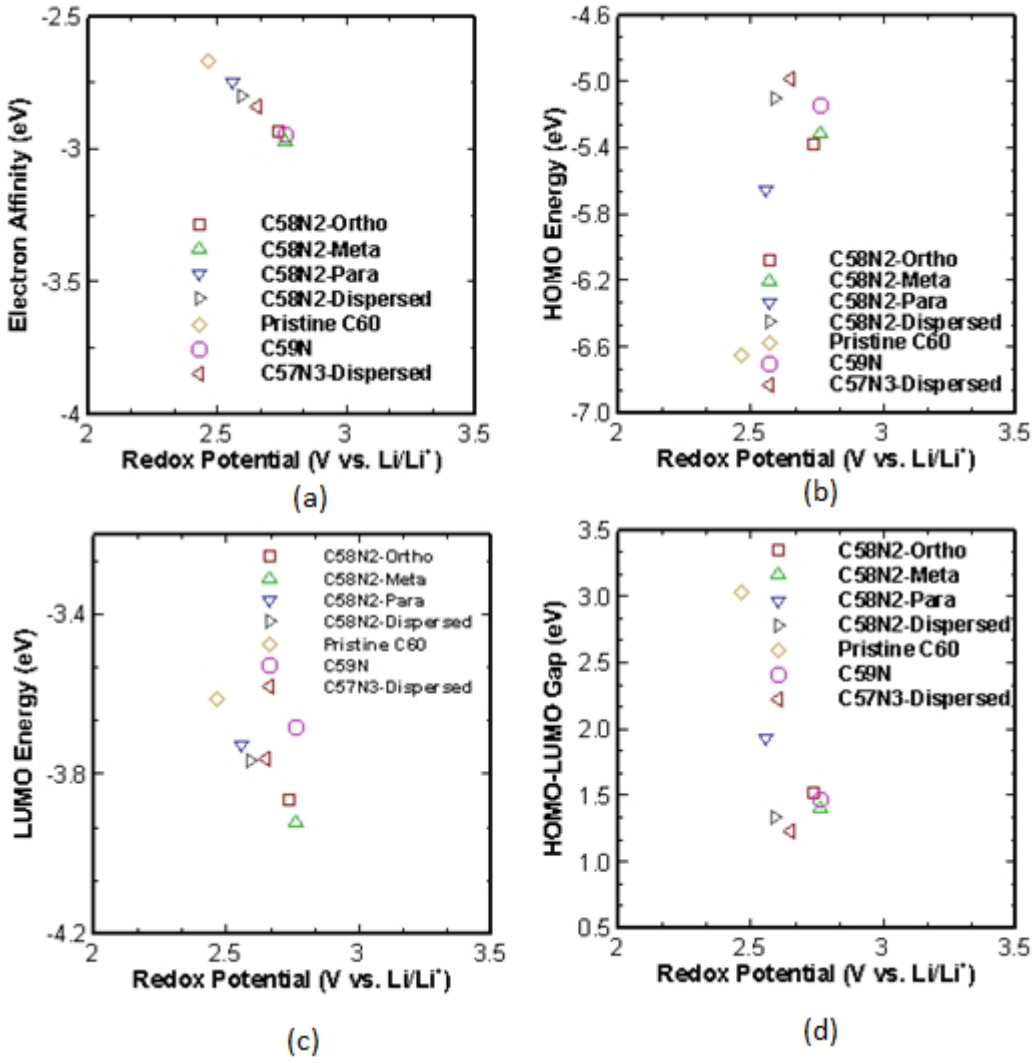

Figure 29: Variations of computed electronic properties with respect to redox potentials for $C_{60-x}N_x$ (x=2,3): (a) electron affinity; (b) HOMO; (c) LUMO;(d) HOMO-LUMO gap. Values for pristine C_{60} and $C_{59}N$ are also indicated on the figure for comparison.

6.4 Conclusions for $C_{59}N$ based materials

For materials obtained by functionalizing $C_{59}N$, it is concluded that functionalization has a limited effect on increasing the redox potential relative to $C_{59}N$.The redox potentials were observed to be relatively insensitive to the position of the OCFGs and SEWFGs, relative to nitrogen, on the hexagonal face of C_{60}. For both OCFGs and SEWFGs, it was found that solvation contributes a minor portion to redox

potential at most 20 percent. Molecular structure is the main determinant of the redox potential contributing atleast 80 percent. For closed shell systems, the intrinsic molecular structure contribution to redox potential correlates quite strongly with the LUMO of these molecules. The minimum redox potential of 2.447 V is obtained for functionalization with trifluoride at the ortho position while the maximum redox potential of 3.135V is obtained by functionalizing with epoxide at the ortho position. This work shows that within this range of redox potentials, multiple choices are available from the functionalized $C_{59}N$ materials. We have also found that some of these molecules are quite close to one another on the redox potential scale and in this sense equivalent. However, these molecules will be non-equivalent in a specific chemical environment with respect to stability and ease of operation. They will also be non-equivalent in terms of ease of synthesis even though their redox potentials are in close proximity to one another. This provides alternatives for designing materials for a specific application within a specific range of redox potentials. Our studies also showed that multiple nitrogen dopants do not have synergistic effect on redox potentials. The small effects of functional groups can be used to fine tune the redox potentials.

CHAPTER 7

REDOX AND ELECTRONIC PROPERTIES OF FUNCTIONALIZED BORON DOPED FULLERENE

In this chapter, we will present the results of our investigations on boron doped fullerene, $C_{59}B$, functionalized with OCFGs and SEWFGs. Our calculations showed that boron doped C_{60}, $C_{59}B$, has about 50 percent higher redox potential compared to C_{60}. From the view point of obtaining high energy density, this is a promising material. Based on chemical intuition, the B-doped fullerene would provide a high positive redox potential that could be possibly be augmented further by introducing functional groups on $C_{59}B$. Besides, the functional groups can also serve as sites for Faradaic reaction with lithium ions thereby giving a high energy and power density material. As described in chapter 3, the OCFGs considered in this work are hydroxyl (-OH), carboxyl (-COOH), epoxide (-O-) and aldehyde (-CHO). The SEWFGs explored in this work are triflouride ($-CF_3$), cyano (-CN), nitro ($-NO_2$) and sulfonates ($-SO_3H$). We have also investigated C_{60} doped with multiple numbers of boron atoms, $C_{58}B_2$ and $C_{57}B_3$, to probe if boron doping has a synergistic effect. This allows us to inquire if a material with higher positive redox potential than $C_{59}B$ can be obtained by simply increasing the number of boron dopants on C_{60}.

7.1 Electronic structure of Pristine C_{60} and $C_{59}B$

When boron is substituted for carbon on the fullerene cage, a relatively electron deficient region is created in the vicinity of boron. Figure 30 shows the comparison of the molecular electrostatic potential profile for pristine C_{60} and $C_{59}B$, expressed in kcal/mole,

superimposed on an iso-charge density surface corresponding to the charge density of 0.001 a.u. Although the wave function extends up to infinity, an iso-value of charge density corresponding to 0.001 a.u. delineates the outer boundary of the molecule. We observe that a region of high positive ESP exists just above the boron atom in $C_{59}B$ indicating that the presence of boron creates a relative electron deficiency in C_{60}.

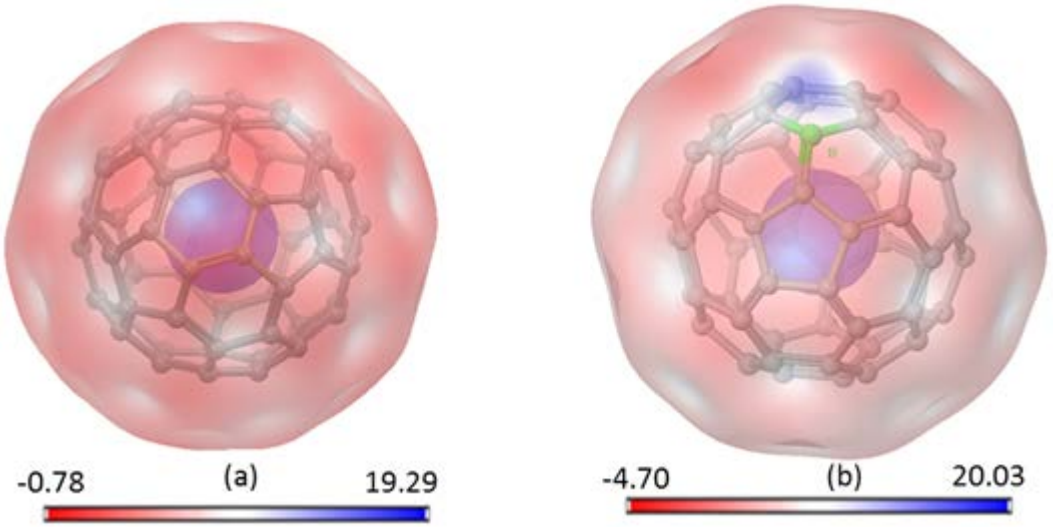

Figure 30: Electrostatic potential profiles, in kcal/mole, superimposed on a 0.001 a.u. charge density profile for (a) Pristine C_{60} and (b) $C_{59}B$. There is an electron deficient region just above boron in (b)

C_{60} doped with one boron atom has one less electron compared to pristine C_{60}, forming an open shell structure. Since frontier orbitals determine the chemical activity of the molecule, the electronic energy levels in the vicinity of HOMO and LUMO are of interest. The electronic energy levels in the vicinity of HOMO and LUMO for pristine C_{60} and $C_{59}B$ are shown in Figure 31.

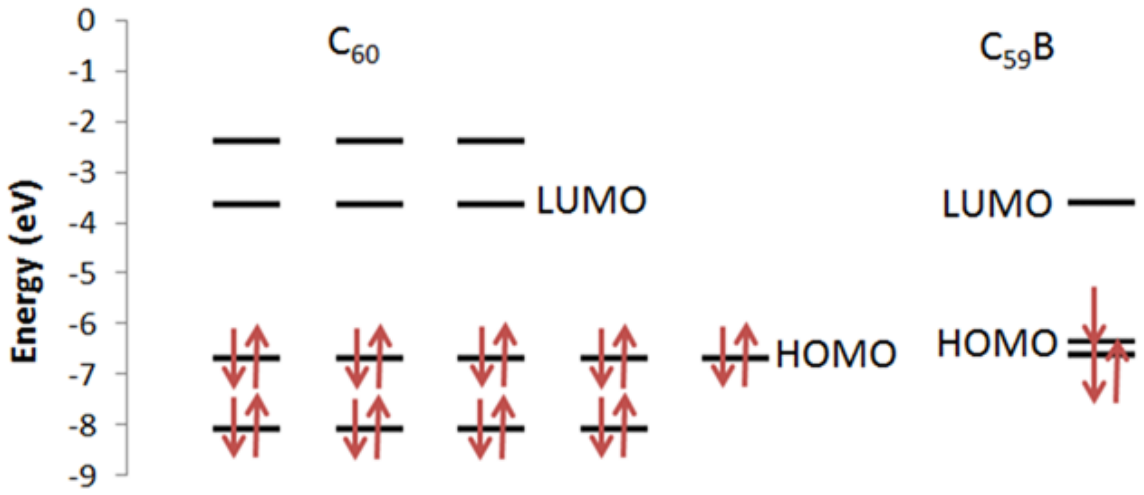

Figure 31: Energy levels and degeneracies in the vicinity of frontier orbitals for pristine C_{60} (left) and $C_{59}B$ (right)

Due to the reduction in symmetry caused by boron doping C_{60} with boron, the degeneracy of the HOMO levels found in pristine C_{60} is broken and a partially occupied HOMO orbital is created with energy of -6.327 eV which is 0.320 eV above the HOMO of pristine C_{60}. This is lower than the LUMO of pristine C_{60}, and so $C_{59}B$ has a strong tendency for accepting an electron in comparison with pristine C_{60}, which accounts for its high electron affinity, an attribute desirable for positive electrode material with high redox potential.

In Figure 32, the HOMO of $C_{59}B$ is compared to that of pristine C_{60} showing that the HOMO of $C_{59}B$ is prominently localized on the boron atom.

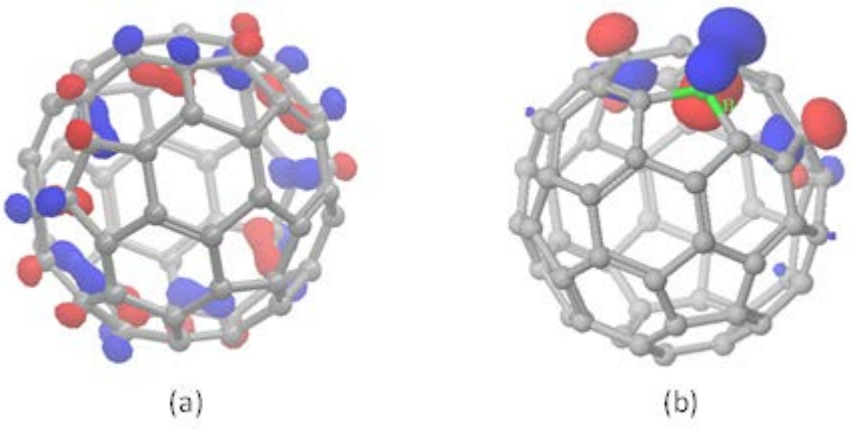

Figure 32: Iso-profile of highest occupied molecular orbital at iso-value of 0.05 (a) Pristine C_{60} and (b) $C_{59}B$. Notice the localization of HOMO on boron atom in (b)

This indicates that boron makes a dominant contribution to create a partially occupied molecular orbital which can accept one more electron to form a closed shell system. Because boron contributes strongly to singly occupied HOMO and is the site of asymmetry in an otherwise symmetric C_{60}, the region around boron is reactive. That is why we have considered functionalization and doping of $C_{59}B$ on positions in close proximity to boron.

7.2 Redox and electronic properties of pristine C_{60}, $C_{59}B$ and functionalized $C_{59}B$

The representative geometry optimized structures for molecules obtained by functionalizing $C_{59}B$, along with the description of their nomenclature is shown in Figure 33.

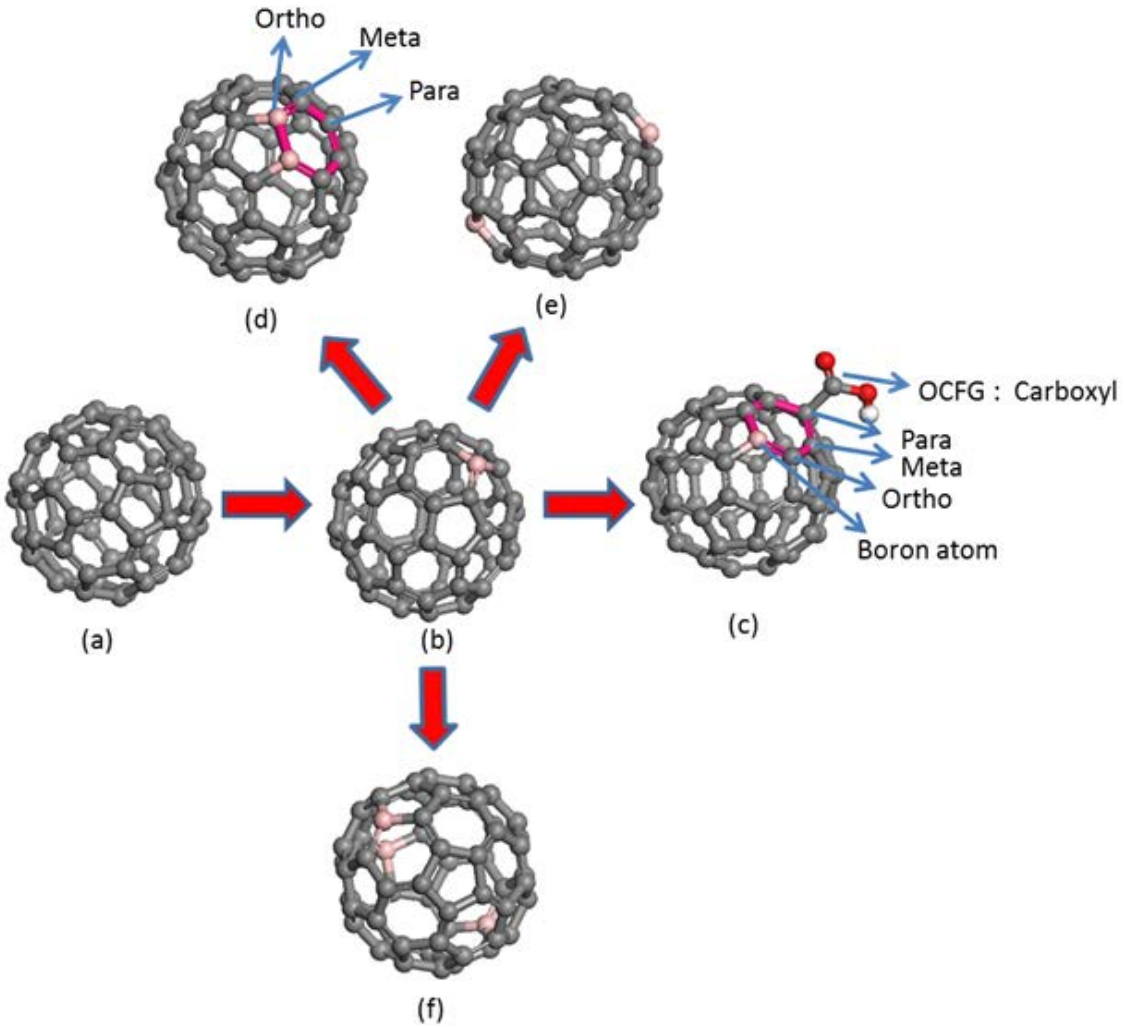

Figure 33: Nomenclature of functionalized and doped $C_{59}B$ based materials investigated in this study (a) Pristine C_{60}, for reference (b) Boron doped C_{60}, $C_{59}B$ (c) $C_{59}B$ functionalized with OCFGs and SEWFGs at different positions relative to boron atom as described in the text: *Ortho, meta and para* positions are indicated for clarity (d) $C_{58}B_2$ with possible *ortho, meta and para* configurations of two boron atoms. (e) $C_{58}B_2$-dispersed configuration (f) $C_{57}B_3$.

All chemical structures considered in this work were optimized for multiple multiplicities to find the multiplicity with the lowest energy. The computed redox potentials and electronic properties of $C_{59}B$, functionalized with OCFGs at ortho, meta and para position relative to the boron atom, as shown schematically in Figure 33, are presented in Table 8.

Table 8 Redox potentials and electronic properties of C_{60}, $C_{59}B$, and OCFG-functionalized $C_{59}B$s. Ortho, meta, and para are the position of OCFG with respect to boron

	Redox Potential (V vs. Li/Li^+)	Electron affinity (eV)	HOMO (eV)	LUMO (eV)	Gap (eV)
C_{60}	2.462	-2.666	-6.648	-3.614	3.034
$C_{59}B$	3.709	-3.835	-6.327	-3.603	2.724
Ortho					
Hydroxyl	2.571	-2.777	-6.520	-3.751	2.770
Carboxyl	2.518	-2.889	-6.643	-3.859	2.783
Epoxide	3.790	-3.939	-6.179	-3.712	2.466
Aldehyde	2.476	-2.779	-6.538	-3.783	2.755
Meta					
Hydroxyl	3.477	-3.667	-5.976	-4.555	1.421
Carboxyl	3.449	-3.772	-6.240	-4.595	1.646
Epoxide	3.668	-3.801	-6.450	-3.675	2.774
Aldehyde	2.521	-2.813	-6.559	-3.790	2.769
Para					
Hydroxyl	2.920	-3.126	-6.550	-3.952	2.598
Carboxyl	2.800	-3.157	-6.683	-4.038	2.645
Epoxide	3.572	-3.690	-6.240	-3.647	2.593
Aldehyde	2.757	-3.040	-6.599	-3.975	2.623

The HOMO and LUMO levels are negative and the HOMO-LUMO gap for the neutral species is positive[204, 205] as expected for the ground state geometry optimized structure of the neutral species. It is observed that amongst the OCFGs, epoxide gives the highest redox potential at ortho, meta and para positions. The hydroxyl and carboxyl groups in the meta positions are strongly reducing than in ortho and para positions. Redox potentials were quite sensitive to the position of the functional group relative to boron atom.

The relationship between the redox and electronic properties of $C_{59}B$-OCFG materials investigated in this work is displayed in Figure 34.

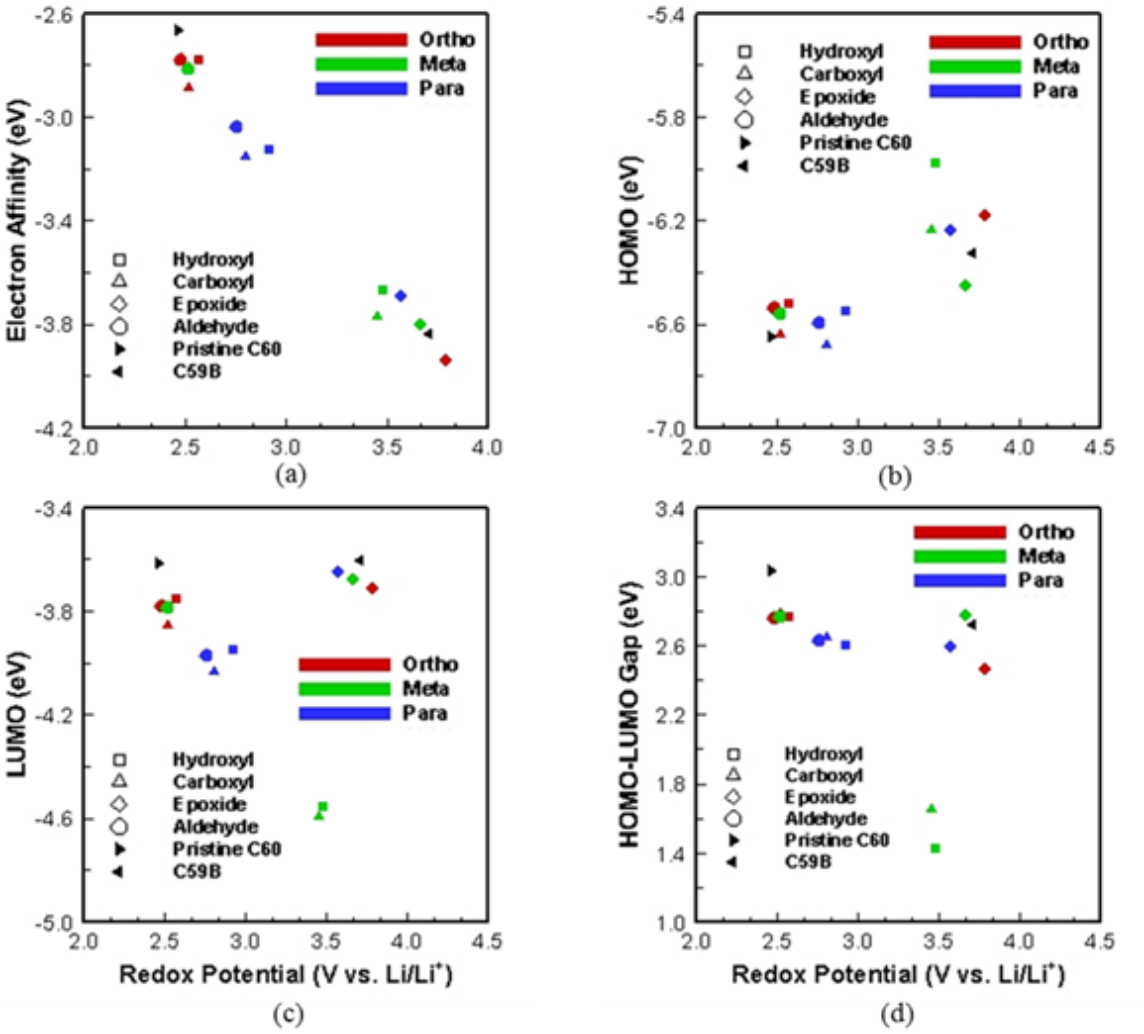

Figure 34: Relationship between computed electronic properties and redox potential for OCFG functionalized $C_{59}B$ in *ortho, meta and para* position with respect to boron: (a) Electron affinity; (b) HOMO level; (c) LUMO level; (d) HOMO-LUMO gap. The *ortho, meta and para* positions are designated with red, green and blue color respectively. Values for pristine C_{60} and $C_{59}B$ are also included for comparison.

It is observed from Figure 34(a) that the electron affinity shows a good correlation with redox potential. However, the correlation of other electronic properties computed in this work i.e. HOMO, LUMO and HOMO-LUMO gap for $C_{59}B$ functionalized with OCFGs is not so strong as seen in Figure 34 (b)-(d) respectively.

The computed redox potentials and electronic properties of $C_{59}B$, functionalized with SEWFGs at ortho, meta and para position relative to the boron atom, as depicted schematically in Figure 33, are shown in Table 9.

Table 9 Redox potentials and electronic properties of C_{60}, $C_{59}B$, and SEWFG-functionalized $C_{59}B$s. Ortho, meta, and para are the position of SEWFG with respect to boron

	Redox Potential (V vs. Li/Li$^+$)	**Electron affinity (eV)**	**HOMO (eV)**	**LUMO (eV)**	**Gap (eV)**
C_{60}	2.462	-2.666	-6.648	-3.614	3.034
$C_{59}B$	3.709	-3.835	-6.327	-3.603	2.724
Ortho					
Trifluoride	2.588	-2.867	-6.599	-3.823	2.776
Cyano	2.634	-2.960	-6.725	-3.918	2.806
Nitro	2.597	-2.771	-6.488	-3.884	2.604
Sulfonate	2.612	-2.988	-6.666	-3.904	2.762
Meta					
Trifluoride	3.373	-3.631	-6.114	-4.571	1.543
Cyano	3.469	-3.755	-6.231	-4.659	1.572
Nitro	3.595	-3.852	-6.216	-4.761	1.455
Sulfonate	3.478	-3.831	-6.198	-4.675	1.524
Para					
Trifluoride	2.839	-3.102	-6.635	-4.017	2.618
Cyano	2.903	-3.209	-6.745	-4.114	2.631
Nitro	3.016	-3.292	-6.734	-4.184	2.550
Sulfonate	2.961	-3.366	-6.650	-4.059	2.591

It is observed that amongst the SEWFGs, the cyano group is most effective in increasing the redox potential when it is present at the meta position. The cyano and nitro groups in meta positions are strongly electron withdrawing than in ortho and para positions. The redox potentials have a strong dependence on the position of functional group relative to the boron atom. The correlation of redox potential with electron affinity, HOMO, LUMO and HOMO-LUMO gap of C_{59}B-SEWFG materials investigated in this work is displayed in Figure 35

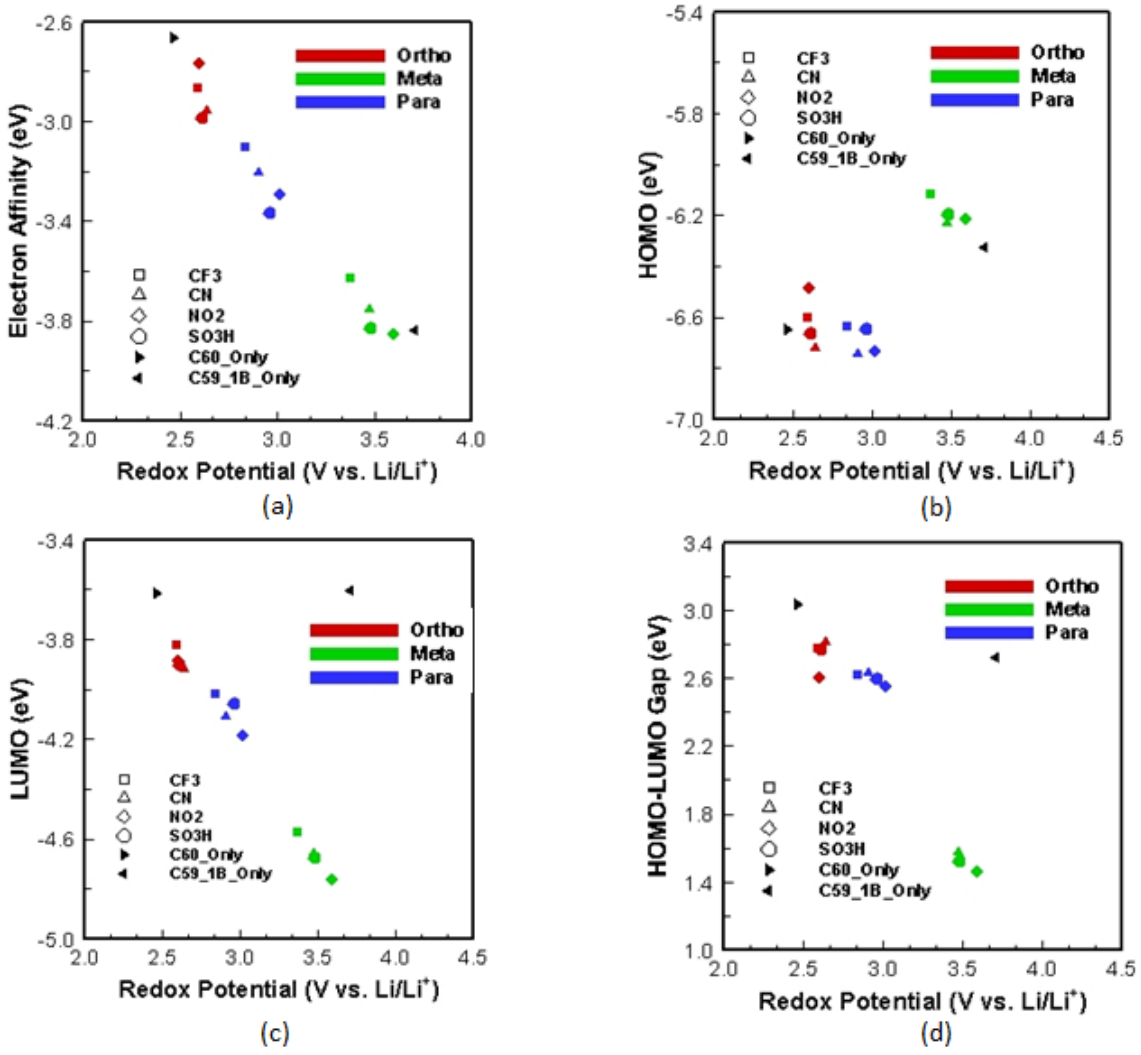

Figure 35: Relationship between computed electronic properties and redox potential for SEWFG functionalized $C_{59}B$ in *ortho, meta and para* position with respect to boron: (a) Electron affinity; (b) HOMO level; (c) LUMO level; (d) HOMO-LUMO gap. The *ortho, meta and para* positions are designated with red, green and blue color respectively. Values for pristine C_{60} and $C_{59}B$ are also included for comparison

It is observed from Figure 35 (a) that the electron affinity shows a good correlation with redox potential. LUMO also shows relatively good correlation with redox potential as is evident in Figure 35 (c). However, HOMO, and HOMO-LUMO gap do not correlate so well with the redox potential. Similarly weak correlation was observed for $C_{59}B$ functionalized with OCFGs.

This is because the overall redox potential is composed of an intrinsic electronic structure part and a solvation part. The intrinsic electronic structure part depends only on the molecular structure while the solvation part depends also on the interaction of the molecule with the solvation medium. The solvation part can be altered by changing the solvation medium and hence the correlation of overall redox potential with any electronic property will be medium dependent. In order to develop molecular descriptors which refer only to the molecular structure and can be used to rapidly screen promising materials for redox potentials, we have decomposed the overall redox potential in an intrinsic electronic structure part and a solvation part. The decomposition of redox potential for $C_{59}B$ based materials functionalized with OCFGs is shown in Figure 36.

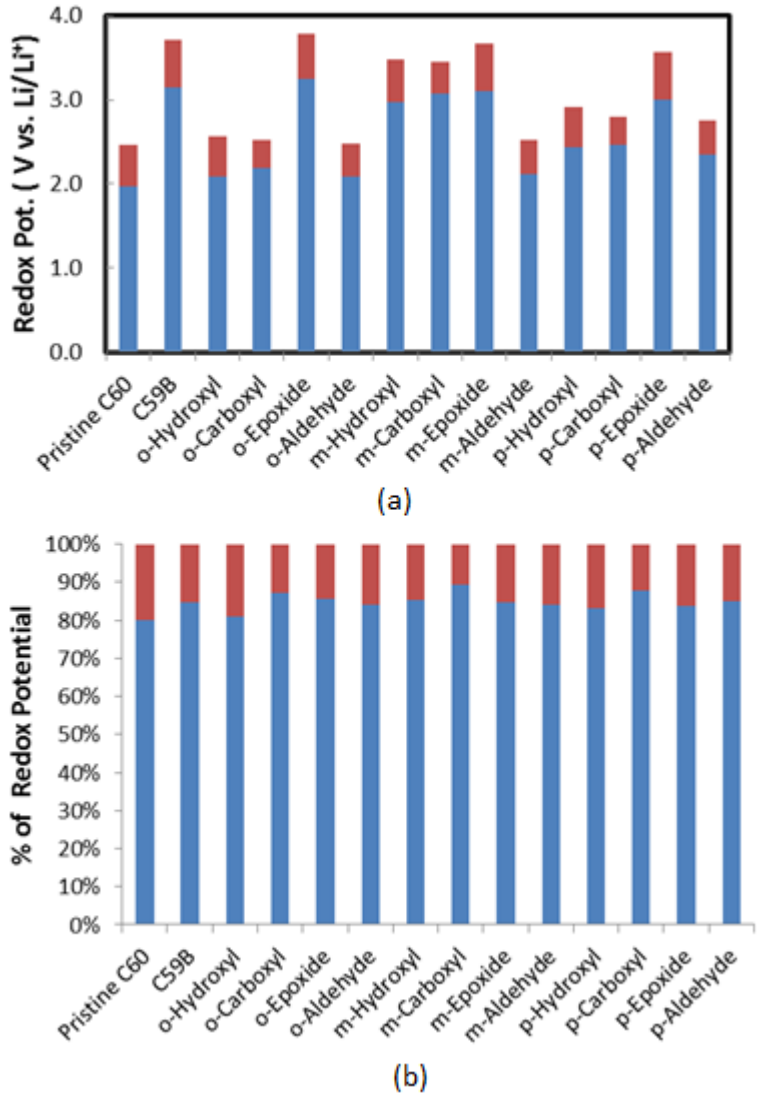

Figure 36: Contributions of electronic structure (blue) and solvation (red) to redox potential for OCFG-functionalized $C_{59}B$ (a) absolute values (b) percentage contributions

The decomposition of redox potential into intrinsic electronic structure part and solvation for $C_{59}B$ functionalized with SEWFGs is shown in Figure 37.

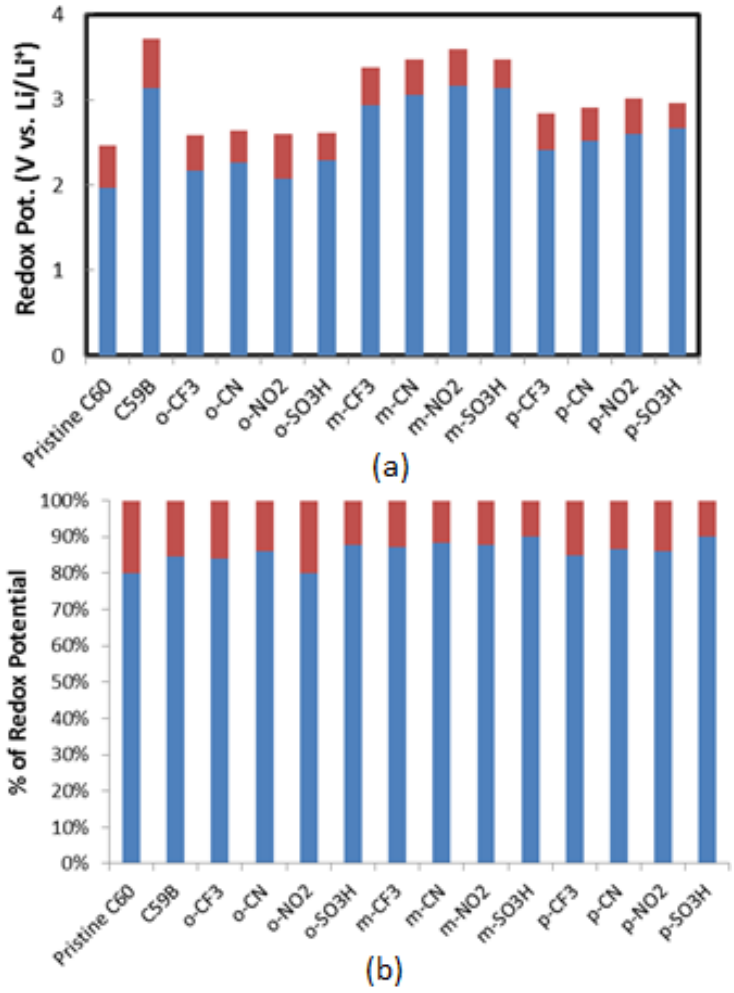

Figure 37: Contributions of electronic structure (blue) and solvation (red) to redox potential for SEWFG-functionalized $C_{59}B$ (a) absolute values (b) percentage contributions

For comparison between the ortho, meta and para positions of OCFGs and SEWFGs, both absolute and percentage contributions are prsented in Figure 36 and Figure 37. It is observed from Figure 36 and Figure 37 that solvation contributes at the most 20 percent of the redox potential and mostly lower. The contribution of intrinsic electronic structure to redox potential is atleast 80 percent. Therefore, the intrinsic electronic structure is the major determinant of the redox potential of the material. Since the details of intrinsic electronic structure can be predicted and investigated using DFT, this emphasizes the

utility of computational approaches in research, development and design of new materials for redox applications. From Figure 36 and Figure 37, it is observed that the percentage of solvation contribution depends on the functional group but is relatively independent of the position of the functional group relative to the boron atom. The electronic affinity part of redox potential refers only to the molecular structure. Therefore, the correlation between the intrinsic electronic structure contribution to redox and the LUMO of the closed shell system has been investigated. The results are presented in Figure 38.

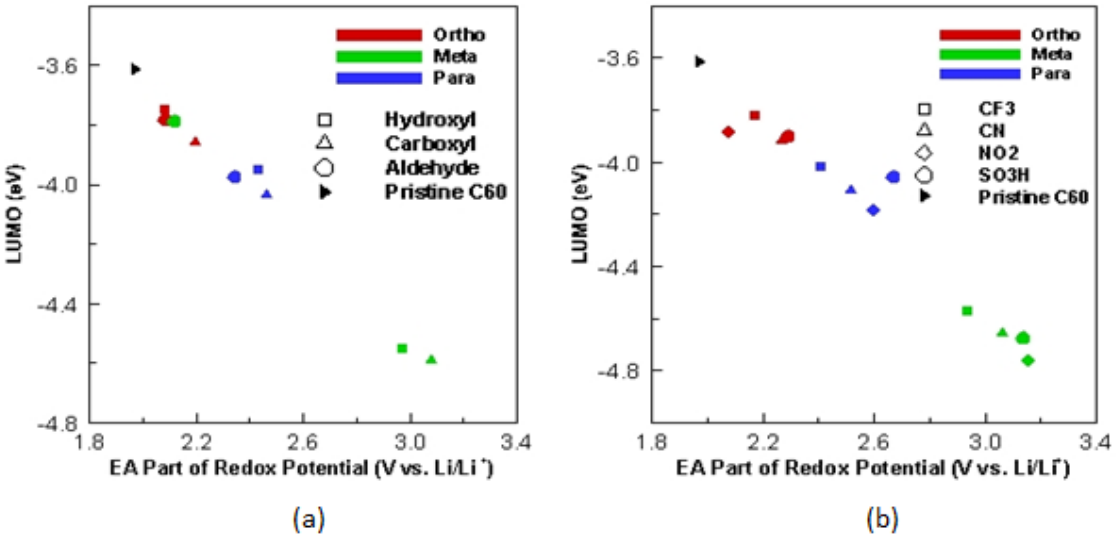

Figure 38: Correlation of LUMO with the redox potential contributed from the electron affinity for (a) closed shell OCFG- functionalized $C_{59}Bs$ (a) closed shell SEWFG-functionalized $C_{59}Bs$

Clearly, a strong correlation is observed between the intrinsic electronic structure part and LUMO for both OCFGs and SEWFGs for closed shell systems. Hence, we infer that LUMO level, which is one of the descriptors of the electronic structure, can be used to rapidly screen high redox potential materials with closed shell structure for which the solvation contribution to redox is small compared to intrinsic electronic structure

contribution. This strong correlation can be explained because the LUMO level is the lowest energy level available for the closed shell system to gain an electron to form an anion.

It is observed from Table 8 and Table 9 that the presence of functional groups on $C_{59}B$ actually reduces the redox potential with respect to $C_{59}B$ although OCFGs and SEWFGs have been considered to increase power densities of carbon based electrode materials. We think that such reduction of redox potential is mainly due to the electronic structures of functionalized $C_{59}Bs$. When a functional group is added to $C_{59}B$, the SOMO of $C_{59}B$ is filled with the electrons from the functional group to form a covalent bond. Thus, the tendency of the electrochemical reduction happens to decrease. The preference of the attached position for OCFG and SEWFG is summarized in Table 10.

Table 10 Relative stabilities (kcal/mole), of ortho, meta and para positions of OCFGs and SEWFGs in functionalized $C_{59}B$ at 298.15K

	Ortho	**Meta**	**Para**
Hydroxyl	0.000	25.391	3.943
Carboxyl	0.000	24.999	9.430
Epoxide	0.000	-6.645	-19.082
Aldehyde	0.000	-2.973	6.448
Trifluoride	0.000	28.499	8.997
Cyano	0.000	29.647	10.549
Nitro	0.000	37.141	17.263
Sulfonate	0.000	28.589	12.181

Hydroxyl and carboxyl groups prefer ortho position from boron while epoxide and aldehyde groups prefer para and meta positons, respectively. The ortho position is the most stable position for all the SEWFGs investigated in this work.

7.3 Electronic structure and redox properties of $C_{58}B_2$ and $C_{57}B_3$

The computed redox potentials and electronic properties for multi-boron doped fullerenes are given in Table 11.

Table 11 Redox potentials and electronic properties of multi-boron doped C_{60}

	Redox Potential (V vs. Li/Li^+)	**Electron affinity (eV)**	**HOMO (eV)**	**LUMO (eV)**	**Gap (eV)**
C_{60}	2.462	-2.666	6.648	3.614	3.034
$C_{59}B$	3.709	-3.835	6.327	3.603	2.724
$C_{58}B_2$-Ortho	3.503	-3.690	6.320	4.580	1.740
$C_{58}B_2$-Meta	3.652	-3.770	6.264	3.567	2.698
$C_{58}B_2$-Para	3.233	-3.407	6.541	4.293	2.248
$C_{58}B_2$-Dispersed	3.298	-3.436	6.510	4.991	1.519
$C_{57}B_3$-Dispersed	3.893	-4.058	6.446	4.844	1.602

It is observed that the redox potentials are quite sensitive to the number of boron substituents on the C_{60} cage with $C_{57}B_3$ showing the highest redox potential of 3.893 V. Although the redox potentials of $C_{58}B_2$ are lower than $C_{59}B$, they are quite high relative to pristine C_{60} showing upto 40 percent increase. The variation of computed electronic properties with redox potentials for multi-boron doped fullerenes is presented in Figure 39.

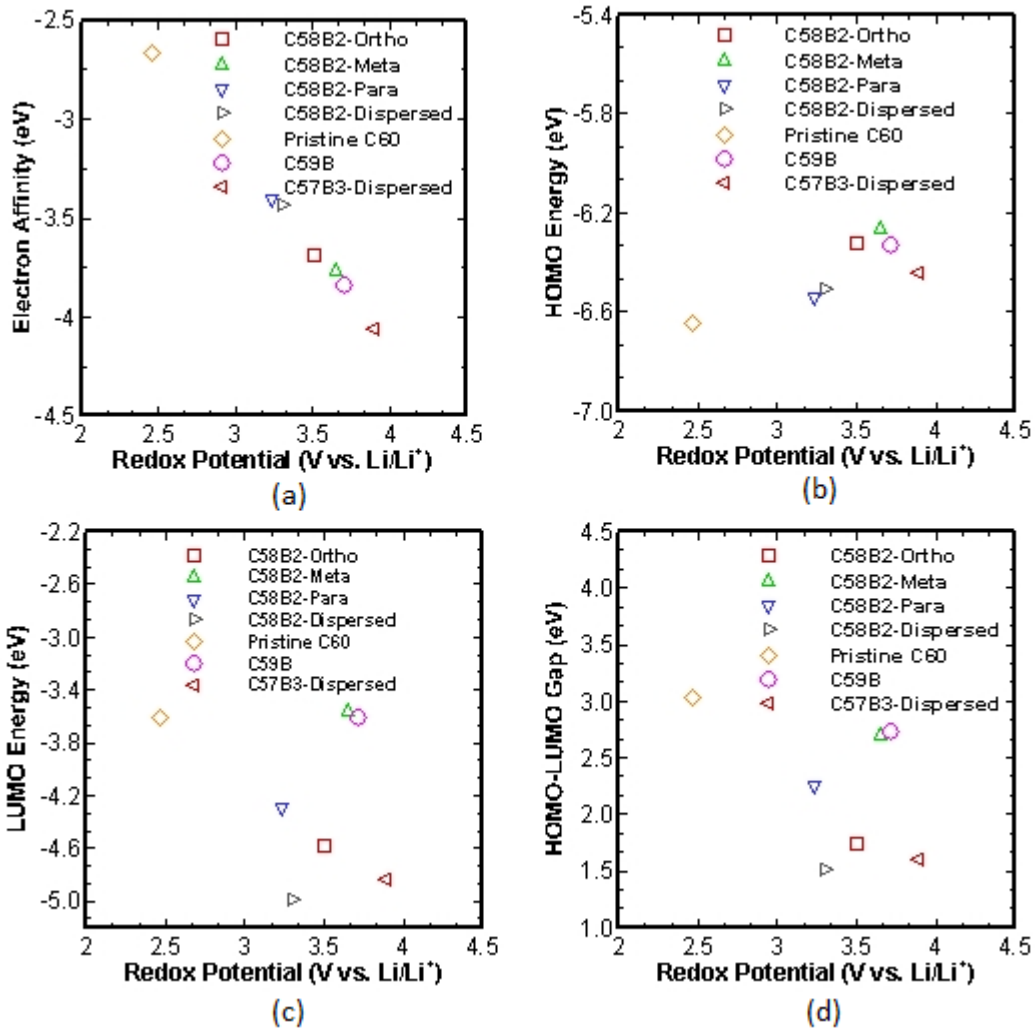

Figure 39: Variations of Computed electronic properties with respect to redox potentials for $C_{60-x}B_x$ (x=2,3): (a) electron affinity; (b) HOMO; (c) LUMO;(d) HOMO-LUMO gap. Values for pristine C_{60} and $C_{59}B$ are also indicated on the figure for comparison.

It is observed from Figure 39 that the electron affinity shows a good correlation with redox potential and LUMO level shows good correlation with redox potential for $C_{58}B_2$ molecules. The relative stabilities of $C_{58}B_2$ molecules is presented in Table 12

Table 12: Relative stabilities (kcal/mole), of ortho, meta, para and dispersed positions of $C_{58}B_2$ at 298.15K

$C_{58}B_2$ - Ortho	$C_{58}B_2$ - Meta	$C_{58}B_2$ -Para	$C_{58}B_2$ -Dispersed
0.000	-11.608	-30.066	-9.694

It is observed from Table 12 that para position is the most stable position for the second boron atom on the fullerene cage.

7.4 Conclusions for $C_{59}B$ based materials

For $C_{59}B$ based materials, it is concluded, the redox potentials are quite sensitive to the position of the OCFGs and SEWFGs, relative to boron, on C_{60} cage. The intrinsic electronic structure is the major contributor to redox potential with solvation contribution being substantially smaller, at the most 20 percent. LUMO level can be used as a reliable predictor of intrinsic contribution to redox potential for $C_{59}B$ based materials functionalized with OCFGs and SEWFGs. The minimum and maximum values of redox potentials (vs. Li/Li^+) for $C_{59}B$ based materials are respectively 2.476 V for $C_{59}B$-CHO and 3.893 for $C_{57}B_3$. This study shows that $C_{59}B$ based materials present multiple choices for material selection within this range of redox potentials. Some of the molecules investigated in this study have similar redox potentials. However, these molecules will be non-equivalent in a specific chemical environment with respect to stability and ease of operation. They will also be non-equivalent in terms of ease of synthesis even though their redox potentials are in close proximity to one another. This provides alternatives for designing materials for a specific application within a specific range of redox potentials.

CHAPTER 8

SUMMARY AND FUTURE WORK

A review of literature on the computational and electrochemical aspects of fullerene based materials shows that doped and functionalized fullerene based materials have not been systematically investigated for their electrochemical and related electronic aspects. This is a first study of its kind to systematically investigate the redox properties of pristine and doped fullerenes functionalized with OCFGs and SEWFGs. Using DFT we have obtained converged wave functions, electronic structure and minimal energy ground state chemical structures which are the starting point for obtaining all other structural, chemical and electronic properties of the molecule. These properties also constitute the input for higher temporal and spatial scale methods such as MD, mesoscale modeling and continuum level FEM models in a multiscale modeling framework. Using DFT, we have obtained thermochemical information for the materials which is essential input for thermodynamic modeling in the CALPHAD paradigm[73]. This work quantitatively explores the redox properties of fullerene based materials and investigates the relationship between the electrochemical properties and the electronic structure.

The research and development of novel materials for lithium ion batteries is a continuing work both computationally and experimentally. The rich chemistry of carbon means that even a compendium of structures of carbon based materials will fill several volumes. Thus, in this sense, this work is scratching the surface of the possibilities and potential for investigation of fullerene based materials for lithium ion battery applications. In order to get a deeper and more comprehensive insight into the calculated

electronic and electrochemical properties of fullerene based materials for lithium ion batteries, we intend to build on the foundation laid down in this work and carry it forward in future in the following direction:

1. Based on the DFT study of lithium interaction with C_{60} carried out in this work, a force field for modeling interaction of Li with C_{60} for MD simulations will be developed. The development of an accurate and reliable force field is an essential requirement for carrying out MD simulations
2. Perform MD simulations to simulate a bulk C60-Li system. MD simulations will give insight into Li diffusion and distribution in the vicinity of C_{60} in bulk systems. This aspect is important since a realistic cell system can only be modeled using several thousand atoms for which DFT method is computationally unfeasible.
3. The interactions in MD are modeled as two body terms. It is anticipated that a high quality, accurate Li-C_{60} force field will also be useful for future simulations as more components such as electrolytes are added to the model Li-C_{60} system.
4. Multiply charged anionic states of $C_{59}N$ and $C_{59}B$ will be explored for stability, electronic structure and properties. Compared to $C_{60,}$ $C_{59}N$ and $C_{59}B$ are asymmetric. It would be interesting to see how and where additional electrons are accommodated on the fullerene cage as the anionic charge on the molecule is increased. We are also interested in investigating the variation of electron affinity of $C_{59}N$ and $C_{59}B$ with increasing anionic charge and how it compares to pristine $C_{60.}$ The simulations for this study are currently in progress and have been partially completed.

5. A systematic study of lithium insertion and binding energies on nitrogen doped fullerene ($C_{59}N$) and boron doped fullerene ($C_{59}B$) will be carried out. It would be interesting to observe how the Lithium insertion behavior of these two materials compares with pristine $C_{60.}$ The simulations for this study are currently in progress.
6. We would like to study the redox and electronic properties of C_{60} cage functionalized with multiple numbers of OCFGs and SEWFGs. It is anticipated that redox properties can be modified and tailored in a specific direction by changing the relative position and number of functional groups on the fullerene cage. The quantitative extent of this change, its relationship to the electronic structure, the possibility of observing patterns in the evolution of redox and electronic properties from which additional general guidelines for designing fullerene based materials for lithium ion battery applications is of interest to us.
7. Lastly, we would like to explore functionalization of C_{60} with other more complex functional groups[161, 208]. Fullerene has a rich chemistry and fullerene based materials are being reported continuously[209-211]. Because of the anticipation of base high electron affinity due to the presence of fullerene cage, these materials are of interest.

REFERENCES

[1] Goodenough, J. B. and Park, K.-S., "The Li-Ion Rechargeable Battery: A Perspective," Journal of the American Chemical Society, vol. 135 (4), pp. 1167-1176, 2013.

[2] Du Pasquier, A., Plitz, I., Menocal, S. and Amatucci, G., "A comparative study of Li-ion battery, supercapacitor and nonaqueous asymmetric hybrid devices for automotive applications," Journal of Power Sources, vol. 115 (1), pp. 171-178, 2003.

[3] Tarascon, J. M. and Armand, M., "Issues and challenges facing rechargeable lithium batteries," Nature, vol. 414 (6861), pp. 359-367, 2001.

[4] Van Noorden, R., "The rechargeable revolution: A better battery," Nature, vol. 507 (7490), pp. 26-8, 2014.

[5] Padhi, A. K., Nanjundaswamy, K. S. and Goodenough, J. B., "Phospho-olivines as Positive-Electrode Materials for Rechargeable Lithium Batteries," Journal of The Electrochemical Society, vol. 144 (4), pp. 1188-1194, 1997.

[6] Winter, M., Besenhard, J. O., Spahr, M. E. and Novák, P., "Insertion Electrode Materials for Rechargeable Lithium Batteries," Advanced Materials, vol. 10 (10), pp. 725-763, 1998.

[7] Li, H., Wang, Z., Chen, L. and Huang, X., "Research on Advanced Materials for Li-ion Batteries," Advanced Materials, vol. 21 (45), pp. 4593-4607, 2009.

[8] Hirsch, A., "The era of carbon allotropes," Nat Mater, vol. 9 (11), pp. 868-871, 2010.

[9] de las Casas, C. and Li, W., "A review of application of carbon nanotubes for lithium ion battery anode material," Journal of Power Sources, vol. 208 pp. 74-85, 2012.

[10] Goriparti, S., Miele, E., De Angelis, F., Di Fabrizio, E., Proietti Zaccaria, R. and Capiglia, C., "Review on recent progress of nanostructured anode materials for Li-ion batteries," Journal of Power Sources, vol. 257 pp. 421-443, 2014.

[11] Zhang, L. L., Zhou, R. and Zhao, X. S., "Graphene-based materials as supercapacitor electrodes," Journal of Materials Chemistry, vol. 20 (29), pp. 5983-5992, 2010.

[12] Pandolfo, A. G. and Hollenkamp, A. F., "Carbon properties and their role in supercapacitors," Journal of Power Sources, vol. 157 (1), pp. 11-27, 2006.

[13] McCreery, R. L., "Advanced carbon electrode materials for molecular electrochemistry," Chemical reviews, vol. 108 (7), pp. 2646-87, 2008.

[14] Balandin, A. A., Ghosh, S., Bao, W., Calizo, I., Teweldebrhan, D., Miao, F. and Lau, C. N., "Superior Thermal Conductivity of Single-Layer Graphene," Nano Letters, vol. 8 (3), pp. 902-907, 2008.

[15] Kumar, A., Reddy, A. L. M., Mukherjee, A., Dubey, M., Zhan, X., Singh, N., Ci, L., Billups, W. E., Nagurny, J., Mital, G. and Ajayan, P. M., "Direct Synthesis of Lithium-Intercalated Graphene for Electrochemical Energy Storage Application," ACS Nano, vol. 5 (6), pp. 4345-4349, 2011.

[16] Luo, J.-Y., Cui, W.-J., He, P. and Xia, Y.-Y., "Raising the cycling stability of aqueous lithium-ion batteries by eliminating oxygen in the electrolyte," Nat Chem, vol. 2 (9), pp. 760-765, 2010.

[17] Kohn, W. and Sham, L. J., "Self-Consistent Equations Including Exchange and Correlation Effects," Physical Review, vol. 140 (4A), pp. A1133-A1138, 1965.

[18] Karplus, M. and Petsko, G. A., "Molecular dynamics simulations in biology," Nature, vol. 347 (6294), pp. 631-639, 1990.

[19] Groot, R. D. and Warren, P. B., "Dissipative particle dynamics: Bridging the gap between atomistic and mesoscopic simulation," The Journal of Chemical Physics, vol. 107 (11), pp. 4423-4435, 1997.

[20] Newman, J. and Tiedemann, W., "Porous-electrode theory with battery applications," AIChE Journal, vol. 21 (1), pp. 25-41, 1975.

[21] Persson, K., Hinuma, Y., Meng, Y. S., Van der Ven, A. and Ceder, G., "Thermodynamic and kinetic properties of the Li-graphite system from first-principles calculations," Physical Review B, vol. 82 (12), pp. 125416, 2010.

[22] Loftager, S., García-Lastra, J. M. and Vegge, T., "A Density Functional Theory Study of the Ionic and Electronic Transport Mechanisms in $LiFeBO_3$ Battery Electrodes," The Journal of Physical Chemistry C, vol. 120 (33), pp. 18355-18364, 2016.

[23] Kim, K. C., Liu, T., Lee, S. W. and Jang, S. S., "First-Principles Density Functional Theory Modeling of Li Binding: Thermodynamics and Redox Properties of Quinone Derivatives for Lithium-Ion Batteries," Journal of the American Chemical Society, vol. 138 (7), pp. 2374-2382, 2016.

[24] Doyle, M., Fuller, T. F. and Newman, J., "Modeling of Galvanostatic Charge and Discharge of the Lithium/Polymer/Insertion Cell," Journal of The Electrochemical Society, vol. 140 (6), pp. 1526-1533, 1993.

[25] Nitta, N., Wu, F., Lee, J. T. and Yushin, G., "Li-ion battery materials: present and future," Materials Today, vol. 18 (5), pp. 252-264, 2015.

[26] In *Materials Selection in Mechanical Design (Fourth Edition)*, Ashby, M. F., Ed. Butterworth-Heinemann: Oxford, 2011; pp i-ii.

[27] Bhatt, M. D. and O'Dwyer, C., "Recent progress in theoretical and computational investigations of Li-ion battery materials and electrolytes," Physical Chemistry Chemical Physics, vol. 17 (7), pp. 4799-4844, 2015.

[28] Whittingham, M. S., "Lithium Batteries and Cathode Materials," Chemical Reviews, vol. 104 (10), pp. 4271-4302, 2004.

[29] Tarascon, J. M., Wang, E., Shokoohi, F. K., McKinnon, W. R. and Colson, S., "The Spinel Phase of $LiMn_2O_4$ as a Cathode in Secondary Lithium Cells," Journal of The Electrochemical Society, vol. 138 (10), pp. 2859-2864, 1991.

[30] Guohua, L., Ikuta, H., Uchida, T. and Wakihara, M., "The Spinel Phases $LiM_yMn_{2-y}O_4$ (M = Co, Cr, Ni) as the Cathode for Rechargeable Lithium Batteries," Journal of The Electrochemical Society, vol. 143 (1), pp. 178-182, 1996.

[31] Park, K.-Y., Hong, J., Kim, J., Park, Y.-U., Kim, H., Seo, D.-H., Kim, S.-W., Choi, J.-W. and Kang, K., "Factors that Affect the Phase Behavior of Multi-Component Olivine ($LiFe_xMn_yCo1_{-x-y}PO_4$; $0 < x, y < 1$) in Lithium Rechargeable Batteries: One-Phase Reaction vs. Two-Phase Reaction," Journal of The Electrochemical Society, vol. 160 (3), pp. A444-A448, 2013.

[32] Li, D. and Zhou, H., "Two-phase transition of Li-intercalation compounds in Li-ion batteries," Materials Today, vol. 17 (9), pp. 451-463, 2014.

[33] Julien, C., Mauger, A., Zaghib, K. and Groult, H., "Comparative Issues of Cathode Materials for Li-Ion Batteries," Inorganics, vol. 2 (1), pp. 132, 2014.

[34] Islam, M. S. and Fisher, C. A. J., "Lithium and sodium battery cathode materials: computational insights into voltage, diffusion and nanostructural properties," Chemical Society Reviews, vol. 43 (1), pp. 185-204, 2014.

[35] He, H., Liu, B., Abouimrane, A., Ren, Y., Liu, Y., Liu, Q. and Chao, Z.-S., "Dynamic Lithium Intercalation/Deintercalation in 18650 Lithium Ion Battery by Time-Resolved High Energy Synchrotron X-Ray Diffraction," Journal of The Electrochemical Society, vol. 162 (10), pp. A2195-A2200, 2015.

[36] Aurbach, D., Gamolsky, K., Markovsky, B., Salitra, G., Gofer, Y., Heider, U., Oesten, R. and Schmidt, M., "The Study of Surface Phenomena Related to Electrochemical Lithium Intercalation into Li_xMO_y Host Materials (M = Ni, Mn)," Journal of The Electrochemical Society, vol. 147 (4), pp. 1322-1331, 2000.

[37] Ohzuku, T., Iwakoshi, Y. and Sawai, K., "Formation of Lithium-Graphite Intercalation Compounds in Nonaqueous Electrolytes and Their Application as a Negative Electrode for a Lithium Ion (Shuttlecock) Cell," Journal of The Electrochemical Society, vol. 140 (9), pp. 2490-2498, 1993.

[38] Jache, B. and Adelhelm, P., "Use of Graphite as a Highly Reversible Electrode with Superior Cycle Life for Sodium-Ion Batteries by Making Use of Co-Intercalation Phenomena," Angewandte Chemie International Edition, vol. 53 (38), pp. 10169-10173, 2014.

[39] Ammundsen, B. and Paulsen, J., "Novel Lithium-Ion Cathode Materials Based on Layered Manganese Oxides," Advanced Materials, vol. 13 (12-13), pp. 943-956, 2001.

[40] Fergus, J. W., "Recent developments in cathode materials for lithium ion batteries," Journal of Power Sources, vol. 195 (4), pp. 939-954, 2010.

[41] Mueller, T., Hautier, G., Jain, A. and Ceder, G., "Evaluation of Tavorite-Structured Cathode Materials for Lithium-Ion Batteries Using High-Throughput Computing," Chemistry of Materials, vol. 23 (17), pp. 3854-3862, 2011.

[42] Longo, R. C., Xiong, K., Kc, S. and Cho, K., "Crystal structure and multicomponent effects in Tetrahedral Silicate Cathode Materials for Rechargeable Li-ion Batteries," Electrochimica Acta, vol. 121 pp. 434-442, 2014.

[43] Thackeray, M. M., "Structural Considerations of Layered and Spinel Lithiated Oxides for Lithium Ion Batteries," Journal of The Electrochemical Society, vol. 142 (8), pp. 2558-2563, 1995.

[44] Li, R. F., Wu, S. Q., Yang, Y. and Zhu, Z. Z., "Structural and Electronic Properties of Li-Ion Battery Cathode Material FeF_3," The Journal of Physical Chemistry C, vol. 114 (39), pp. 16813-16817, 2010.

[45] Wu, S. Q., Zhang, J. H., Zhu, Z. Z. and Yang, Y., "Structural and electronic properties of the Li-ion battery cathode material Li_xCoSiO_4," Current Applied Physics, vol. 7 (6), pp. 611-616, 2007.

[46] Li, A. Y., Wu, S. Q., Yang, Y. and Zhu, Z. Z., "Structural and electronic properties of Li-ion battery cathode material MoF_3 from first-principles," Journal of Solid State Chemistry, vol. 227 pp. 25-29, 2015.

[47] Melot, B. C., Rousse, G., Chotard, J. N., Ati, M., Rodríguez-Carvajal, J., Kemei, M. C. and Tarascon, J. M., "Magnetic Structure and Properties of the Li-Ion Battery Materials $FeSO_4F$ and $LiFeSO_4F$," Chemistry of Materials, vol. 23 (11), pp. 2922-2930, 2011.

[48] Shin, D., Kercher, A. K., Kiggans, J. and Dudney, N. J., "Computational Thermodynamic Modeling of Mixed Polyanion Glasses for Lithium Ion Battery Cathode Materials," Meeting Abstracts, vol. MA2013-02 (8), pp. 597, 2013.

[49] Shang, S. L., Wang, Y., Mei, Z. G., Hui, X. D. and Liu, Z. K., "Lattice dynamics, thermodynamics, and bonding strength of lithium-ion battery materials $LiMPO_4$ (M = Mn, Fe, Co, and Ni): a comparative first-principles study," Journal of Materials Chemistry, vol. 22 (3), pp. 1142-1149, 2012.

[50] Ceder, G., "Opportunities and challenges for first-principles materials design and applications to Li battery materials," MRS Bulletin, vol. 35 (09), pp. 693-701, 2010.

[51] Shi, S., Qi, Y., Li, H. and Hector, L. G., "Defect Thermodynamics and Diffusion Mechanisms in Li_2CO_3 and Implications for the Solid Electrolyte Interphase in Li-Ion Batteries," The Journal of Physical Chemistry C, vol. 117 (17), pp. 8579-8593, 2013.

[52] Kim, Y., Kim, D. and Kang, S., "Experimental and First-Principles Thermodynamic Study of the Formation and Effects of Vacancies in Layered Lithium Nickel Cobalt Oxides," Chemistry of Materials, vol. 23 (24), pp. 5388-5397, 2011.

[53] Ceder, G. and Van Der Ven, A., "Phase diagrams of lithium transition metal oxides: investigations from first principles," Electrochimica Acta, vol. 45 (1), pp. 131-150, 1999.

[54] Burke, K. and Wagner, L. O., "DFT in a nutshell," International Journal of Quantum Chemistry, vol. 113 (2), pp. 96-101, 2013.

[55] Kikuchi, R. and Masuda-Jindo, K., "Cluster variation method in the computational materials science," Calphad, vol. 26 (1), pp. 33-54, 2002.

[56] Ceder, G., Hautier, G., Jain, A. and Ong, S. P., "Recharging lithium battery research with first-principles methods," MRS Bulletin, vol. 36 (03), pp. 185-191, 2011.

[57] Longo, R. C., Kong, F. T., Kc, S., Park, M. S., Yoon, J., Yeon, D. H., Park, J. H., Doo, S. G. and Cho, K., "Phase stability of Li-Mn-O oxides as cathode materials for Li-ion batteries: insights from ab initio calculations," Physical Chemistry Chemical Physics, vol. 16 (23), pp. 11233-11242, 2014.

[58] Wang, L., Maxisch, T. and Ceder, G., "A First-Principles Approach to Studying the Thermal Stability of Oxide Cathode Materials," Chemistry of Materials, vol. 19 (3), pp. 543-552, 2007.

[59] Kang, K. and Ceder, G., "Factors that affect Li mobility in layered lithium transition metal oxides," Physical Review B, vol. 74 (9), pp. 094105, 2006.

[60] Borg, Richard J. In *An Introduction to Solid State Diffusion*, Dienes, G. J., Ed. Academic Press: San Diego, 1988.

[61] Jang, Y.-I., Neudecker, B. J. and Dudney, N. J., "Lithium Diffusion in Li_xCoO_2 ($0.45 < x < 0.7$) Intercalation Cathodes," Electrochemical and Solid-State Letters, vol. 4 (6), pp. A74-A77, 2001.

[62] Van der Ven, A. and Ceder, G., "Lithium Diffusion in Layered Li_xCoO_2," Electrochemical and Solid-State Letters, vol. 3 (7), pp. 301-304, 2000.

[63] Dathar, G. K. P., Sheppard, D., Stevenson, K. J. and Henkelman, G., "Calculations of Li-Ion Diffusion in Olivine Phosphates," Chemistry of Materials, vol. 23 (17), pp. 4032-4037, 2011.

[64] Ouyang, C., Shi, S., Wang, Z., Huang, X. and Chen, L., "First-principles study of Li ion diffusion in $LiFePO_4$," Physical Review B, vol. 69 (10), pp. 104303, 2004.

[65] Chen Yong-Chang, H. M., Liu Yang, Chen Tong, Leng Cheng-Cai, Li Qiang, Sun Zhao-Lin, Song Li-Juan, "Structural, Electrical, and Lithium Ion Dynamics of Li_2MnO_3 from Density Functional Theory," Chin. Phys. Lett., vol. 32 (01), pp. 17102-, 2015.

[66] Xiao, R., Li, H. and Chen, L., "Density Functional Investigation on Li_2MnO_3," Chemistry of Materials, vol. 24 (21), pp. 4242-4251, 2012.

[67] Reed, J. and Ceder, G., "Charge, Potential, and Phase Stability of Layered $Li(Ni_{0.5}Mn_{0.5})O_2$," Electrochemical and Solid-State Letters, vol. 5 (7), pp. A145-A148, 2002.

[68] Winget, P., Cramer, C. J. and Truhlar, D. G., "Computation of equilibrium oxidation and reduction potentials for reversible and dissociative electron-transfer reactions in solution," Theor Chem Acc, vol. 112 (4), pp. 217-227, 2004.

[69] Winget, P., Weber, E. J., Cramer, C. J. and Truhlar, D. G., "Computational electrochemistry: aqueous one-electron oxidation potentials for substituted anilines," Physical Chemistry Chemical Physics, vol. 2 (6), pp. 1231-1239, 2000.

[70] Kelly, C. P., Cramer, C. J. and Truhlar, D. G., "Single-Ion Solvation Free Energies and the Normal Hydrogen Electrode Potential in Methanol, Acetonitrile, and Dimethyl Sulfoxide," The Journal of Physical Chemistry B, vol. 111 (2), pp. 408-422, 2007.

[71] Rychnovsky, S. D., Vaidyanathan, R., Beauchamp, T., Lin, R. and Farmer, P. J., "AM1-SM2 Calculations Model the Redox Potential of Nitroxyl Radicals Such as TEMPO," The Journal of Organic Chemistry, vol. 64 (18), pp. 6745-6749, 1999.

[72] Marenich, A. V., Ho, J., Coote, M. L., Cramer, C. J. and Truhlar, D. G., "Computational electrochemistry: prediction of liquid-phase reduction potentials," Physical Chemistry Chemical Physics, vol. 16 (29), pp. 15068-15106, 2014.

[73] Miodownik, A. P., Phenomenological Calculations of Phase-Equilibria: the Calphad Approach. In *Statics and Dynamics of Alloy Phase Transformations*, Turchi, P. A.; Gonis, A., Eds. Springer US: 1994; Vol. 319, pp 45-79.

[74] Goel, P., Gupta, M. K., Mittal, R., Rols, S., Patwe, S. J., Achary, S. N., Tyagi, A. K. and Chaplot, S. L., "Phonons, lithium diffusion and thermodynamics of $LiMPO_4$ (M = Mn, Fe)," Journal of Materials Chemistry A, vol. 2 (35), pp. 14729-14738, 2014.

[75] Shang, S. L., Hector Jr, L. G., Shi, S., Qi, Y., Wang, Y. and Liu, Z. K., "Lattice dynamics, thermodynamics and elastic properties of monoclinic Li_2CO_3 from density functional theory," Acta Materialia, vol. 60 (13-14), pp. 5204-5216, 2012.

[76] Ganesh, P., Jiang, D.-e. and Kent, P. R. C., "Accurate Static and Dynamic Properties of Liquid Electrolytes for Li-Ion Batteries from ab initio Molecular Dynamics," The Journal of Physical Chemistry B, vol. 115 (12), pp. 3085-3090, 2011.

[77] Johari, P., Qi, Y. and Shenoy, V. B., "The Mixing Mechanism during Lithiation of Si Negative Electrode in Li-Ion Batteries: An Ab Initio Molecular Dynamics Study," Nano Letters, vol. 11 (12), pp. 5494-5500, 2011.

[78] Meunier, V., Kephart, J., Roland, C. and Bernholc, J., "Ab Initio Investigations of Lithium Diffusion in Carbon Nanotube Systems," Physical review letters, vol. 88 (7), pp. 075506, 2002.

[79] Tan, X., Cabrera, C. R. and Chen, Z., "Metallic BSi3 Silicene: A Promising High Capacity Anode Material for Lithium-Ion Batteries," The Journal of Physical Chemistry C, vol. 118 (45), pp. 25836-25843, 2014.

[80] Armstrong, A. R., Lyness, C., Panchmatia, P. M., Islam, M. S. and Bruce, P. G., "The lithium intercalation process in the low-voltage lithium battery anode $Li_{1+x}V_{1-x}O_2$," Nat Mater, vol. 10 (3), pp. 223-229, 2011.

[81] Kazemiabnavi, S., Dutta, P. and Banerjee, S., "Density Functional Theory Based Study of the Electron Transfer Reaction at the Lithium Metal Anode in a Lithium–Air Battery with Ionic Liquid Electrolytes," The Journal of Physical Chemistry C, vol. 118 (47), pp. 27183-27192, 2014.

[82] Arrouvel, C., Parker, S. C. and Islam, M. S., "Lithium Insertion and Transport in the TiO_2-B Anode Material: A Computational Study," Chemistry of Materials, vol. 21 (20), pp. 4778-4783, 2009.

[83] Zhang, T., Li, D., Tao, Z. and Chen, J., "Understanding electrode materials of rechargeable lithium batteries via DFT calculations," Progress in Natural Science: Materials International, vol. 23 (3), pp. 256-272, 2013.

[84] Tasaki, K., "Density Functional Theory Study on Structural and Energetic Characteristics of Graphite Intercalation Compounds," The Journal of Physical Chemistry C, vol. 118 (3), pp. 1443-1450, 2014.

[85] Grimme, S., "Semiempirical GGA-type density functional constructed with a long-range dispersion correction," Journal of computational chemistry, vol. 27 (15), pp. 1787-99, 2006.

[86] Grimme, S., "Density functional theory with London dispersion corrections," Wiley Interdisciplinary Reviews: Computational Molecular Science, vol. 1 (2), pp. 211-228, 2011.

[87] Grimme, S. and Steinmetz, M., "Effects of London dispersion correction in density functional theory on the structures of organic molecules in the gas phase," Physical Chemistry Chemical Physics, vol. 15 (38), pp. 16031-16042, 2013.

[88] Chan, T.-L. and Chelikowsky, J. R., "Controlling Diffusion of Lithium in Silicon Nanostructures," Nano Letters, vol. 10 (3), pp. 821-825, 2010.

[89] Wu, D.-h. and Zhou, Z., "Recent progress of computational investigation on anode materials in Li ion batteries," Front. Phys., vol. 6 (2), pp. 197-203, 2011.

[90] Koh, W., Choi, J. I., Donaher, K., Lee, S. G. and Jang, S. S., "Mechanism of Li Adsorption on Carbon Nanotube-Fullerene Hybrid System: A First-Principles Study," ACS Applied Materials & Interfaces, vol. 3 (4), pp. 1186-1194, 2011.

[91] Koh, W., Choi, J. I., Lee, S. G., Lee, W. R. and Jang, S. S., "First-principles study of Li adsorption in a carbon nanotube-fullerene hybrid system," Carbon, vol. 49 (1), pp. 286-293, 2011.

[92] Koh, W., Lee, J. H., Lee, S. G., Choi, J. I. and Jang, S. S., "Li adsorption on a graphene-fullerene nanobud system: density functional theory approach," RSC Advances, vol. 5 (41), pp. 32819-32825, 2015.

[93] Koh, W., Moon, H. S., Lee, S. G., Choi, J. I. and Jang, S. S., "A First-Principles Study of Lithium Adsorption on a Graphene–Fullerene Nanohybrid System," ChemPhysChem, vol. 16 (4), pp. 789-795, 2015.

[94] Márquez, A. and Balbuena, P. B., "Molecular Dynamics Study of Graphite/Electrolyte Interfaces," Journal of The Electrochemical Society, vol. 148 (6), pp. A624-A635, 2001.

[95] Xing, L., Vatamanu, J., Borodin, O., Smith, G. D. and Bedrov, D., "Electrode/Electrolyte Interface in Sulfolane-Based Electrolytes for Li Ion Batteries: A Molecular Dynamics Simulation Study," The Journal of Physical Chemistry C, vol. 116 (45), pp. 23871-23881, 2012.

[96] An, S. J., Li, J., Daniel, C., Mohanty, D., Nagpure, S. and Wood Iii, D. L., "The state of understanding of the lithium-ion-battery graphite solid electrolyte interphase (SEI) and its relationship to formation cycling," Carbon, vol. 105 pp. 52-76, 2016.

[97] Borodin, O., "Polarizable Force Field Development and Molecular Dynamics Simulations of Ionic Liquids," The Journal of Physical Chemistry B, vol. 113 (33), pp. 11463-11478, 2009.

[98] Borodin, O., Zhuang, G. V., Ross, P. N. and Xu, K., "Molecular Dynamics Simulations and Experimental Study of Lithium Ion Transport in Dilithium Ethylene Dicarbonate," The Journal of Physical Chemistry C, vol. 117 (15), pp. 7433-7444, 2013.

[99] Lee, S., Park, J., Sastry, A. M. and Lu, W., "Molecular Dynamics Simulations of SOC-Dependent Elasticity of LixMn2O4 Spinels in Li-Ion Batteries," Journal of The Electrochemical Society, vol. 160 (6), pp. A968-A972, 2013.

[100] Kim, S.-P., Duin, A. C. T. v. and Shenoy, V. B., "Effect of electrolytes on the structure and evolution of the solid electrolyte interphase (SEI) in Li-ion batteries: A molecular dynamics study," Journal of Power Sources, vol. 196 (20), pp. 8590-8597, 2011.

[101] Agubra, V. A. and Fergus, J. W., "The formation and stability of the solid electrolyte interface on the graphite anode," Journal of Power Sources, vol. 268 pp. 153-162, 2014.

[102] Tachikawa, H., "A Direct Molecular Orbital−Molecular Dynamics Study on the Diffusion of the Li Ion on a Fluorinated Graphene Surface," The Journal of Physical Chemistry C, vol. 112 (27), pp. 10193-10199, 2008.

[103] Tachikawa, H., "Diffusion of the Li^+ Ion on C60: A DFT and Molecular Dynamics Study," The Journal of Physical Chemistry C, vol. 115 (42), pp. 20406-20411, 2011.

[104] Tachikawa, H., "Diffusion Dynamics of the Li Ion on C_{60}: A Direct Molecular Orbital−Molecular Dynamics Study," The Journal of Physical Chemistry C, vol. 111 (35), pp. 13087-13091, 2007.

[105] Cai, L. and White, R. E., "Mathematical modeling of a lithium ion battery with thermal effects in COMSOL Inc. Multiphysics (MP) software," Journal of Power Sources, vol. 196 (14), pp. 5985-5989, 2011.

[106] Martínez-Rosas, E., Vasquez-Medrano, R. and Flores-Tlacuahuac, A., "Modeling and simulation of lithium-ion batteries," Computers & Chemical Engineering, vol. 35 (9), pp. 1937-1948, 2011.

[107] Ramadesigan, V., Northrop, P. W. C., De, S., Santhanagopalan, S., Braatz, R. D. and Subramanian, V. R., "Modeling and Simulation of Lithium-Ion Batteries from a Systems Engineering Perspective," Journal of The Electrochemical Society, vol. 159 (3), pp. R31-R45, 2012.

[108] Kim, G.-H., Smith, K., Lee, K.-J., Santhanagopalan, S. and Pesaran, A., "Multi-Domain Modeling of Lithium-Ion Batteries Encompassing Multi-Physics in Varied Length Scales," Journal of The Electrochemical Society, vol. 158 (8), pp. A955-A969, 2011.

[109] "Allen J. Bard and Larry R. Faulkner, Electrochemical Methods: Fundamentals and Applications, New York: Wiley, 2001, 2nd ed," Russian Journal of Electrochemistry, vol. 38 (12), pp. 1364-1365, 2002.

[110] Newman, J., "Stefan–Maxwell mass transport," Chemical Engineering Science, vol. 64 (22), pp. 4796-4803, 2009.

[111] Newman, J., "Numerical Solution of Coupled, Ordinary Differential Equations," Industrial & Engineering Chemistry Fundamentals, vol. 7 (3), pp. 514-517, 1968.

[112] White, R. E., "On Newman's Numerical Technique for Solving Boundary Value Problems," Industrial & Engineering Chemistry Fundamentals, vol. 17 (4), pp. 367-369, 1978.

[113] West, K., Jacobsen, T. and Atlung, S., "Modeling of Porous Insertion Electrodes with Liquid Electrolyte," Journal of The Electrochemical Society, vol. 129 (7), pp. 1480-1485, 1982.

[114] Krishna, R. and Wesselingh, J. A., "The Maxwell-Stefan approach to mass transfer," Chemical Engineering Science, vol. 52 (6), pp. 861-911, 1997.

[115] Song, Y., Song, J., Gong, M., Cao, B., Yang, Y. and Ma, X., "Modeling of Mass Transfer in Nonideal Multicomponent Mixture with Maxwell-Stefan Approach," Chinese Journal of Chemical Engineering, vol. 18 (3), pp. 362-371, 2010.

[116] Onsager, L., "THEORIES AND PROBLEMS OF LIQUID DIFFUSION," Annals of the New York Academy of Sciences, vol. 46 (5), pp. 241-265, 1945.

[117] Lightfoot, E. N., Cussler, E. L. and Rettig, R. L., "Applicability of the Stefan-Maxwell equations to multicomponent diffusion in liquids," AIChE Journal, vol. 8 (5), pp. 708-710, 1962.

[118] Laity, R. W., "General Approach to the Study of Electrical Conductance and Its Relation to Mass Transport Phenomena," The Journal of Chemical Physics, vol. 30 (3), pp. 682-691, 1959.

[119] Laity, R. W., "An Application of Irreversible Thermodynamics to the Study of Diffusion," The Journal of Physical Chemistry, vol. 63 (1), pp. 80-83, 1959.

[120] Fan, D. and White, R. E., "Modification of Newman's BAND(J) Subroutine to Multi-Region Systems Containing Interior Boundaries: MBAND," Journal of The Electrochemical Society, vol. 138 (6), pp. 1688-1691, 1991.

[121] Fuller, T. F., Doyle, M. and Newman, J., "Simulation and Optimization of the Dual Lithium Ion Insertion Cell," Journal of The Electrochemical Society, vol. 141 (1), pp. 1-10, 1994.

[122] Kimble, M. C. and White, R. E., "A five-point finite difference method for solving parabolic partial differential equations," Computers & Chemical Engineering, vol. 14 (8), pp. 921-924, 1990.

[123] Smith, K. A., Rahn, C. D. and Chao-Yang, W., "Model-Based Electrochemical Estimation and Constraint Management for Pulse Operation of Lithium Ion Batteries," Control Systems Technology, IEEE Transactions on, vol. 18 (3), pp. 654-663, 2010.

[124] Biesheuvel, P. M., Fu, Y. and Bazant, M. Z., "Electrochemistry and capacitive charging of porous electrodes in asymmetric multicomponent electrolytes," Russian Journal of Electrochemistry, vol. 48 (6), pp. 580-592, 2012.

[125] Zheng, G., Popov, B. N. and White, R. E., "Application of Porous Electrode Theory on Metal Hydride Electrodes in Alkaline Solution," Journal of The Electrochemical Society, vol. 143 (2), pp. 435-441, 1996.

[126] Lei, Y. Q., Wang, C. S., Yang, X. G., Pan, H. G., Wu, J. and Wang, Q. D., "A mathematical model for the cycle life of hydride electrodes," Journal of Alloys and Compounds, vol. 231 (1–2), pp. 611-615, 1995.

[127] Subramanian, V. R., Ploehn, H. J. and White, R. E., "Shrinking Core Model for the Discharge of a Metal Hydride Electrode," Journal of The Electrochemical Society, vol. 147 (8), pp. 2868-2873, 2000.

[128] Zhang, W., Srinivasan, S. and Ploehn, H. J., "Analysis of Transient Hydrogen Uptake by Metal Alloy Particles," Journal of The Electrochemical Society, vol. 143 (12), pp. 4039-4047, 1996.

[129] Srinivasan, V. and Newman, J., "Discharge Model for the Lithium Iron-Phosphate Electrode," Journal of The Electrochemical Society, vol. 151 (10), pp. A1517-A1529, 2004.

[130] Ferguson, T. R. and Bazant, M. Z., "Nonequilibrium Thermodynamics of Porous Electrodes," Journal of The Electrochemical Society, vol. 159 (12), pp. A1967-A1985, 2012.

[131] Bazant, M. Z., "Theory of Chemical Kinetics and Charge Transfer based on Nonequilibrium Thermodynamics," Accounts of Chemical Research, vol. 46 (5), pp. 1144-1160, 2013.

[132] Gurtin, M. E., "Generalized Ginzburg-Landau and Cahn-Hilliard equations based on a microforce balance," Physica D: Nonlinear Phenomena, vol. 92 (3–4), pp. 178-192, 1996.

[133] Gomadam, P. M., Weidner, J. W., Dougal, R. A. and White, R. E., "Mathematical modeling of lithium-ion and nickel battery systems," Journal of Power Sources, vol. 110 (2), pp. 267-284, 2002.

[134] Botte, G. G., Subramanian, V. R. and White, R. E., "Mathematical modeling of secondary lithium batteries," Electrochimica Acta, vol. 45 (15–16), pp. 2595-2609, 2000.

[135] Chabre, Y., Djurado, D., Armand, M., Romanow, W. R., Coustel, N., McCauley, J. P., Fischer, J. E. and Smith, A. B., "Electrochemical intercalation of lithium into solid fullerene C60," Journal of the American Chemical Society, vol. 114 (2), pp. 764-766, 1992.

[136] Wang, H. H., Kini, A. M., Savall, B. M., Carlson, K. D., Williams, J. M., Lykke, K. R., Wurz, P., Parker, D. H., Pellin, M. J. and et al., "First easily reproduced solution-phase synthesis and confirmation of superconductivity in the fullerene K_xC_{60} (T_c = 18.0 .+-. 0.1 K)," Inorganic Chemistry, vol. 30 (14), pp. 2838-2839, 1991.

[137] McCauley, J. P., Zhu, Q., Coustel, N., Zhou, O., Vaughan, G., Idziak, S. H. J., Fischer, J. E., Tozer, S. W. and Groski, D. M., "Synthesis, structure, and superconducting properties of single-phase Rb_3C_{60}. A new, convenient method for the preparation of M_3C_{60} superconductors," Journal of the American Chemical Society, vol. 113 (22), pp. 8537-8538, 1991.

[138] Yokoji, T., Matsubara, H. and Satoh, M., "Rechargeable organic lithium-ion batteries using electron-deficient benzoquinones as positive-electrode materials with high discharge voltages," Journal of Materials Chemistry A, vol. 2 (45), pp. 19347-19354, 2014.

[139] Lee, S. W., Yabuuchi, N., Gallant, B. M., Chen, S., Kim, B.-S., Hammond, P. T. and Shao-Horn, Y., "High-power lithium batteries from functionalized carbon-nanotube electrodes," Nat Nano, vol. 5 (7), pp. 531-537, 2010.

[140] Byon, H. R., Gallant, B. M., Lee, S. W. and Shao-Horn, Y., "Role of Oxygen Functional Groups in Carbon Nanotube/Graphene Freestanding Electrodes for High Performance Lithium Batteries," Advanced Functional Materials, vol. 23 (8), pp. 1037-1045, 2013.

[141] Frackowiak, E. and Béguin, F., "Carbon materials for the electrochemical storage of energy in capacitors," Carbon, vol. 39 (6), pp. 937-950, 2001.

[142] Lee, S. W., Gallant, B. M., Lee, Y., Yoshida, N., Kim, D. Y., Yamada, Y., Noda, S., Yamada, A. and Shao-Horn, Y., "Self-standing positive electrodes of oxidized few-walled carbon nanotubes for light-weight and high-power lithium batteries," Energy & Environmental Science, vol. 5 (1), pp. 5437-5444, 2012.

[143] Byon, H. R., Lee, S. W., Chen, S., Hammond, P. T. and Shao-Horn, Y., "Thin films of carbon nanotubes and chemically reduced graphenes for electrochemical micro-capacitors," Carbon, vol. 49 (2), pp. 457-467, 2011.

[144] Lee, S. W., Gallant, B. M., Byon, H. R., Hammond, P. T. and Shao-Horn, Y., "Nanostructured carbon-based electrodes: bridging the gap between thin-film lithium-ion batteries and electrochemical capacitors," Energy & Environmental Science, vol. 4 (6), pp. 1972-1985, 2011.

[145] Lota, G., Fic, K. and Frackowiak, E., "Carbon nanotubes and their composites in electrochemical applications," Energy & Environmental Science, vol. 4 (5), pp. 1592-1605, 2011.

[146] Frackowiak, E., "Carbon materials for supercapacitor application," Physical Chemistry Chemical Physics, vol. 9 (15), pp. 1774-1785, 2007.

[147] Lota, G., Grzyb, B., Machnikowska, H., Machnikowski, J. and Frackowiak, E., "Effect of nitrogen in carbon electrode on the supercapacitor performance," Chemical Physics Letters, vol. 404 (1–3), pp. 53-58, 2005.

[148] Burkhardt, S. E., Lowe, M. A., Conte, S., Zhou, W., Qian, H., Rodriguez-Calero, G. G., Gao, J., Hennig, R. G. and Abruna, H. D., "Tailored redox functionality of small organics for pseudocapacitive electrodes," Energy & Environmental Science, vol. 5 (5), pp. 7176-7187, 2012.

[149] Qu, D., "Studies of the activated carbons used in double-layer supercapacitors," Journal of Power Sources, vol. 109 (2), pp. 403-411, 2002.

[150] Liang, Y., Tao, Z. and Chen, J., "Organic Electrode Materials for Rechargeable Lithium Batteries," Advanced Energy Materials, vol. 2 (7), pp. 742-769, 2012.

[151] Xie, J. and Zhang, Q., "Recent progress in rechargeable lithium batteries with organic materials as promising electrodes," Journal of Materials Chemistry A, vol. 4 (19), pp. 7091-7106, 2016.

[152] Liu, C., Neale, Z. G. and Cao, G., "Understanding electrochemical potentials of cathode materials in rechargeable batteries," Materials Today, vol. 19 (2), pp. 109-123, 2016.

[153] Xu, J., Dou, S., Liu, H. and Dai, L., "Cathode materials for next generation lithium ion batteries," Nano Energy, vol. 2 (4), pp. 439-442, 2013.

[154] Zettergren, H., Alcamí, M. and Martín, F., "First- and second-electron affinities of C_{60} and C_{70} isomers," Physical Review A, vol. 76 (4), pp. 043205, 2007.

[155] Prato, M., "[60]Fullerene chemistry for materials science applications," Journal of Materials Chemistry, vol. 7 (7), pp. 1097-1109, 1997.

[156] Kroto, H. W., "The stability of the fullerenes C_n, with n = 24, 28, 32, 36, 50, 60 and 70," Nature, vol. 329 (6139), pp. 529-531, 1987.

[157] Vostrowsky, O. and Hirsch, A., "Heterofullerenes," Chemical Reviews, vol. 106 (12), pp. 5191-5207, 2006.

[158] Lips, K., Waiblinger, M., Pietzak, B. and Weidinger, A., "Atomic Nitrogen Encapsulated in Fullerenes: Realization of a Chemical Faraday Cage," physica status solidi (a), vol. 177 (1), pp. 81-91, 2000.

[159] Olah, G. A., Bucsi, I., Aniszfeld, R. and Surya Prakash, G. K., "Chemical reactivity and functionalization of C_{60} and C_{70} fullerenes," Carbon, vol. 30 (8), pp. 1203-1211, 1992.

[160] Nebhani, L. and Barner-Kowollik, C., "Functionalization of Fullerenes with Cyclopentadienyl and Anthracenyl Capped Polymeric Building Blocks via Diels–Alder Chemistry," Macromolecular Rapid Communications, vol. 31 (14), pp. 1298-1305, 2010.

[161] Yan, W., Seifermann, S. M., Pierrat, P. and Brase, S., "Synthesis of highly functionalized C60 fullerene derivatives and their applications in material and life sciences," Organic & Biomolecular Chemistry, vol. 13 (1), pp. 25-54, 2015.

[162] Yannoni, C. S., Wendt, H. R., de Vries, M. S., Siemens, R. L., Salem, J. R., Lyerla, J., Johnson, R. D., Hoinkis, M., Crowder, M. S., Brown, C. A., Bethune, D. S., Taylor, L., Nguyen, D., Jedrzejewski, P. and Dorn, H. C., "Characterization of fullerenes and doped fullerenes," Synthetic Metals, vol. 59 (3), pp. 279-295, 1993.

[163] Chen, Z., Jiao, H., Hirsch, A. and Thiel, W., "BN-Doped Fullerenes: An NICS Characterization," The Journal of Organic Chemistry, vol. 66 (10), pp. 3380-3383, 2001.

[164] Andreoni, W., Gygi, F. and Parrinello, M., "Impurity states in doped fullerenes: C59B and C59N," Chemical Physics Letters, vol. 190 (3–4), pp. 159-162, 1992.

[165] Churilov, G. N., Alikhanyan, A. S., Nikitin, M. I., Glushchenko, G. A., Vnukova, N. G., Bulina, N. V. and Emelina, A. L., "Synthesis and investigation of boron-doped fullerene and scandium-containing fullerene," Technical Physics Letters, vol. 29 (2), pp. 168-170, 2003.

[166] Ratnikova, O. V., Melenevskaya, E. Y., Amsharov, K. Y., Vlasova, E. N., Volchek, B. Z., Gribanov, A. V., Shibaev, L. A. and Zgonnik, V. N., "The New Method for the Synthesis of Fullerols Based on Radical Reaction," Fullerenes, Nanotubes and Carbon Nanostructures, vol. 12 (1-2), pp. 155-158, 2005.

[167] Periya, V. K., Koike, I., Kitamura, Y., Iwamatsu, S.-i. and Murata, S., "Hydrophilic [60]fullerene carboxylic acid derivatives retaining the original 60π electronic system," Tetrahedron Letters, vol. 45 (45), pp. 8311-8313, 2004.

[168] Yasukawa, M. and Yamanaka, S., "Synthesis of Li_xC_{60}(x=1-28) fullerides under high-pressure and high-temperature conditions and their electrical properties," Chemical Physics Letters, vol. 341 (5-6), pp. 467-475, 2001.

[169] Giglio, F., Pontiroli, D., Gaboardi, M., Aramini, M., Cavallari, C., Brunelli, M., Galinetto, P., Milanese, C. and Riccò, M., "$Li_{12}C_{60}$: A lithium clusters intercalated fulleride," Chemical Physics Letters, vol. 609 pp. 155-160, 2014.

[170] Zimmermann, U., Burkhardt, A., Malinowski, N., Näher, U. and Martin, T. P., "Quantum chemical study of lithium–C_{60} clusters," The Journal of Chemical Physics, vol. 101 (3), pp. 2244-2249, 1994.

[171] Green, W. H., Gorun, S. M., Fitzgerald, G., Fowler, P. W., Ceulemans, A. and Titeca, B. C., "Electronic Structures and Geometries of C_{60} Anions via Density

Functional Calculations," The Journal of Physical Chemistry, vol. 100 (36), pp. 14892-14898, 1996.

[172] Dubois, D., Kadish, K. M., Flanagan, S. and Wilson, L. J., "Electrochemical detection of fulleronium and highly reduced fulleride ($C60^{5-}$) ions in solution," Journal of the American Chemical Society, vol. 113 (20), pp. 7773-7774, 1991.

[173] Pavanello, M., Jalbout, A. F., Trzaskowski, B. and Adamowicz, L., "Fullerene as an electron buffer: Charge transfer in Li@C60," Chemical Physics Letters, vol. 442 (4–6), pp. 339-343, 2007.

[174] Mantina, M., Wang, Y., Chen, L. Q., Liu, Z. K. and Wolverton, C., "First principles impurity diffusion coefficients," Acta Materialia, vol. 57 (14), pp. 4102-4108, 2009.

[175] Soscún, H., Hernández, J., Escobar, R., Toro-Mendoza, C., Alvarado, Y. and Hinchliffe, A., "Ab initio and density functional theory calculations of the dipole polarizability and the second dipole hyperpolarizability of benzene," International Journal of Quantum Chemistry, vol. 90 (2), pp. 497-506, 2002.

[176] Franco, A. A., "Multiscale modelling and numerical simulation of rechargeable lithium ion batteries: concepts, methods and challenges," RSC Advances, vol. 3 (32), pp. 13027-13058, 2013.

[177] Mohr, S., Ratcliff, L. E., Genovese, L., Caliste, D., Boulanger, P., Goedecker, S. and Deutsch, T., "Accurate and efficient linear scaling DFT calculations with universal applicability," Physical Chemistry Chemical Physics, vol. 17 (47), pp. 31360-31370, 2015.

[178] Fermeglia, M. and Pricl, S., "Multiscale modeling for polymer systems of industrial interest," Progress in Organic Coatings, vol. 58 (2–3), pp. 187-199, 2007.

[179] Hohenberg, P. and Kohn, W., "Inhomogeneous Electron Gas," Physical Review, vol. 136 (3B), pp. B864-B871, 1964.

[180] Cederbaum, L. S., "Born–Oppenheimer approximation and beyond for time-dependent electronic processes," The Journal of Chemical Physics, vol. 128 (12), pp. 124101, 2008.

[181] Becke, A. D., "Perspective: Fifty years of density-functional theory in chemical physics," The Journal of Chemical Physics, vol. 140 (18), pp. 18A301, 2014.

[182] Parr, R. G., Density Functional Theory of Atoms and Molecules. In *Horizons of Quantum Chemistry: Proceedings of the Third International Congress of Quantum Chemistry Held at Kyoto, Japan, October 29 - November 3, 1979*, Fukui, K.; Pullman, B., Eds. Springer Netherlands: Dordrecht, 1980; pp 5-15.

[183] Foldy, L. L., "Antisymmetric Functions and Slater Determinants," Journal of Mathematical Physics, vol. 3 (3), pp. 531-539, 1962.

[184] Echenique, P. and Alonso, J. L., "A mathematical and computational review of Hartree–Fock SCF methods in quantum chemistry," Molecular Physics, vol. 105 (23-24), pp. 3057-3098, 2007.

[185] Slamet, M. and Sahni, V., "Coulomb holes and correlation potentials in the helium atom," Physical Review A, vol. 51 (4), pp. 2815-2825, 1995.

[186] Ceperley, D. M. and Alder, B. J., "Ground State of the Electron Gas by a Stochastic Method," Physical review letters, vol. 45 (7), pp. 566-569, 1980.

[187] Perdew, J. P., Burke, K. and Ernzerhof, M., "Generalized Gradient Approximation Made Simple," Physical review letters, vol. 77 (18), pp. 3865-3868, 1996.

[188] Vosko, S. H., Wilk, L. and Nusair, M., "Accurate spin-dependent electron liquid correlation energies for local spin density calculations: a critical analysis," Canadian Journal of Physics, vol. 58 (8), pp. 1200-1211, 1980.

[189] Perdew, J. P. and Zunger, A., "Self-interaction correction to density-functional approximations for many-electron systems," Physical Review B, vol. 23 (10), pp. 5048-5079, 1981.

[190] Perdew, J. P. and Wang, Y., "Accurate and simple analytic representation of the electron-gas correlation energy," Physical Review B, vol. 45 (23), pp. 13244-13249, 1992.

[191] Bachelet, G. B., Hamann, D. R. and Schlüter, M., "Pseudopotentials that work: From H to Pu," Physical Review B, vol. 26 (8), pp. 4199-4228, 1982.

[192] Kresse, G. and Furthmüller, J., "Efficient iterative schemes for *ab initio* total-energy calculations using a plane-wave basis set," Physical Review B, vol. 54 (16), pp. 11169-11186, 1996.

[193] Payne, M. C., Teter, M. P., Allan, D. C., Arias, T. A. and Joannopoulos, J. D., "Iterative minimization techniques for ab initio total-energy calculations: molecular dynamics and conjugate gradients," Reviews of Modern Physics, vol. 64 (4), pp. 1045-1097, 1992.

[194] Paolo, G., Stefano, B., Nicola, B., Matteo, C., Roberto, C., Carlo, C., Davide, C., Guido, L. C., Matteo, C., Ismaila, D., Andrea Dal, C., Stefano de, G., Stefano, F., Guido, F., Ralph, G., Uwe, G., Christos, G., Anton, K., Michele, L., Layla, M.-S., Nicola, M., Francesco, M., Riccardo, M., Stefano, P., Alfredo, P., Lorenzo, P., Carlo, S., Sandro, S., Gabriele, S., Ari, P. S., Alexander, S., Paolo, U. and Renata, M. W., "QUANTUM ESPRESSO: a modular and open-source software project for quantum simulations of materials," Journal of Physics: Condensed Matter, vol. 21 (39), pp. 395502, 2009.

[195] Heine, V., "The Pseudopotential Concept," Solid State Physics, vol. 24 pp. 1-36, 1970.

[196] Fuchs, M. and Scheffler, M., "Ab initio pseudopotentials for electronic structure calculations of poly-atomic systems using density-functional theory," Computer Physics Communications, vol. 119 (1), pp. 67-98, 1999.

[197] Vanderbilt, D., "Soft self-consistent pseudopotentials in a generalized eigenvalue formalism," Physical Review B, vol. 41 (11), pp. 7892-7895, 1990.

[198] Hamann, D. R., "Generalized norm-conserving pseudopotentials," Physical Review B, vol. 40 (5), pp. 2980-2987, 1989.

[199] Kresse, G. and Furthmüller, J., "Efficiency of ab-initio total energy calculations for metals and semiconductors using a plane-wave basis set," Computational Materials Science, vol. 6 (1), pp. 15-50, 1996.

[200] Tannor, D. J., Marten, B., Murphy, R., Friesner, R. A., Sitkoff, D., Nicholls, A., Honig, B., Ringnalda, M. and Goddard, W. A., "Accurate First Principles Calculation of Molecular Charge Distributions and Solvation Energies from Ab Initio Quantum Mechanics and Continuum Dielectric Theory," Journal of the American Chemical Society, vol. 116 (26), pp. 11875-11882, 1994.

[201] Bochevarov, A. D., Harder, E., Hughes, T. F., Greenwood, J. R., Braden, D. A., Philipp, D. M., Rinaldo, D., Halls, M. D., Zhang, J. and Friesner, R. A., "Jaguar: A high-performance quantum chemistry software program with strengths in life and materials sciences," International Journal of Quantum Chemistry, vol. 113 (18), pp. 2110-2142, 2013.

[202] Politzer, P. and Abu-Awwad, F., "A comparative analysis of Hartree-Fock and Kohn-Sham orbital energies," Theor Chem Acc, vol. 99 (2), pp. 83-87, 1998.

[203] Hamel, S., Duffy, P., Casida, M. E. and Salahub, D. R., "Kohn–Sham orbitals and orbital energies: fictitious constructs but good approximations all the same," Journal of Electron Spectroscopy and Related Phenomena, vol. 123 (2–3), pp. 345-363, 2002.

[204] Clayborne, P. A., Gupta, U., Reber, A. C., Melko, J. J., Khanna, S. N. and Jr., A. W. C., "The applicability of three-dimensional aromaticity in BiSnn− Zintl analogues," The Journal of Chemical Physics, vol. 133 (13), pp. 134302, 2010.

[205] Lynam, M. M., Kuty, M., Damborsky, J., Koca, J. and Adriaens, P., "Molecular orbital calculations to describe microbial reductive dechlorination of polychlorinated dioxins," Environmental Toxicology and Chemistry, vol. 17 (6), pp. 988-997, 1998.

[206] Chen, G., Cookscor, R. G., Corpuz, E. and Scott, L. T., "Estimation of the electron affinities of C60, corannulene, and coronene by using the kinetic method," Journal of the American Society for Mass Spectrometry, vol. 7 (7), pp. 619-627, 1996.

[207] Wang, L.-S., Conceicao, J., Jin, C. and Smalley, R. E., "Threshold photodetachment of cold C−60," Chemical Physics Letters, vol. 182 (1), pp. 5-11, 1991.

[208] Functionalized fullerenes : proceedings of the international symposium. Martin, N.; Maggini, M.; Guldi, D. M., Eds. Electrochemical Society: Pennington, New Jersey :, 2000.

[209] Maggini, M., Scorrano, G. and Prato, M., "Addition of azomethine Ylides to C_{60}: synthesis, characterization, and functionalization of fullerene pyrrolidines," Journal of the American Chemical Society, vol. 115 (21), pp. 9798-9799, 1993.

[210] Lai, Y.-Y., Cheng, Y.-J. and Hsu, C.-S., "Applications of functional fullerene materials in polymer solar cells," Energy & Environmental Science, vol. 7 (6), pp. 1866-1883, 2014.

[211] Goldshleger, N. F., "FULLERENES AND FULLERENE-BASED MATERIALS IN CATALYSIS," Fullerene Science and Technology, vol. 9 (3), pp. 255-280, 2001.